MARMARA UNIVERSITY
INSTITUTE FOR GRADUATE STUDIES
IN PURE AND APPLIED SCIENCES

EXPERIMENTAL AND THEORETICAL INVESTIGATION OF FLUIDIZED BED GASIFICATION WITH COLD AND HOT SYSTEMS

SERHAT GÜL

Ph.D. THESIS

Department of Mechanical Engineering

Thesis Supervisor
Prof. Dr. Z. Sibel ÖZDOĞAN

Thesis CO- Supervisor
Assoc. Prof. Dr. Emre ALPMAN

ISTANBUL, 2017

MARMARA UNIVERSITY
INSTITUTE FOR GRADUATE STUDIES
IN PURE AND APPLIED SCIENCES

EXPERIMENTAL AND THEORETICAL INVESTIGATION OF FLUIDIZED BED GASIFICATION WITH COLD AND HOT SYSTEMS

SERHAT GÜL
(724608004)

Ph.D. THESIS
Department of Mechanical Engineering

Thesis Supervisor
Prof. Dr. Z. Sibel ÖZDOĞAN

Thesis CO- Supervisor
Assoc. Prof. Dr. Emre ALPMAN

ISTANBUL, 2017

ACKNOWLEDGMENT

I would like to thank my supervisor Prof. Dr. Z. Sibel Özdoğan for her guidance and support during the research of this thesis.

I would like thank to committee members Prof. Dr. Hayati Olgun and Prof Dr. Ersan Kalafatoğlu for their encouragement and valuable comments.

I would like to thank to TUBITAK-MRC Energy Institute, Marmara University Institute of Pure and Applied Sciences and Mechanical Engineering Department.

I would like to thank my friend Ufuk Kayahan from the beginning of my engineering life to the end.

Lastly, I would like to thank my family and my wife for their material and spiritual support, encouragement and unconditional love along my life.

Serhat Gül

January, 2017

"Truth is ever to be found in the simplicity and not in the multiplicity and confusion of things"

Isaac Newton

TABLE OF CONTENTS **PAGE**

1. INTRODUCTION 1
1.1. Global Energy Profile and Turkey 1
1.2. Background of Gasification 3
1.3. Circulating Fluidized Bed (CFB) Reactors 5
1.4. Solid Circulation Systems at CFB Reactors 6
1.5. Problem Statement for Solid Circulation at CFB Reactors 8
1.6. Proposed Novel Solid Circulation Method at CFB Reactors 8
1.7. Literature Survey for Novel Solid Circulation Methods 13
1.8. Aim of the Study 22
2. MATERIAL and METHOD 24
2.1. Computational Fluid Dynamics (CFD) Model and Validation 25
2.1.1. CFD Model assumptions 26
2.1.1.1. Mesh type 26
2.1.1.2. Boundary conditions 28
2.1.1.3. Solver 29
2.1.1.4. Energy 30
2.1.1.5. Viscous model 30
2.1.1.6. Material 30
2.1.1.7. Turbulence model 30
2.1.1.8. Pressure-velocity coupling 30
2.1.1.9. Discretization 31
2.1.1.10. Convergence criteria 31
2.1.2. Experimental system for CFD Model validation 33
2.2. CFD Model Analysis and Validation Methodology 35
2.2.1. CFD analysis matrix 35
2.2.1.1. Performance criteria of ejector system 36
2.2.1.2. Motive gas flowrate 36
2.2.1.3. Ejector tube length 37
2.2.1.4. Ejector tube diameter 37
2.2.1.5. Ejector nozzle diameter 37

2.2.1.6. Motive gas temperature 37
2.2.1.7. Induced gas temperature 38
2.2.1.8. Induced gas static pressure 38
2.2.2. CFD model validation methodology 38
2.3. Experimental Cold Test Facility Design 38
2.3.1. Hydrodynamic calculations 41
2.3.2. Distributor plate 43
2.3.3. Riser 43
2.3.4. Cyclone 43
2.3.5. Downcomer 45
2.3.6. Air blower 45
2.3.7. Orifice flowmeter 46
2.3.8. Ejector motive gas 47
2.3.9. Ejector motive gas flowmeter 47
2.3.10. Bed material 48
2.3.11. Pressure measurement along the CFB loop 48
2.3.12. Ejector design 48
2.4. Experimental Cold Tests Methodology 49
2.4.1. Experimental matrix for cold tests 49
2.4.2. Measurement method for pressure profile 51
2.4.3. Determination of the solid circulation rate 51
2.4.4. Determination of the cyclone efficiency 52
2.4.5. Determination of the dense bed and freeboard densities 52
2.5. Experimental Hot Test Facility Design (Gasifier) 52
2.5.1. Fuel properties 54
2.5.2. Gasifier energy and mass balance (HYSYS) 55
2.5.3. Hydrodynamic calculations 57
2.5.4. Distributor plate 60
2.5.5. Riser 61
2.5.6. Cyclone 61
2.5.7. Downcomer 61
2.5.8. Fluidization agent 61

2.5.9. Fluidization agent flowmeter 61
2.5.10. Ejector motive gas 62
2.5.11. Bed material 62
2.5.12. Control system 62
2.5.13. Fuel feeding system 63
2.5.14. Gas analyzing system 64
2.6. Experimental Hot Test Methodology 64
2.6.1. Experimental method for hot tests 64
2.6.2. Measurement method for pressure profile 65
3. RESULTS AND DISCUSSION 66
3.1. CFD Analysis of Ejector System 66
3.1.1. CFD Model validation results 66
3.1.2. Flow characteristics of ejector model 67
3.1.2.1. Velocity magnitude along the axis of the ejector 67
3.1.2.2. Mach Number along the axis of the ejector 68
3.1.2.3. Static pressure along the axis of the ejector 69
3.1.2.4. Static temperature change along the axis of the ejector 70
3.1.2.5. Static pressure along the inside wall of the ejector 71
3.1.2.6. Density along the axis of the ejector 72
3.1.2.7. Thermodynamic Properties through the Axis 73
3.1.3. CFD model validation with positive pressure conditions 74
3.1.4. Ejector analysis with CFD (both side open) 77
3.1.4.1. Comparison of maximum vacuum pressure & back pressure without induced flow 82
3.1.4.2. Comparison of maximum positive pressure & back pressure with reverse flow 83
3.1.4.3. Entrainment ratio 84
3.1.5. Flow profiles of motive gas through the ejector tube 86
3.1.6. CFD results for different operational and geometric ejector design parameters 87
3.1.6.1. Ejector type: Central nozzle vs. radial nozzles 87
3.1.6.2. Effect of ejector length 88

3.1.6.3. Effect of motive gas flowrate 90
3.1.6.4. Effect of nozzle diameter 92
3.1.6.5. Effect of ejector tube diameter 95
3.1.6.6. Effect of induced gas static pressure 96
3.1.6.7. Effect of induced gas temperature 98
3.1.6.7. Effect of motive gas temperature 99
3.2. Semi Empirical Correlation for Ejector Design 100
3.2.1. Vacuum pressure & motive gas momentum relation 100
3.2.2. Conditions for the comparison of semi-empirical correlation and CFD results 104
3.2.3. Mach number correction factor 105
3.2.4. Derivation of Mach number 106
3.2.5. Comparison of semi-empirical correlation with CFD results 107
3.3. Cold Model Experimental Results 108
3.3.1. Effect of ejector system at CFB without solid bed inventory 108
3.3.2. Effect of ejector system at CFB with solid bed inventory 110
3.3.2.1. Experimental results of CFB cold model without ejector system 110
3.3.2.2. Experimental results of CFB cold model with ejector system 112
3.3.3. Solid particle flowrate at ejector vortex region 118
3.3.4. Solid column formation conditions during cold experiment 119
3.4. Hot Model Experimental Results 121
3.4.1. Operating conditions of hot experiment 121
3.4.2. Pressure profile along the CFB loop 124
3.4.3. Solid circulation rate (Gs) 126
3.4.4. Gas composition 127
4. CONCLUSIONS 128
5. FUTURE WORKS 131
REFERENCES 132
VITA 136

ÖZET

AKIŞKAN YATAKLI GAZLAŞTIRMA İŞLEMİNİN SOĞUK VE SICAK SİSTEMLER İLE DENEYSEL VE TEORİK OLARAK İNCELENMESİ

Stabil katı dolaşımı, dolaşımlı akışkan yataklı sistemler için büyük bir önem arz etmektedir. Dolaşımlı akışkan yataklı sistemlerde katı dolaşımının stabil şekilde sağlanması için, geri dönüş ayağında ters gaz akışını önlemek için basınç bariyeri/direnci olması gerekmektedir. Konvansiyonel sistemlerde, döngü kilidi veya L, J, V vanaları basınç bariyeri olarak kullanılmaktadır. Konvansiyonel sistemlerde, özellikle döngü kilitlerinde, operasyon, reaktör içerisindeki basınç dalgalanmalarına karşı çok hassastır ve basınç bariyerinin anlık şekilde kırılması sonucunda operasyonun durdurulması gerekmektedir ve döngü kilidinin tekrar yeni yatak malzemesi ile doldurulması gerekmektedir.

Önerilen yeni konseptte, dolaşımlı akışkan yataklı sistemin geri dönüş ayağında ejektör sistemi kullanılmıştır. Gerekli olan basınç bariyeri, basınçlı ve yüksek hızlı gazın geri dönüş ayağına paralel şekilde yerleştirilen ejektör püskürtme borusundan püskürtülmesi ile elde edilmektedir. Ejektör sistemi temel olarak Venturi etkisi prensibine dayanmaktadır. Ejektör püskürtme borusundan hava, su buharı, azot veya herhangi bir gaz akımı püskürtülebilir. Bu çalışmada, ejektör tipinde katı dolaşımının sağlanmasının daha stabil olduğu iddia edilmektedir ve herhangi bir operasyon kesintisinde yatak malzemesi olmaksızın tekrar operasyona devam edebilmektedir. Bundan dolayı kesintisiz operasyon süresi daha uzun olmaktadır.

Bahsedilen ejektör sistemi ile katı dolaşımının sağlandığı dolaşımlı akışkan yataklı sistemlerde, ejektör itici gazı debisine ve geri dönüş ayağındaki katı akısına bağlı olarak 2 farklı operasyon durumu gözlenmiştir. Birinci operasyon durumunda, düşük katı akısından dolayı geri dönüş ayağında herhangi bir katı birikimi olmamaktadır. Basınç bariyeri, yüksek hızlı püskürtülen ejektör itici gazının momentumunun, geri dönüş ayağındaki düşük hızlı gaza transfer edilmesi ile sağlanmaktadır ve bu durum ejektör sistemi boyunca basınç farkı oluşmasını sağlamaktadır.

İkinci operasyon durumunda, geri dönüş ayağındaki göreceli olarak yüksek katı akısından dolayı ejektör sisteminin hemen üzerinde katı birikimi olmaktadır. Ejektör püskürtme borusunun çıkışındaki yüksek hızlı gaz, ejektör püskürtme borusu çıkışının

hemen altında halka şeklinde girdaplar meydana getirmektedir. Bu girdaplar katı akışına karşı bir direnç oluşturmaktadır. Ejektör itici gazının hızı artırıldığında oluşan girdapların şiddeti artmaktadır ve katı akışına karşı direnç artmaktadır. Ejektör gaz hızı belirli bir seviyeye kadar artırıldığında, ejektörün hemen üst bölgesinde akışkan olmayan ama yavaş bir şekilde aşağı yönlü hareket eden bir katı sütunu oluşmaktadır. Bu noktada, oluşan katı sütunun yüksekliği ejektör püskürtme borusu gaz çıkış hızı ile kontrol edilmektedir (ejektör itici gaz debisi ile). Ejektör sistemi ile birlikte oluşan katı sütunu basınç bariyeri olarak çalışmaktadır. Birinci operasyon durumundan farklı olarak, gerekli olan basınç farkının bir kısmı oluşan katı sütunu ile sağlandığından dolayı gerekli ejektör itici gazı debisi önemli derecede azalmaktadır.

Bu çalışmada, ejektör sistemi için istenilen tasarım ve operasyon şartları (maksimum basınç farkına karşılık minimum yüksek basınçlı gaz debisi) aranmıştır. Bahsi geçen iki farklı operasyon durumu dolaşımlı akışkan yataklı soğuk sistem (94 mm iç çapında ve 7800 mm yüksekliğinde) ile incelenmiştir. Deneysel çalışmalara ilave olarak ejektör sistemi, temel geometrik ve operasyon parametrelerinin, oluşturulan basınç farkına etkilerini incelemek üzere hesaplamalı akışkanlar dinamiği modeli ile analiz edilmiştir. Ayrıca, ejektör performansını tahmin etmek üzere hesaplamalı akışkanlar dinamiği sonuçları ile kıyaslanabilir yeni bir yarı-ampirik metot önerilmiştir. Son olarak soğuk sistem ile aynı geometrik ölçülere sahip dolaşımlı akışkan yataklı gazlaştırma reaktöründe ejektör sistemi test edilmiştir.

ABSTRACT

EXPERIMENTAL AND THEORETICAL INVESTIGATION OF FLUIDIZED BED GASIFICATION WITH COLD AND HOT SYSTEM

Stable solid circulation is of utmost importance in circulating fluidized bed operation. In order to maintain stable solid circulation at circulating fluidized bed systems, there should be a pressure barrier/resistance between riser and the downcomer for the purpose of avoiding reverse gas flow through the downcomer. In conventional systems, loop seals, L, J, V valves are used as pressure barriers. In conventional circulation methods especially for loop seals, operation is very sensitive to the pressure fluctuations inside the riser and if the pressure barrier is broken, the operation has to be stopped to re-charge the loop seal with the new bed material.

Within the proposed novel concept, an ejector system is used at the downcomer of the CFB reactor. The pressure barrier is provided with the pressurized high speed gas flow through the ejector nozzle exit placed parallel to the downcomer which is mainly based on Venturi effect principle. Gases which can be air, steam, nitrogen or any other gas streams flow through the ejector nozzle exit. It is claimed that the operation of the ejector type circulation is more stable and in case of an interruption, it can be rebuilt operation whether there is bed material or not. Therefore the latter appears to increase uninterrupted operation time.

For CFB systems with that ejector type circulation, there appear 2 different cases which are the function of gas velocity and solid flux through the downcomer. In the first case, there is no solid accumulation through the downcomer because of the low solid flux. The pressure barrier is obtained by the momentum transfer of high speed gas flow at ejector nozzle exit to the low speed gas flow at downcomer which causes the pressure difference through the ejector system.

In the second case, there is solid accumulation just above the ejector system because of relatively higher solid flux through the downcomer. High speed gas flow through the ejector nozzle exit causes severe vortices just below the nozzle exit which is torus in shape. These vortices cause resistance to the flow of solid particles. If the velocity of the motive gas is increased, the severeness of the vortices is increased and the resistance to the solid particle flow is increased. At some point of motive gas velocity, solid column

is formed just above the ejector which is not fluidized and moving quite slowly to the reactor. At that point, solid column height is controlled by the nozzle exit gas velocity (motive gas flow rate). This solid column and ejector system work as a pressure barrier. Different from the first case, some portion of the required pressure difference is contributed by the accumulated solid column which causes considerable amount of decrease in required high pressure motive gas flow rate.

In this study, the desired design and operational conditions (maximum pressure difference & minimum high pressure gas flow rate) are sought for the ejector system. The before mentioned two cases have been investigated with the CFB cold model (94 mm in diameter and 7800 mm in height) experiments . In addition to the experimental study, ejector system was analyzed with CFD model in order to investigate the effect of basic geometric and operational parameters on the pressure difference generated by the ejector. Furthermore a novel semi-empirical method was proposed as a tool for predicting the ejector performance comparable with CFD results. Finally, ejector system was tested with hot gasifier system which has same dimensions with the cold CFB test facility.

CLAIM FOR ORIGINALITY

In this study, an alternative method for solid circulation at circulating fluidized bed systems was developed. In conventional circulation methods especially for loop seals, operation is very sensitive to the pressure fluctuations inside the riser and if the pressure barrier is broken, the operation has to be stopped to re-charge the loop seal with the new bed material.

Within the proposed novel concept, an ejector system is used at the downcomer of the CFB reactor in order to provide pressure barrier. The pressure barrier is provided with the pressurized high speed gas flow through the ejector nozzle exit placed parallel to the downcomer. The original points of this study different from the other systems are summarized below:

- Using ejector for creating pressure barrier for the solid circulation at circulating fluidized bed is new concept and there is no published literature about ejector type circulation for circulating fluidized beds.
- Patent application has been done related with the new circulation concept with the patent application number of PCT/IB2015/054852. International preliminary report on patentability has been taken with 4/5 claims are accepted.
- The operation of the ejector type circulation is more stable and in case of an interruption, it can be rebuilt operation whether there is bed material or not. Therefore the latter appears to increase uninterrupted operation time.
- In conventional loop seals, there is bubbling fluidized bed that has to be operated as a separate reactor. In this new concept, there is no bubbling bed and the operation is simpler.
- The volume of ejector type circulation system is considerably smaller than the conventional ones and manufacturing cost is lower than the conventional ones.
- With CFD analysis of ejector system, a new semi-empirical equation was developed.

LIST OF SYMBOLS

A_d : Ejector nozzle cross-section area

A_D : Ejector tube cross-section area

Ar : Archimedes number

C : Speed of sound

C_D : Ejector tube diameter correction factor

C_p : Specific heat of motive gas (Constant pressure)

C_v : Specific heat of motive gas (Constant volume)

C_{Ma} : Mach number correction factor

d_p : Particle diameter

D : Ejector tube diameter

D_r : Reactor diameter

g : Gravitational acceleration

Gs : Solid circulation rate

k : Specific heat ratio

K : Kelvin

m : Meter

$\dot{m}$: Motive gas mass flowrate

Ma : Mach number

Pa : Pascal

P_{vacuum} : Vacuum pressure generated by the ejector

P_e : Motive gas nozzle exit static pressure

R : Specific gas constant

Re : Reynolds number

T_e : Motive gas nozzle exit temperature

T_a : Temperature of the motive gas at the inlet of the ejector nozzle

T_e : Temperature of the motive gas at the exit of the ejector nozzle

$\mathbf{U_g}$: Superficial gas velocity

$\mathbf{U_t}$: Terminal velocity of solid particle

V : Volumetric flow rate of the motive gas

$\dot{V}_e$: Volumetric flow rate of the motive gas at the exit of the ejector nozzle

V_e : Motive gas nozzle exit velocity

$\boldsymbol{\rho_g}$: Gas density

$\boldsymbol{\rho_p}$: Particle density

$\boldsymbol{\mu}$: Gas dynamic viscosity

$\boldsymbol{\varepsilon}$: Void fraction

ABBREVIATIONS

Bara : Absolute bar

ER : Equivalence Ratio

Mbarg : Milibar gage

Mtoe : Million Tons Oil Equivalent

CFB : Circulating Fluidized Bed

CFD : Computational Fluid Dynamics

C : Carbon

H : Hydrogen

O : Oxygen

N : Nitrogen

S : Sulfur

H_2O : Water

LHV : Lower Heating Value

FT : Fisher-Tropsch

MWth : Mega Watt Thermal

MWe : Mega Watt Electricity

IGCC : Integrated Gasification and Combustion Cycle

SNG : Synthetic Natural Gas

LIST OF FIGURES **Page**

Figure 1.1.	L valve	6
Figure 1.2.	Loop seal	7
Figure 1.3.	General principle of the experimental Venturi ejector	10
Figure 1.4.	Ejector type circulation for 2 different operation modes	11
Figure 1.5.	Vortices at ejector nozzle exit	12
Figure 1.6.	Combustion system according to invention	14
Figure 1.7.	Gasification system according to invention	15
Figure 1.8.	New type of fluidized bed combustion device according to invention	16
Figure 1.9.	New type of power plant according to invention	17
Figure 1.10.	Polymerization device according to invention	18
Figure 1.11.	New type drying apparatus with ejector according to the invention	19
Figure 1.12.	Circulating fluidized bed system according to the invention	20
Figure 1.13.	New type of particle processing system according to invention	21
Figure 1.14.	Vertically oriented fines ejector according to the invention	22
Figure 2.1.	Base procedure for the experimental and computational study	24
Figure 2.2.	Reference Ejector System	26
Figure 2.3.	Axisymmetric Plane of Ejector (0.5 mm mesh size)	26

Figure 2.4.	Gambit axisymmetric plane drawing and mesh of the ejector exit	27
Figure 2.5.	CFD results with different convergence criterions	31
Figure 2.6.	Reference Ejector System Drawing for CFD Calibration	33
Figure 2.7.	Reference Ejector System for CFD Calibration	34
Figure 2.8.	Fluent solution for velocity magnitude @ 28Nm^3/h	35
Figure 2.9.	Experimental CFB Cold Model	39
Figure 2.10.	Cold CFB model	40
Figure 2.11.	Hydrodynamic calculation procedure	41
Figure 2.12.	Cyclone dimensions	44
Figure 2.13.	Cold CFB test facility cyclone dimensions	45
Figure 2.14.	Orifice plate pressure difference and volumetric air flowrate relation	47
Figure 2.15.	Bed material size distribution	48
Figure 2.16.	Ejector dimensions	49
Figure 2.17.	Pressure measurement at 6 m/s gas velocity	51
Figure 2.18.	Hot CFB Gasifier	54
Figure 2.19.	Simulation flow diagram of gasifier reactor	55
Figure 2.20.	Hydrodynamic calculation procedure (hot system)	58
Figure 2.21.	Distributor plate of hot system	60
Figure 2.22.	Control screen of PLC system	63

Figure 3.1.	Experimental and Fluent Results (0.5 mm mesh size)	67
Figure 3.2.	Velocity magnitude along the axis of the ejector	68
Figure 3.3.	Mach Number along the axis of the ejector	69
Figure 3.4.	Static pressure along the axis of the ejector	70
Figure 3.5.	Static temperature change along the axis of the ejector	71
Figure 3.6.	Static pressure along the inside wall of the ejector	72
Figure 3.7.	Density along the axis of the ejector	73
Figure 3.8.	Apparatus for Positive Pressure Effect Investigation	75
Figure 3.9.	Experimental and Fluent Results for Positive Pressure (0.5 mm mesh size)	77
Figure 3.10.	Ejector Model (both side open) for Entrainment Analysis with CFD Model	78
Figure 3.11.	Velocity Profile along the Axis of the Ejector (both side open– zero back pressure)	79
Figure 3.12.	Velocity Profile along the Axis of the Ejector (295 mm ejector length)	80
Figure 3.13.	Motive Air Flow Rate & Back Pressure Chart	82
Figure 3.14.	Entrainment Ratios for Different Motive Air Flow Rates with Zero Back Pressure	85
Figure 3.15.	Flow profile of motive gas (colors represent velocity magnitude)	86
Figure 3.16.	Comparison of ejector types performance	88
Figure 3.17.	Ejector tube length effect on ejector performance	90

Figure 3.18. Motive gas flowrate effect on ejector performance 91

Figure 3.19. Vacuum pressures for different nozzle diameters 93

Figure 3.20. Nozzle inlet pressure change with nozzle diameter 94

Figure 3.21. Vacuum pressures for different ejector tube diameters 96

Figure 3.22. Vacuum pressures for different induced gas pressures 97

Figure 3.23. Induced air flowrate for different temperatures and back pressures 99

Figure 3.24. Vacuum pressures for different motive gas temperatures 100

Figure 3.25. Correction factors for different Mach numbers 105

Figure 3.26. Pressure profile along the CFB model without bed inventory 108

Figure 3.27. Pressure profile with ejector and without bed inventory 109

Figure 3.28. Pressure profile of CFB loop without ejector system 110

Figure 3.29. Pressure profile of CFB loop with/without ejector system for 4 m/s 114

Figure 3.30. Solid column formation 115

Figure 3.31. Pressure profile of CFB loop with (without) ejector system for 5 m/s 116

Figure 3.32. Pressure profile of CFB loop with (without) ejector system for 6 m/s 117

Figure 3.33. Solid particle flow rate through the ejector system 119

Figure 3.34. CFB gasifier reactor control screen 122

Figure 3.35. CFB gasifier Fuel feeding control screen 122

Figure 3.36. Pressure profile of CFB loop at 4 m/s superficial gas velocity 124

Figure 3.37. Pressure profile of CFB loop at 5 m/s superficial gas velocity 125

Figure 3.38. Pressure profile of CFB loop at 6 m/s superficial gas velocity 126

LIST OF TABLES **Page**

Table 2.1.	Mesh independency test results for 4 different mesh sizes	27
Table 2.2.	Pre-processing settings for ejector model	29
Table 2.3.	Equation solver settings for ejector model	32
Table 2.4.	Operational and geometric parameters investigated with CFD model	36
Table 2.5.	Empirical table for cyclone design	44
Table 2.6.	Calibration data for orifice flowmeter	46
Table 2.7.	Experimental matrix for CFB cold tests	50
Table 2.8.	Elemental analysis of selected Turkish coal	55
Table 2.9.	Mass & Energy Balance of Gasifier	56
Table 2.10.	Syngas composition result of simulation study (volumetric)	57
Table 2.11.	Density and viscosity values at gasifier bottom and top	58
Table 2.12.	Archimedes and Reynolds numbers at gasifier bottom and top	59
Table 2.13.	Terminal velocity of the particles at gasifier bottom and top conditions	59
Table 2.14.	Void fraction of the reactor at gasifier bottom and top conditions	59
Table 2.15.	Solid circulation rate of the reactor at gasifier bottom and top conditions	60
Table 3.1.	CFD validation results for 7 different operating conditions	66
Table 3.2.	Thermodynamic Properties through the Axis with 7 Different	74

Flow Rates

Table 3.3.	CFD validation results for 7 different operating conditions (positive pressure)	76
Table 3.4.	Induced air flow rates with various motive air flow rates and back pressures	81
Table 3.5.	Comparison of Maximum Vacuum Pressure & Back Pressure with No Induced Flow	83
Table 3.6.	Comparison of Maximum Positive Pressure & Back Pressure with Reverse Flow (equal to motive gas flowrate)	84
Table 3.7.	Entrainment Ratios for Both Side Open Ejector at Zero Back Pressure Conditions	85
Table 3.8.	CFD results of ejector types for different motive gas flowrates	87
Table 3.9.	Ejector tube length effect on ejector performance	89
Table 3.10.	Motive gas flowrate effect on ejector performance	91
Table 3.11.	Vacuum pressures for different nozzle diameters	92
Table 3.12.	Nozzle inlet pressure change with nozzle diameter	94
Table 3.13.	Vacuum pressures for different ejector tube diameters	95
Table 3.14.	Vacuum pressures for different induced gas pressures	97
Table 3.15.	Vacuum pressure & motive gas momentum relation	101
Table 3.16.	Conditions for the Comparison of Semi-empirical Correlation and CFD Results	104
Table 3.17.	Experimental Parameters without Ejector System	111

Table 3.18.	Experimental Parameters with Ejector System	112
Table 3.19.	Solid Column Formation/ Disappearance Conditions during Cold Experiment	120
Table 3.20.	Main operating conditions of hot experiments	121
Table 3.21.	Gas composition of syngas at gasifier exit	127

1. INTRODUCTION

1.1. Global Energy Profile and Turkey

The energy demand of the world is rapidly increasing with the increase in population and economic development, and the energy sources of fossil fuels such as coal and petroleum are rapidly decreasing. At present situation, fossil fuels are the dominant sources of the global primary energy demand. The world primary energy supply was totally 12150 Mtoe that was consisted of, 32.8% oil, 27.2% coal/peat, 20.9% natural gas, 10.2% biofuels and wastes, 5.8% nuclear, 2.3% hydro power and 0.8% other renewable energy sources [1]. The majority of these primary energy sources are used for, electricity generation, transportation, various industrial applications and residential usage.

Approximately, 31.7% of the world primary energy supply was used for electricity generation [2]. The electricity generation by resources were consist of, 40.6% coal/peat, 21.4% natural gas, 16.2% hydraulic power, 13.4% nuclear, 5.1% oil and 3.3% other renewables. The majority of the electricity was generated with conventional combustion process of solid fuels or gas fuels. This leads to people to improve the conventional process or to investigate new conversion technologies in order to get improved conversion efficiencies.

Turkey's primary energy supply was 106 Mtoe which is the 0.9% of the world primary energy supply and the distribution by resources is, 31.1% coal/lignite, 28.8% oil, 30.9% natural gas, 4.4% biofuels/wastes, 2.9% hydro power and 1.7% other renewable energy sources. Similarly to the average value of the world (31.7%), 35.3% of the primary energy supply of Turkey is used for electricity generation [3].

The electricity generation by resources at Turkey consists of 50.1% natural gas, 37.2% coal/peat, 8.2% hydraulic power, 3.1% oil and 1.4% other renewables. The majority of the electricity is generated with natural gas which the majority portion is imported. Although, coal has the highest portion for the primary energy need, it is the second for the electricity generation which the majority portion is supplied by national resources.

As can be seen that, both for the primary energy need and electricity generation, solid fuels (coal and biomass) have crucial place for both world and Turkey energy demand.

Especially over the past decade, the role of coal as an energy source for the future has gained renewed interest for its proven stability in supply and cost and it is therefore, likely that coal will remain in an important position in the energy supply in the foreseeable future.

At current state, world total recoverable coal reserves are estimated at 948 billion tons which means the reserve to production ratio of 126 years according to world current production rates. The majority of those reserves are mainly consisting of 47% anthracite and bituminous coal with tonnage basis, 30% of sub bituminous coal and 23 % of lignite reserves [4].

There are very limited oil and natural gas reserves at Turkey, but relatively higher reserves of coal. At current state of Turkey, total recoverable coal reserves are estimated at 14.6 billion tones (1.5% of the world coal reserves) of which, 13.3 billion tons of lignite and 1.3 billion tons of hard coal. Total coal production rate was 85.3 million tons of which the majority is lignite (84 million tons) and the reserve to production ratio was 171 years according to coal production rates [5].

Besides the coal reserves as national energy resources for Turkey, biomass has also great potential as a national and renewable energy sources based on forestry and agricultural residues. The annual biomass energy potential of Turkey is estimated as 32 Mtoe. The total economically recoverable biomass energy potential is estimated as 17 Mtoe/year. However, the total biomass consumption in Turkey was 4.8 Mtoe /year. The recoverable biomass energy potential come from agricultural residues, farming wastes, forestry and wood processing residues and municipal wastes. The largest portion of this product is used in rural areas for heating and cooking [6].

As seen from the coal reserves and biomass potential data, solid fuel conversion technologies are getting more important for both world and Turkey. Mainly, the challenge is converting the solid fuels into a desired form (electricity, synthetic fuels, chemicals, heat, etc.), as efficient as possible in a cleaner and economical way. In order to do that, there are many conversion technologies some of whose are mature but still being improved, and new ones about to commercialize.

1.2. Background of Gasification

Gasification is the one of the most promising solid fuel conversion technologies for different purposes. Mainly, gasification is the process of producing combustible gases having usable heating value, from solid fuels. The process is also called "partial oxidation" and the majority of the produced syngas consists of CO, H_2, CH_4, CO_2, N_2 and H_2O gases. Produced syngas from gasification process is generally used for generating power, chemicals, and hydrogen and transportation fuels. World total installed gasification capacity is about 71000 MWth of syngas which is the 0.4 % of world total primary energy supply. There are also some under construction gasifiers which have the total capacity of about 11000 MWth of syngas [7]. The distribution of feedstocks used for producing syngas is, 51 % coal, 25 % petroleum products, 22 % natural gas and 2 % of other feedstock (petcoke, biomass, waste). The products which are converted from syngas are, 45 % chemicals (Ammonia, methanol, oxo alcohols, etc.), 38 % transportation liquid fuels (FT liquids), 11 % power generation (3880 MWe) generally with IGCC applications which is 0.2 % of the world total coal based power plant capacity[8], and 6 % gases fuels (SNG, H_2, etc.) [9].

There are alternative technologies for gasification process determined by mainly fuel properties (fuel type, ash content, fuel size, impurities content, desired syngas properties, etc.) and the syngas production capacity of the gasifier. For main purposes, these technologies can be grouped into three categories; moving bed gasifiers, fluidized bed gasifiers, and entrained flow gasifiers. These three technologies have different strength and weakness with respect to each other. Each of these can be determined as the most convenient technology according to the specifications of the fuel, process conditions and desired syngas properties.

Commercial scale gasification plants which are totally 71000 MWth of syngas are using one of these gasification technologies. The leading technology is entrained flow gasifiers with 65% of total capacity, followed by moving bed gasifiers with 34% and the rest is fluidized bed gasifiers with 1% of total gasification capacity of the world [10].

The main advantages of using entrained flow gasifiers are ability of gasifying all kind of coal (sub-bituminous coals to anthracite) contrary to the moving bed and fluidized bed gasifiers, and produce tar free syngas. It can be preferred especially for hard coals.

However, as it can be used for all type of coal, due to the high reaction temperatures (~1500 °C), entrained flow gasifiers are not attractive for low rank coals (brown coal and lignite) because of high moisture and ash contents [11]. Besides, entrained flow process is preferred for large scale applications and the maximum operating single reactor capacity is 708 MWth of syngas [10].

Moving bed gasifiers can be used for small scale applications (< 1.5 MWth fuel input) especially for biomass gasification [12] and medium scale applications with the maximum operating single gasifier capacity of 176 MWth of syngas, especially for anthracite [10].

Fluidized bed gasifiers are generally preferred for the low rank coals (lignite, peat) and biomass. Because, low rank coals have higher reactivity and relatively lower temperatures of fluidized bed gasifiers are (~ 900 °C) enough for achieving sufficient reaction rates. However, this situation causes the one of the main problems with fluidized bed gasification that is less thermal cracking of tars and increases the tar content of the syngas. In order to minimize the tar content, temperature of the gasifier can be increased but there is also another limitation related with the agglomeration problems. For the sake of maintain stable fluidization, agglomeration of the ash particles should be avoided with providing lower operating temperatures than the softening temperature of the ash particles which is typically in the range of 950 °C – 1100 °C for coal and 800–950 °C for biomass. On the other hand, a fluidized bed reactor can be supposed as a continuously stirred tank reactor because of the high turbulence and mixing conditions of the bed section. It is an advantage with the mass and heat transfer point of view. However, for the steady state operation, ash should be extracted from fluidized bed in which, ash and char particles are highly homogenous distributed over the whole bed (generally %5 char, %95 ash) and for this reason it does not seem possible to extract only ash without unreacted carbon which causes the reduction of carbon conversion level**.**

Furthermore, there are some operational challenges related with fluidized bed gasifiers, especially with circulating fluidized bed gasifiers. Contrary to the bubbling fluidized bed gasifiers which are generally preferred for small scale applications (< 25MWth feed), relatively higher rate of solids must be circulated at circulating fluidized bed

gasifiers. Generally, the circulation loop of a CFB system consists of riser, cyclone separator, downcomer and a solid flow control valve. At commercial scale applications, the most common circulation valve used at CFB reactor is loopseal which is a non-mechanical valve without any moving parts. Basically, it is a bubbling fluidized bed used for providing a pressure barrier in order to prevent gas flow from the riser to the downcomer and also maintaining the stable solid flow from the downcomer to the riser. When the plugging of the loopseal occurred or insufficient backpressure of loopseal regarding with the low solid inventory appears due to the unexpected reasons (pressure fluctuations at riser, formation of small agglomerations, over solid circulation rates, etc.), solid accumulation in the downcomer and the cyclone will stop the all system.

1.3. Circulating Fluidized Bed (CFB) Reactors

One of the most common reactor types for the solid fuel conversion is the circulating fluidized bed (CFB) reactors. In CFB reactors, hot solid particles (mixture of solid fuel and sand/ash) circulate around the reactor. Air or any other agent (steam or oxygen) pass through the reactor and carry the solid particles from bottom of the reactor to the top. In industrial applications, gas superficial velocity inside the reactor is generally in between 4 – 6 m/s which is higher than the terminal velocity of the particles. Generally, mean particle diameter of circulated material is in between 0.05 – 1 mm. In CFB reactors, the solid mixing is very high due to the higher superficial gas velocities and the turbulent regime of gas and solid mixture. Heat transfer coefficient is also very high (100 – 200 $W/m^2.°C$) [13].

The CFB reactors consist of a riser at where the reactions are mainly taking place, a cyclone for the solid separation from the hot gas, a downcomer for the solid flow to the reactor from the cyclone and a non-mechanical solid circulation valve for feedback the solid particles captured by the cyclone to the reactor meanwhile to prevent the reverse gas flow from the reactor to the downcomer. Mainly, loopseal and L valves are used for the circulation of solid material. In industrial scale applications, loop seals are used as non-mechanical valve. Loop seal is mainly consist of a bubbling fluidized bed which is used for generating a pressure barrier between reactor and the downcomer and send back the solid particles to the reactor.

1.4. Solid Circulation Systems at CFB Reactors

L valves: The L-valve consists of L-shaped pipe connecting the downcomer and the reactor at where the solids are transferred (Figure 1.1). The horizontal part of L-valve is connected to the CFB riser and the vertical part is connected to the downcomer.

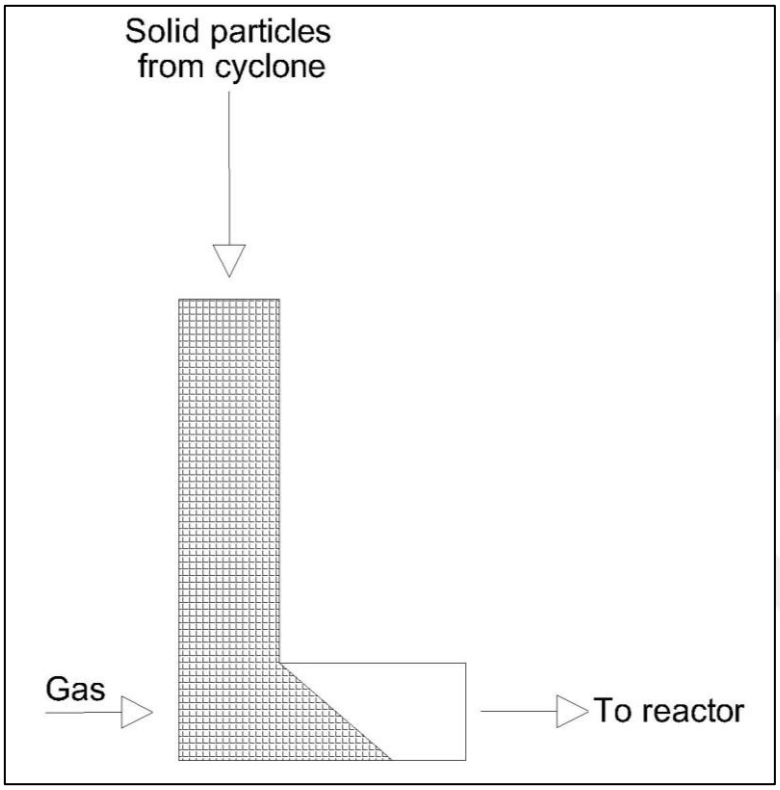

Figure 1.1. L valve

There is moving bed inside the L-valve rather than fluidized bed. Small amount of air is fed into the vertical part of the L-valve in order to facilitate the movement of the solid column. In large scale systems, this air may be fed in multiple points around the L-valve. Unlike loop-seals, L-valves do not work well with Group A and C particles. They work best with Group B particles [13].

Loop Seals: In industrial applications, generally Loop-seals are used in CFB boilers and gasifiers. A loop seal (Figure 1.2) consists of two sections which are supply chamber and recycle chamber. Supply chamber is connected to the downcomer at where the solid material separated by the cyclone, is passing through. Supply chamber supplies solids material to the recycle chamber which transfers the solid materials to the riser. Solid

materials move horizontally from supply chamber to the recycle chamber at where there is a partition wall separating the supply and recycle chambers.

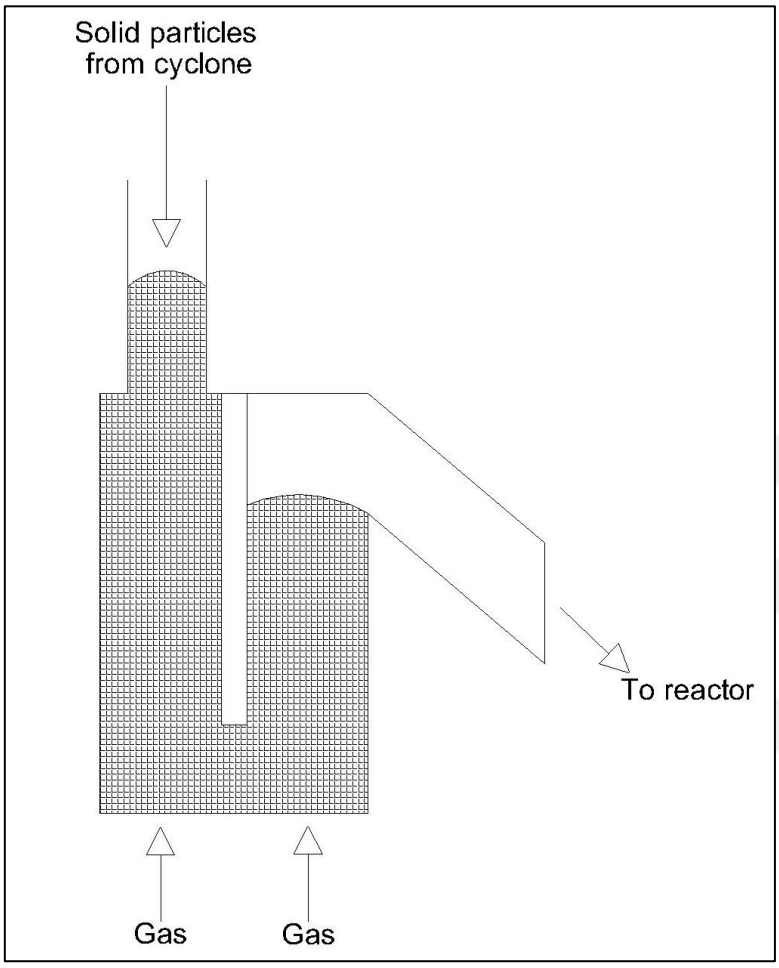

Figure 1.2. Loop seal

Some air is fed to the recycle chamber in order to make it fluidize (bubbling bed) and facilitate to transfer solid material to the reactor. There is one barrier between recycle chamber and the reactor that fluidized solid material overflow this barrier to the reactor through the recycle pipe with the help of gravity. In industrial scale applications, bottom of the supply chamber generally fluidized in order to help move Group B particles. Loop-seals work best with Group A and B particles [13].

1.5. Problem Statement for Solid Circulation at CFB Reactors

Circulating fluidized beds (CFB) are widely used for thermal processes, such as drying, combustion, gasification and mineral processing. Contrary to the bubbling fluidized bed systems, solids must be circulated in circulating fluidized bed systems. Circulation systems are considered as the heart of a CFB system from the viewpoint of its importance and its functions. Poor circulation may result in heat transfer and/or reaction problems along with mechanical problems leading to shut down of the system. It has been reported that the major problem in CFB operation is the interruption of solids circulation through the CFB loop. Therefore, proper operation of solids circulation system is of crucial importance for the stable operation of CFB reactors [13, 14].

Generally, the circulation loop of a CFB system consists of a riser, a cyclone separator, a downcomer and a solid flow control valve. A pressure barrier is necessary to prevent gas flow from the riser to the downcomer so that a stable solid flow is maintained from the downcomer to the riser. At commercial scale applications, the common circulation valve is loop seal which is a non-mechanical valve without any moving parts. If the operations of the loop seal stops, solids accumulate in the downcomer and in the cyclone leading to an interruption in the solid flow from cyclone to the riser. Sometimes the accumulated large amount of solids may suddenly flow into the bed causing massive fluctuations in bed pressure. If the solid inventory in the loop seal is too low to create a pressure barrier a reverse gas flow occurs to the cyclone from the riser through the downcomer and reduces the cyclone efficiency [15]. For both cases, the entire system may have to be stopped to get proper start up conditions.

1.6. Proposed Novel Solid Circulation Method at CFB Reactors

The proposed alternative CFB concept is based on an ejector placed at the downcomer of the CFB system [16]. The pressure difference required for uninterrupted solid circulation can be achieved and/or rebuilt whether there is initial bed material or not and without the need to re-start the entire system. Therefore, the proposed concept is expected to enable continuous high speed gas flow and continuous solids circulation through the ejector forming a pressure barrier enabling increased uninterrupted operation time of the entire system.

Ejector applications first appeared in 1858, based on the invention by Henry Giffard [17] for the purpose of feeding water to the boiler of a steam engine of a locomotive. There are various kinds of ejector applications in the current industry such as, distillation in chemical and petroleum industry, evaporation and drying in food industry, pneumatic conveying or tank drains, vacuum test chambers in aerospace research, refrigeration systems and thermal power plants.

Generally, ejector systems are used for the refrigeration systems and the CFD analyses have been focused on mainly jet ejector system for refrigeration cycle [18 - 35]. The ejector geometry investigated in this study is different from the ejectors used at refrigeration systems. However, the operations are based on the same physics. The main difference between conventional ejectors and the ejector studied in this work is the throat/nozzle area ratios. Generally, the area ratios of throat/motive gas nozzle are in between 6.4 to 10.6 [19]. However, the area ratios studied in this work is in between 25 to 660. The higher area ratios cause lower pressure difference with respect to conventional ejector which is high enough for the operation of the CFB systems. Motive gas nozzle exit velocities/Mach numbers are similar to the conventional ejectors. The CFD analyses of ejector used at refrigeration cycles are mainly supersonic [25, 26, and 27]. There are various studies in published literature related with conventional ejector systems and mainly focus on the effect of nozzle throat to constant section area ratios, converging angle, operating pressure, mixing tube length, motive gas flowrate, throat diameter and working fluids [22, 29, 30, 33, 33, 34]. The main performance parameter for conventional ejectors is entrainment ratio [20, 21]. In this study, validated CFD model was used for investigation of ejector operational and geometric parameters which are outside the experimental range of CFD validation experiments [19, 23]. Due to the symmetric geometry of ejector, 2D axisymmetric space was chosen [24, 31]. The realizable k-ϵ model was chosen as turbulence model in this work [28, 31].

The proposed circulation concept is based on the formation of ejector type pressure barrier. Within this frame, an ejector is placed at the downcomer of the CFB system. An ejector (Figure 1.3.) is a vacuum generating apparatus, generally driven by compressed gas or liquid. Venturi effect is the main principle which the ejector is based on.

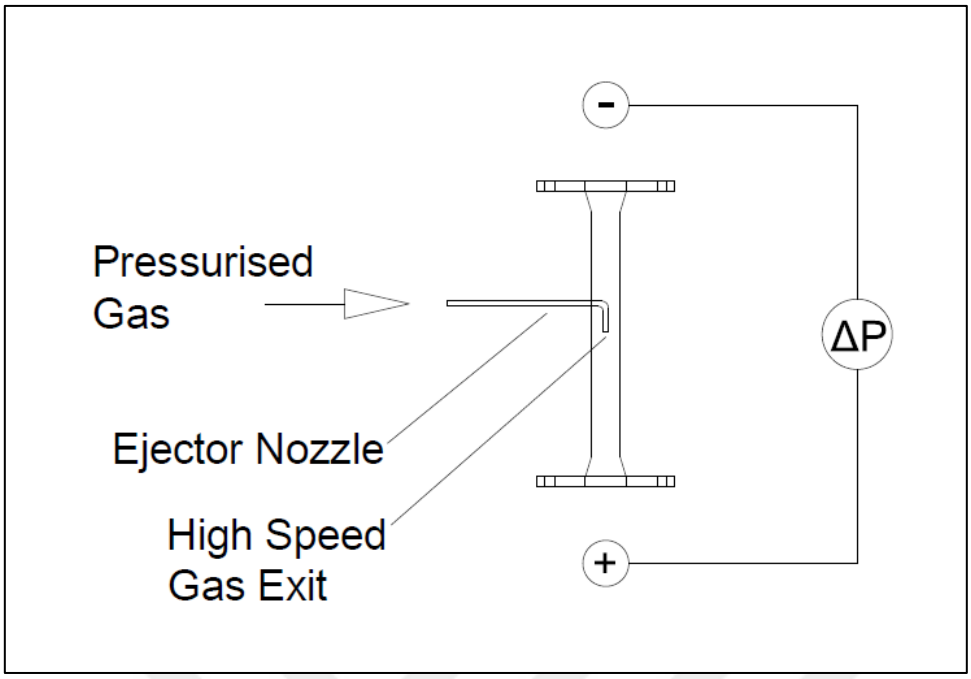

Figure 1.3. General principle of the experimental Venturi ejector

Pressurized gases flow at a high speed through the ejector nozzle exit which is parallel to the downcomer. The pressure of the motive gas is converted to velocity which decreases the pressure level at the high velocity region. The momentum transfer by the high speed gas flow at the ejector nozzle exit to the low speed gas flow at the downcomer causes the pressure difference through the ejector system and builds a pressure barrier.

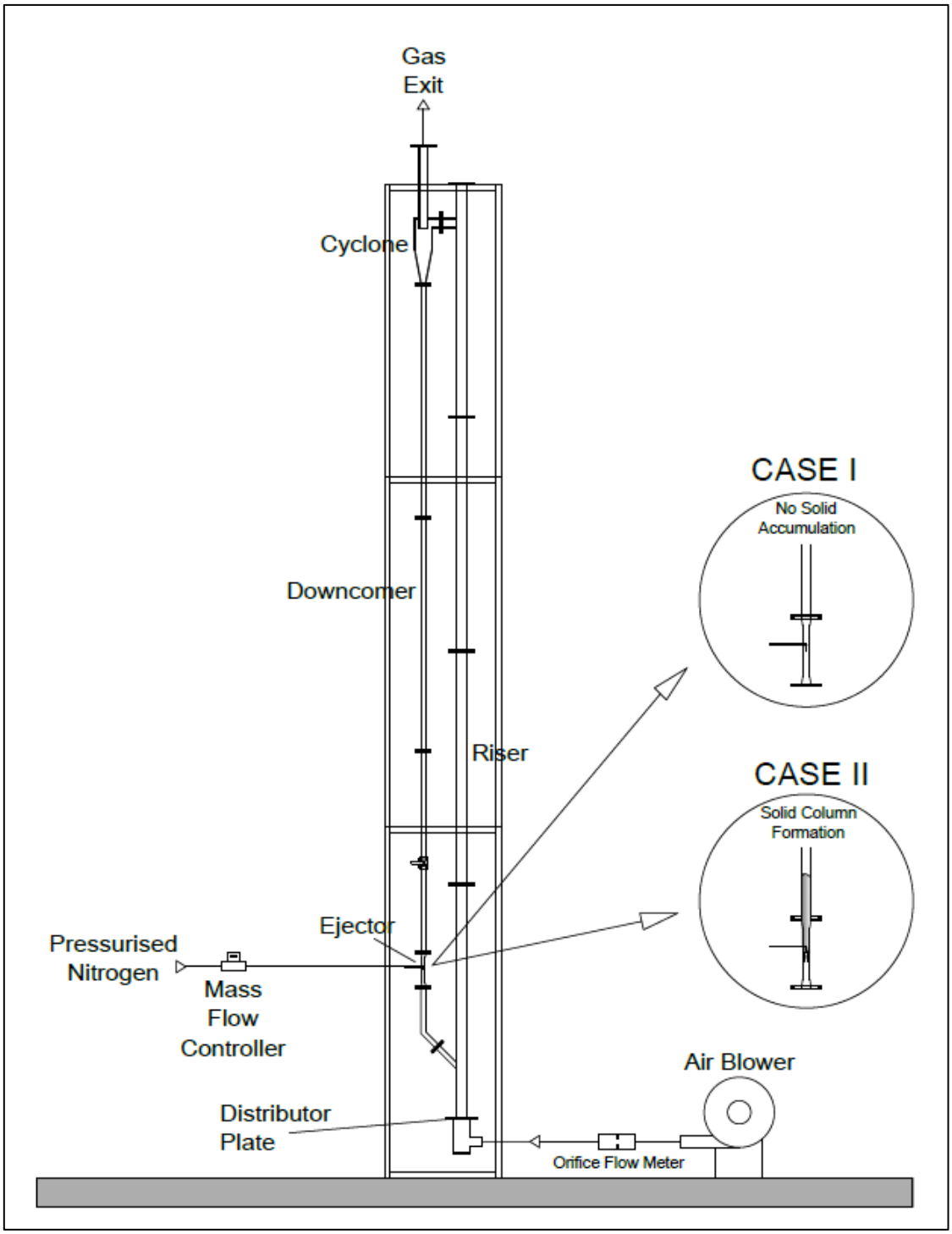

Figure 1.4. Ejector type circulation for 2 different operation modes

There are 2 different operation modes (Figure 1.4.) depending on the operational motive gas velocity and the solid flux through the downcomer. In the first mode, there is no solid accumulation through the downcomer because of the low solid flux. The pressure barrier is obtained by the momentum transfer of high speed gas flow at ejector nozzle

exit to the low speed gas flow at the downcomer. In contrast to the conventional circulation systems, some amount of gas is being recirculated to the reactor due to the pressure difference formed by the ejector. Under these conditions, there is no solid accumulation observed along the downcomer. This circumstance is valid for up to a specific level of solid flux through the downcomer.

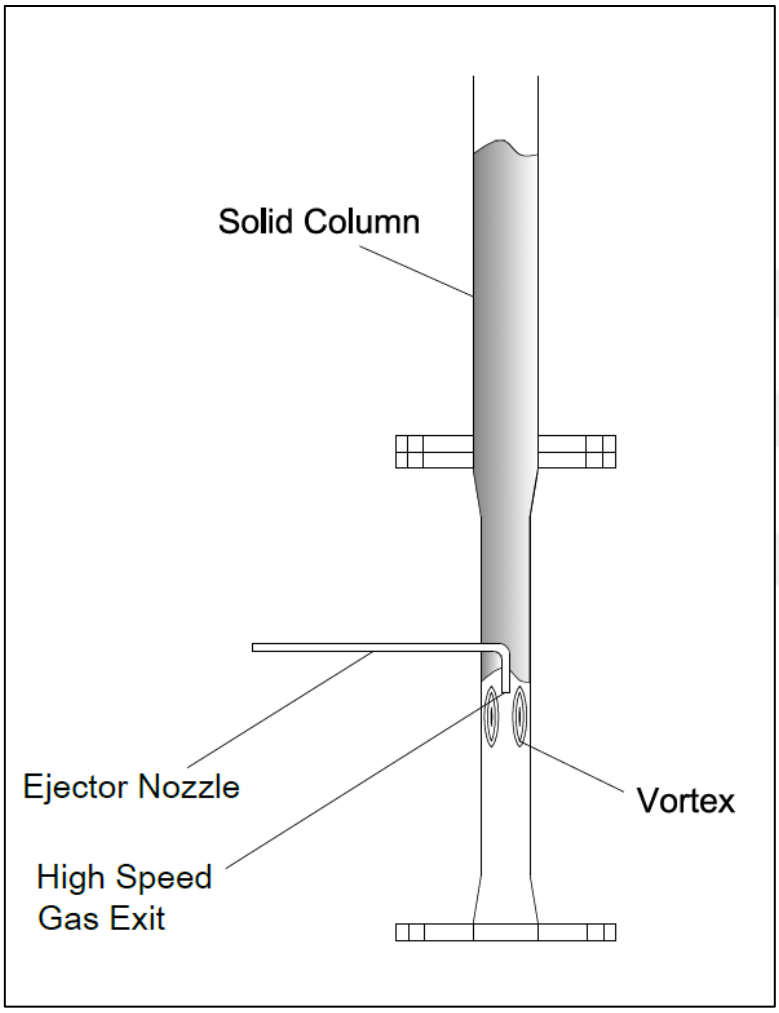

Figure 1.5. Vortices at ejector nozzle exit

In the second mode (Figure 1.5.), solid accumulation is observed just above the ejector system because of relatively higher solid flux through the downcomer. High speed gas flow through the ejector nozzle exit causes severe vortices just below the nozzle exit which is torus in shape. These vortices were realized during the CFD studies which will be mentioned at subsequent sections. These vortices cause resistance to the flow of solid particles. If the solid flux is increased gradually for a specified level of ejector nozzle

exit gas velocity, a solid column is formed just above the ejector at some point of solid flux through the downcomer. This non-fluidized solid column slowly moves to the CFB reactor. Similarly, if the ejector nozzle exit gas velocity is increased gradually to a specified level of solid flux, the severeness of the vortices is increased resulting in increased resistance of the vortices to the solid particle flow. At some point of gas velocity, solid column is formed just above the ejector. As a matter of fact, solid flux through the downcomer and ejector nozzle exit gas velocity has to be sufficient in order to form a solid column. If any of these two parameters is not sufficient, there is no solid column observed. The solid column height is controlled by the nozzle exit gas velocity. The solid column and the ejector both work as a pressure barrier system to the reverse flow of gases from the CFB reactor to the downcomer. Different from the first operation mode without solid column formation, some portion of the required pressure difference is provided by the accumulated solid column in the second mode. Therefore the high pressure motive gas flow rate requirement is considerably lower in the latter case.

In the second mode of operation with constant motive gas and primary air flow rates, the solid column height generally fluctuates at acceptable levels. There may be some disturbances at the CFB reactor which leads to too low or too big solid column heights. The desired solid column height can be automatically re-adjusted with controlling the motive gas flow rate by using solid level switches or transmitters. In this study, solid column height i.e. motive gas flowrate was controlled manually.

1.7. Literature Survey for Novel Solid Circulation Method

As we aware, there is no published literature about ejector type circulation for circulating fluidized beds except 9 related patents which are described below. These are various types of ejector applications to the various types of processes. However, they are not proposed as an alternative method for solid circulation for circulating fluidized bed systems. Additionally, there is no solid column formation (2nd case of this study) and its control at those studies.

At 1st related patent (Figure 1.6.) which has the title of "Particulate solid fuel combustion systems, (1972)", pulverulent fuel is burned in a fluidized bed (1), fly ash and gases are fed to a cyclone (8) mounted in the top of the chamber and unburned particles are returned to the fluidized bed through a pipe by an ejector (12). The ejector

prevents blockage of the pipe due to excess pressure above the fluidized bed. The cyclone may be mounted outside the fluidized bed reactor [36].

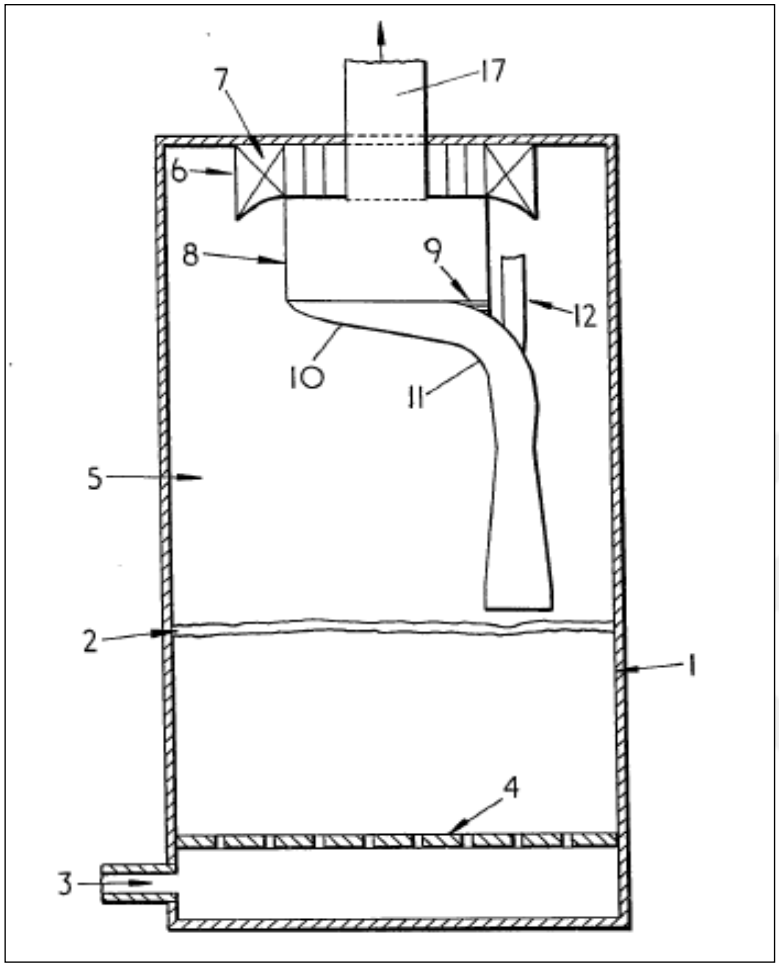

Figure 1.6. Combustion system according to invention [36]

As seen from this patent, the application is bubbling fluidized bed combustion system and ejector is used for feedback the flyash only. Besides, the other difference between new concepts is the geometry and the position of the ejector with respect to reactor.

At 2nd related patent (Figure 1.7.) which has the title of "Two stage gasification of coal, (1975)", entrained bed gasification system is used in which, oxygen and superheated steam is used for gasification process. Unburned char and syngas go through the cyclone (44) for separation of the syngas and char. Then, separated char is fed to the storage tank (60) where char is fluidized with steam. At the bottom of the char storage stank, there is an ejector system(70) which is used for feeding back the fluidized

unburned char bed to the reactor with using superheated steam as motive gas of ejector [37].

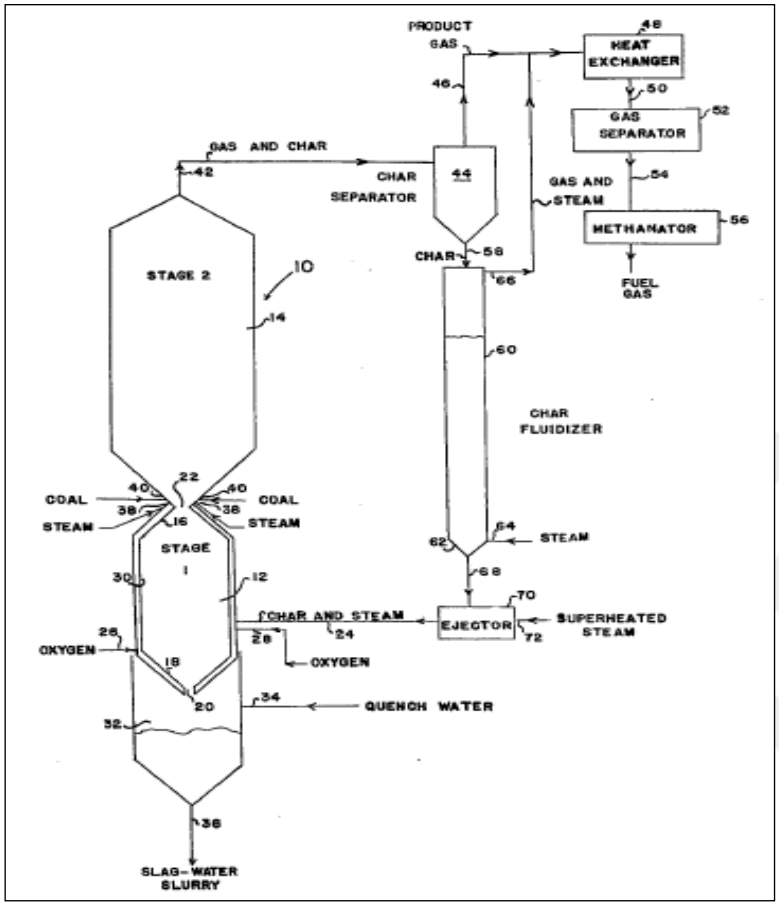

Figure 1.7. Gasification system according to invention [37]

As seen from this patent, the application is entrained bed gasification system and ejector is used for feedback the unburned char only instead of heavy recirculated bed material as in the CFB systems. Besides, the other difference is the fluidized char bed just before the ejector which is also forming a pressure barrier for preventing the gas flow through the return leg.

At 3rd related patent (Figure 1.8.) which has the title of "Fluidized bed combustion device having secondary combustion chamber, (1987)", the purpose is to recirculate the fine particles which are captured by the dust collector. Produced combustion gas is raised with fuel particle through a primary combustion chamber(3) up to the chamber ceiling(3a), and is sucked by means of an injected secondary air flow and lowered down to a position of a secondary combustion chamber floor surface(4b). After fine particles

are lowered down, they change the direction and are discharged from combustion gas exhaust port(6). The fine particles are collected by a cyclone (10), sucked by means of an ejector (11), and returned to a secondary air feed port (5). Since only the fine particles are circulated, wear of a furnace wall can be reduced [38].

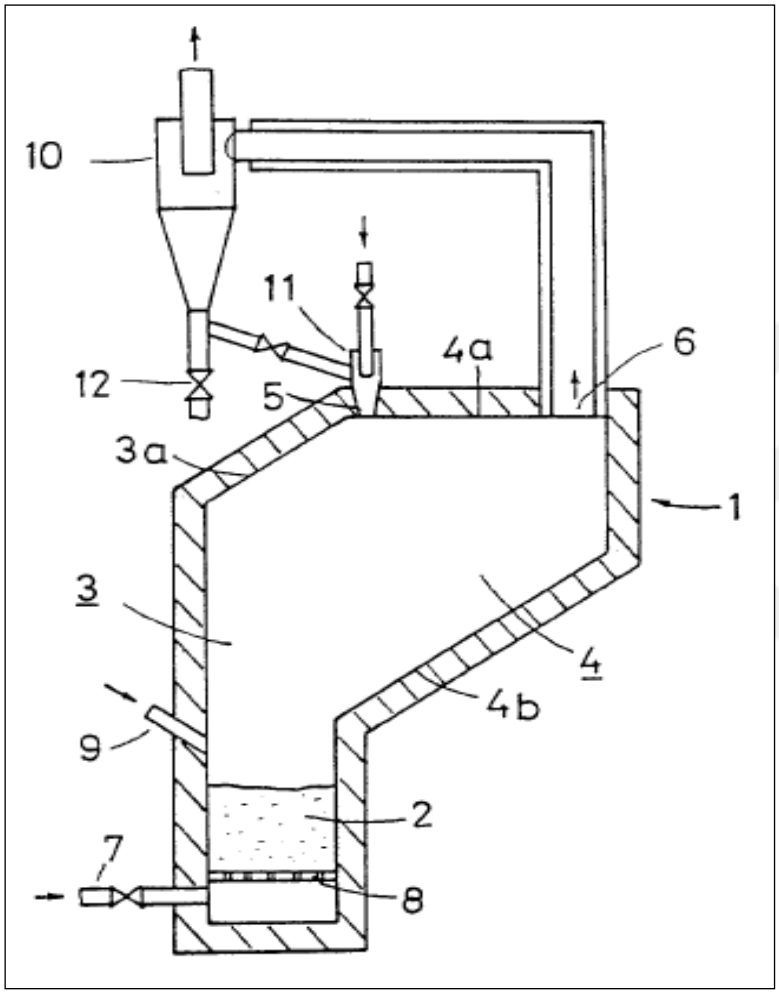

Figure 1.8. New type of fluidized bed combustion device according to invention [38]

As seen from this patent, the application is bubbling fluidized bed combustion system and ejector is used for feedback the fine particles only, instead circulating heavy particle load.

At 4th related patent (Figure 1.9.) which has the title of "Power plant with centrifugal separators for returning material from combustion gases to a fluidized bed, (1988)", the system consists of fluidized bed combustor (14) enclosed within a vessel (11) is used. A gas outlet from the bed vessel is formed as a centrifugal separator (20) intended to

primarily separate coarse material containing unburnt fuel leaving the bed together with the combustion gases. Separator extends into the bed vessel and separated material is returned to the bed (14) through a return conduit (34), which is located close to the bed vessel wall. This conduit opens into the bed vessel, near the bottom (12). For the return of solid material, an ejector (35) is used to overcome the pressure difference existing between the separator and the orifice of the conveying conduit. The propellant gas consists of combustion air. If the pressure difference between generated by the ejector is insufficient to obtain the necessary driving power, a compressor may be used to increase the pressure of the propellant gas [39].

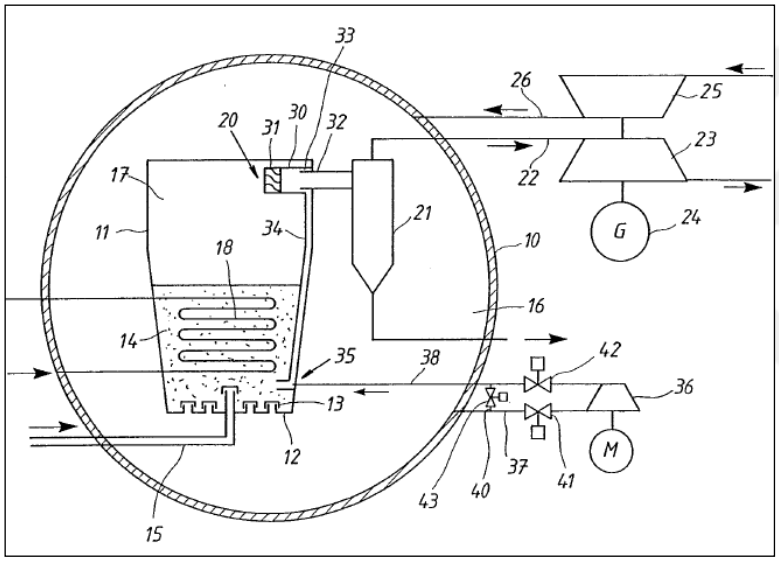

Figure 1.9. New type of power plant according to invention [39]

As seen from this patent, the application is pressurized bubbling fluidized bed combustion system and ejector is used for feedback the fine particles only instead circulating heavy particle load.

At 5th related patent (Figure 1.10.) which has the title of "Process for gas phase polymerization of olefins in a fluidized bed reactor, (1989)", the system consists of gas phase polymerization of olefins using a highly active catalyst in a fluidized bed reactor(1), a reactor body(2) partially occupied by the fluidized bed and a disengagement chamber(3). The gas mixture withdrawn from the disengagement chamber is fed to a dust separator (6) to separate the fine particles entrained by the gas. The particles are withdrawn from the dust separator by an ejector (8) which mixes the

particles and feedback the fine particles to the reactor with a carrier gas. The carrier gas and particles are recycled to the reactor where they are introduced into the reactor body through an opening in the side wall at a position above the fluidized bed, but below the disengagement chamber [40].

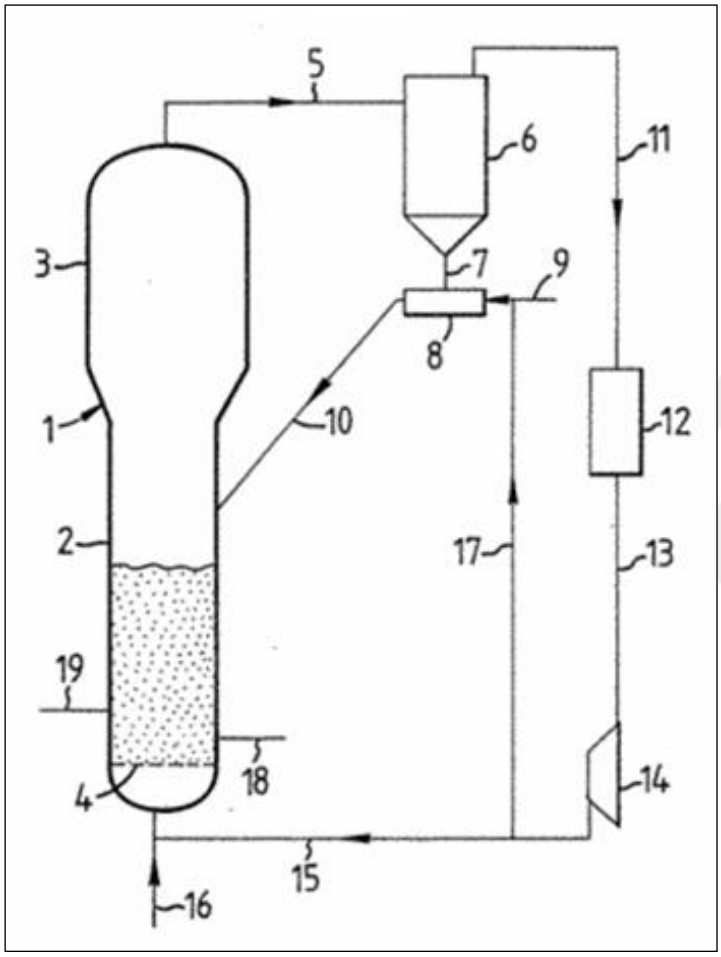

Figure 1.10. Polymerization device according to invention [40]

As seen from this patent, the application is polymerization of olefins in a bubbling fluidized bed system and ejector is used for feedback the fine particles only instead circulating heavy particle load.

At 6th related patent (Figure 1.11.) which has the title of "Circulating fluidized bed dryer apparatus, (1998)", the purpose is to provide a circulating fluidized bed type drying apparatus which differs from a conventional apparatus using a rotary valve. For that reason, an ejector feeder which, supplied with compressed gas and sucks the

powder out of hopper and returns them together with the compressed gas to the inside of the drying apparatus body through the pipe [41].

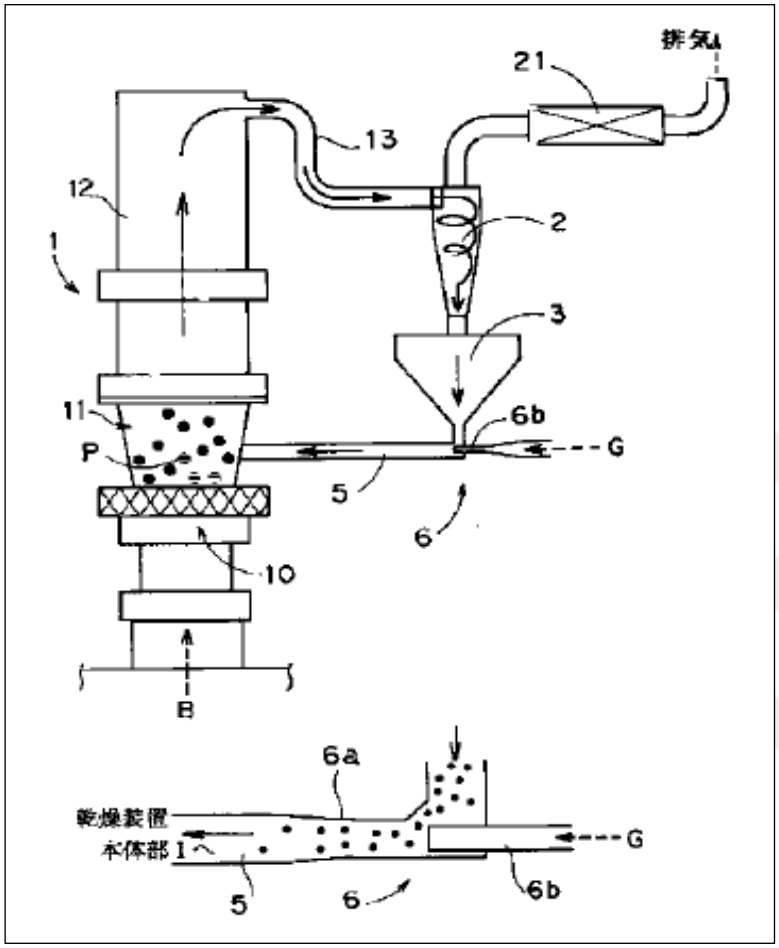

Figure 1.11. New type drying apparatus with ejector according to the invention [41]

As seen from this patent, the application is drying process in a circulating fluidized bed system and ejector is used for feedback the recirculated particles. Besides, the other differences between new concepts are the geometry and the position of the ejector with respect to reactor and using recycled solid storage tank (3) just before the ejector system.

At 7th related patent (Figure 1.12.) which has the title of "Fine solids recycle in a circulating fluidized bed, (2001)", a CFB reactor unit is provided having enhanced circulation of the finest particles. The improved circulation is achieved by recycling gas having entrained fine particles from a solids collection hopper connected to the solids separator back into the reactor. A system of conduits connects the upper portion of the

solids collection hopper with the reactor. The system permits recycling of the finest particles that would otherwise be carried over with the gas flow exiting the separator [42].

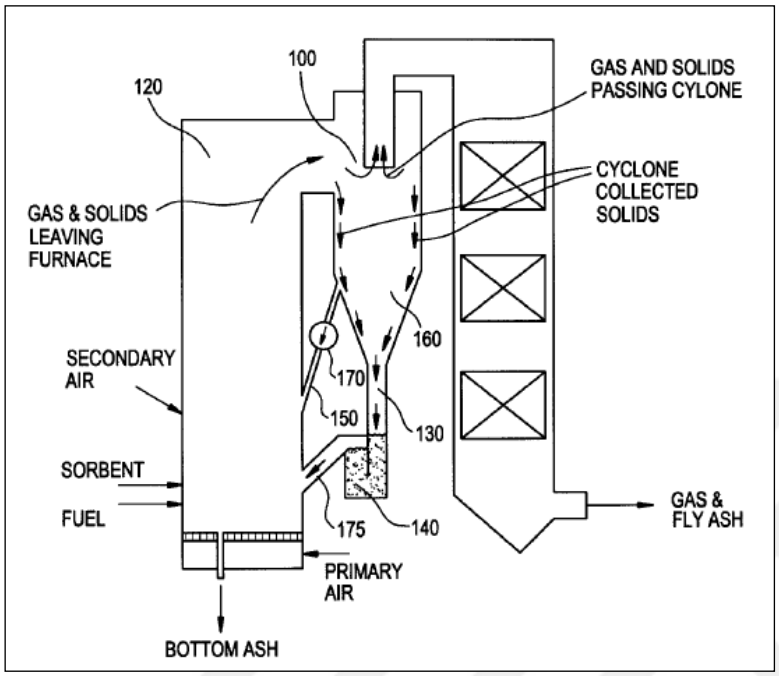

Figure 1.12. Circulating fluidized bed system according to the invention [42]

As seen from this patent, the application is a circulating fluidized bed system and ejector is used for feedback the recirculated fine particles only.

At 8th related patent (Figure 1.13.) which has the title of "Device for processing particles, (2003)", the purpose is to efficiently separate and collects particles of a powder and granular material from a gas to efficiently return the particles to a particle processing zone. A particle collecting for separating and collecting particles in the gas discharged after the particle processing zone has been formed and an ejector (31) for sucking and returning the particles to the particle processing zone are provided [43].

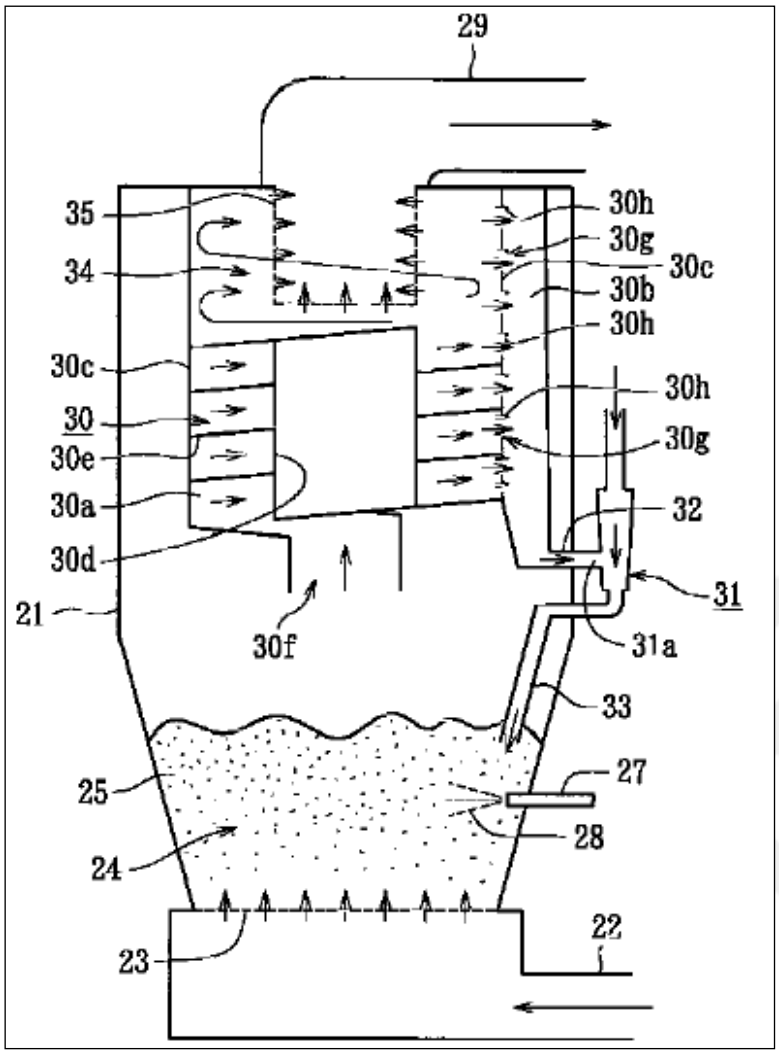

Figure 1.13. New type of particle processing system according to invention [43]

As seen from this patent, the application is a bubbling fluidized bed system and ejector is used for feedback the recirculated fine particles only.

At 9th related patent (Figure 1.14.) which has the title of "Process and apparatus for olefin polymerization in a fluidized bed reactor, (2010)", the purpose is to provide a process for olefin polymerization in a fluidized bed reactor which differs from a conventional process using a horizontal fines ejector, in order to reduce fouling and reactor downtime. A vertically oriented fines ejector is used to convey the fine polymer particles back to the fluidized bed reactor [44].

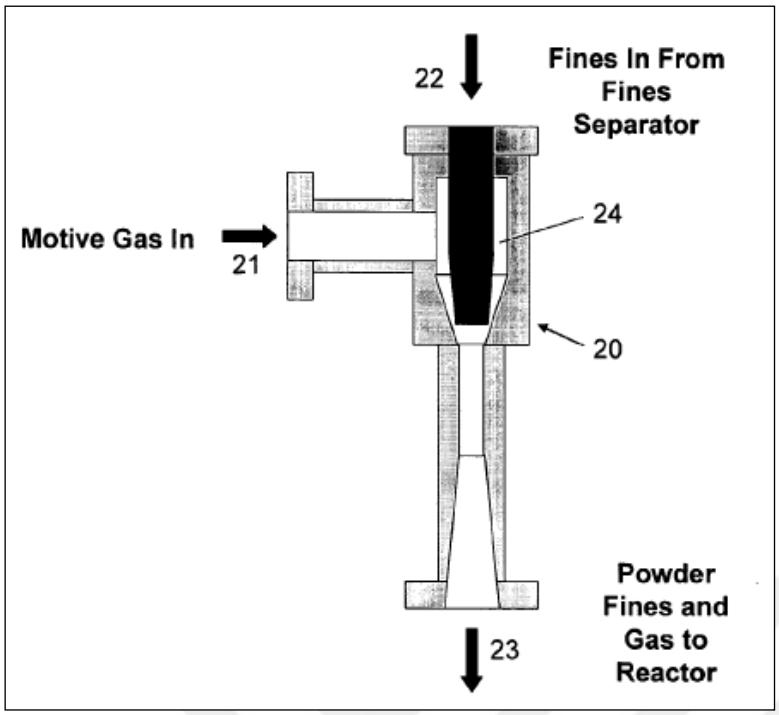

Figure 1.14. Vertically oriented fines ejector according to the invention [44]

As seen from this patent, the application is a process and apparatus for olefin polymerization in a fluidized bed reactor and ejector is used for feedback the recirculated fine particles only.

1.8. Aim of the Study

The aim of this thesis study is to investigate the proposed new solid circulation method for CFB reactor. The concept is new and there is no industrial application of ejector type solid circulation for CFB system. Thus, a good understanding of the performance of the ejector type circulation system for CFBs is essential for a preliminary evaluation of the ejector type circulation systems. The present work attempted to develop a first level understanding of the proper design and operational conditions of an ejector type CFB system, by using computational fluid dynamic (CFD) model, experimental CFB cold system and gasifier system.

At CFD studies, CFD model was built for the gas only homogeneous case by using CFD simulation software tool FLUENT. A reference ejector system has been built to validate the CFD results. Performance analyses of ejector system depending on the basic geometric and operational parameters (ejector tube length and diameter, nozzle

diameter, motive gas flowrate and motive gas temperature) were investigated with CFD model. Furthermore a novel semi-empirical method was proposed as a tool for predicting the ejector performance comparable with CFD results.

At cold model experimental studies, ejector type solid circulation was investigated in an experimental CFB setup. The solid flux at the downcomer and the motive gas flowrate of the ejector were investigated under different cold flow conditions. Pressure profile of CFB loop was also investigated in order to analyze the effect of ejector system on CFB pressure balance.

Finally, ejector system was tested with hot gasifier system which has same dimensions with the cold CFB test facility. Pressure profile of hot system and gas composition of syngas was investigated.

2. MATERIAL and METHOD

In this section, materials and methods of this study are explained in detail. The base procedure for this study is shown in Fig.2.1. Cold circulating fluidized bed system was designed and constructed in order to validate the new concept of circulation with cold model experiments.

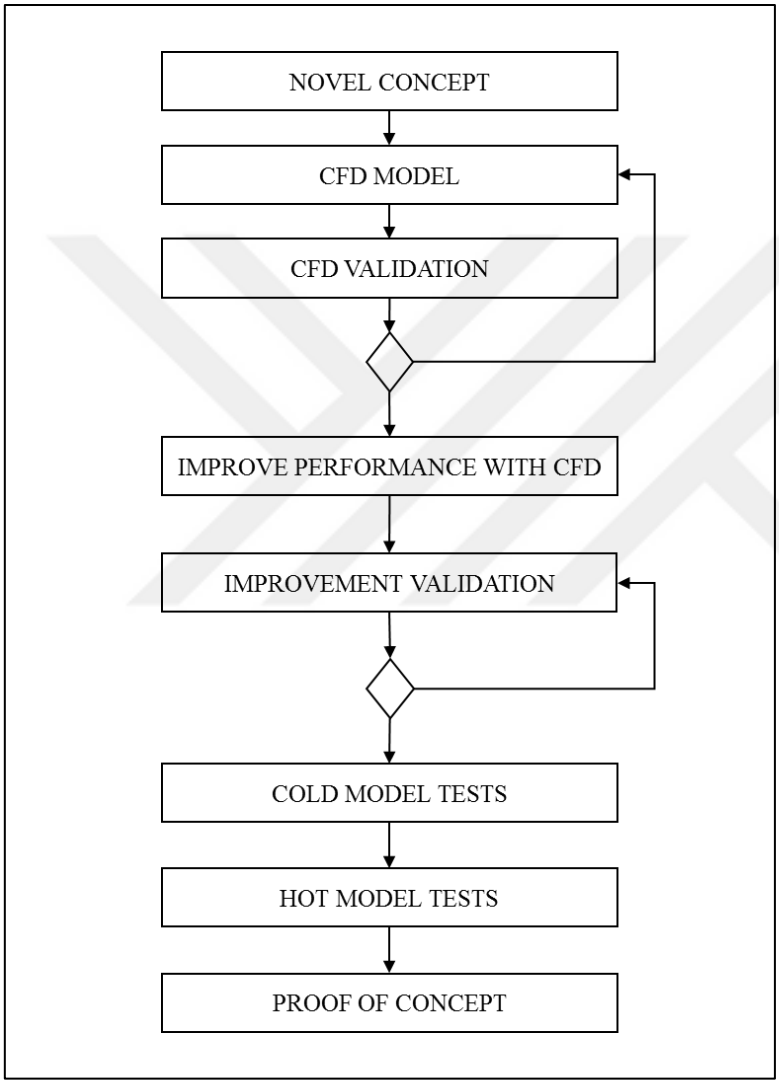

Figure 2.1. Base procedure for the experimental and computational study

After the validation of the new circulation concept, CFD model was developed which was validated with the experimental data in order to make parametric analysis for improving the ejector performance. Critical parameters were analyzed which the performance of the ejector system depends on. With CFD study, design improvements

were done for increasing the ejector performance. Improvements done with CFD model were validated with experimental data. New ejector system was designed and manufactured and tested with cold model. Finally new concept of circulation was tested with hot gasification experiment.

2.1. Computational Fluid Dynamics (CFD) Model and Validation

In order to make some improvements and determine some critical points for the ejector design and operational conditions, Fluent Software was used as the computational fluid dynamics (CFD) tool. Fluent Software is the most common CFD program used for flow and thermal based physical simulation. The main solution procedure of CFD software can be summarized as in two steps. Discretization of the physical model into finite volumes (elements) for making possible to apply partial differential equations as finite volume approach and producing the system of algebraic equations is the first step of the process. Solving the system of algebraic equations in order to obtain approximate solution is the second step of the CFD technique.

Gambit program was used for specifying the geometry (drawing) and discretization of the geometry into finite elements (meshing). It is possible to create 3 dimensional models (drawing and meshing) or 2 dimensional model for specific conditions. In the case of 3 dimensional analyses, it requires more time to solve due to the increase of number of elements. It is easier to solve with 2 dimensional analyses if 3 dimensional real models can be represented with 2 dimensional drawing which is valid for the model which is axisymmetric. As shown in Fig.2.2, reference ejector model is axisymmetric and can be represented with 2 dimensional drawing and meshing as shown in Fig.2.3. Due to the simplicity of this approach and making possible to analyze with much smaller mesh size (discrete element size) in the same solution time, axisymmetric centerline was used for simulating the original 3 dimensional shape with 2 dimensional drawing.

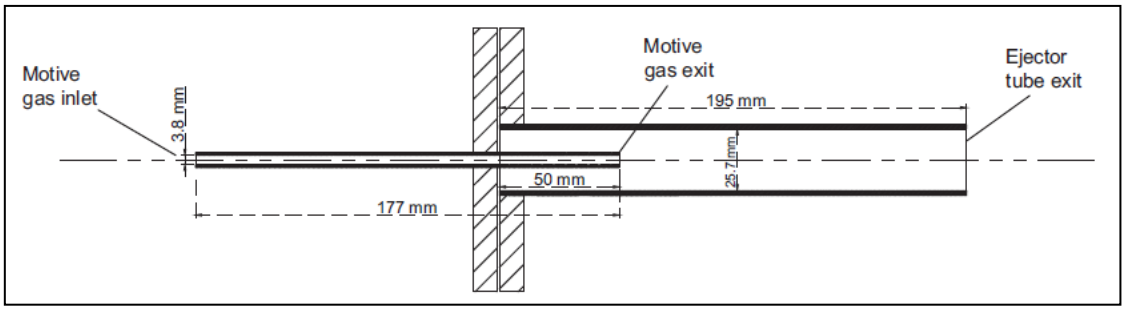

Figure 2.2. Reference Ejector System

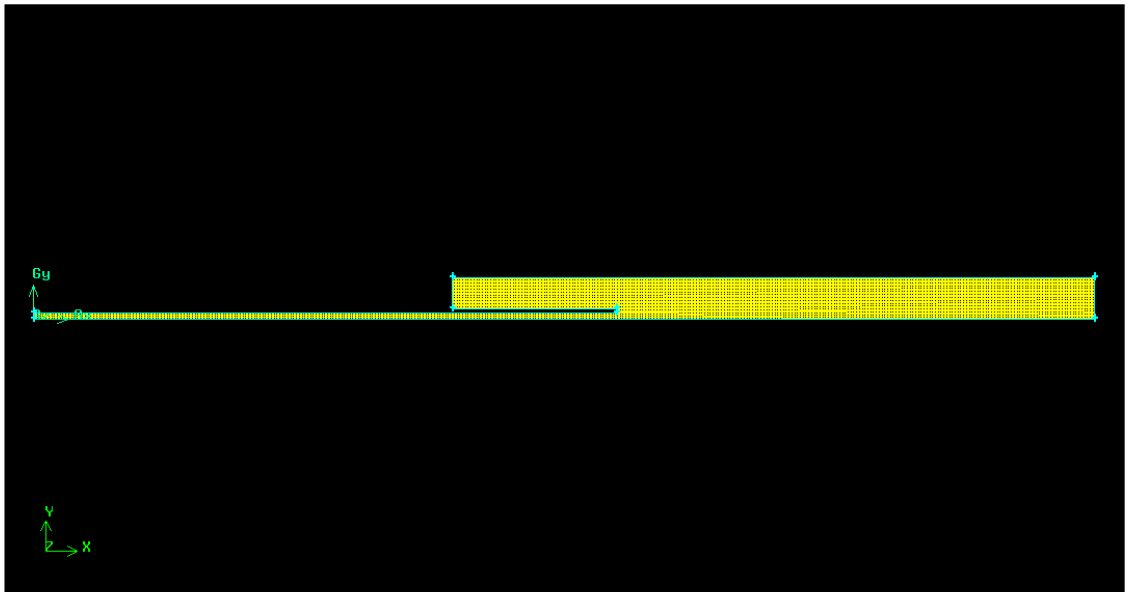

Figure 2.3. Axisymmetric Plane of Ejector (0.5 mm mesh size)

2.1.1. CFD model structure

2.1.1.1. Mesh type

Quadrilateral mesh type was used as shown in Fig.2.4. For the case of 0.5 mm mesh size, there were 10602 elements placed at 2 dimensional axisymmetric plane of the model and if 3 dimensional model was used for analyzing, there should be 522517 elements and it would requires much more time to get convergence conditions.

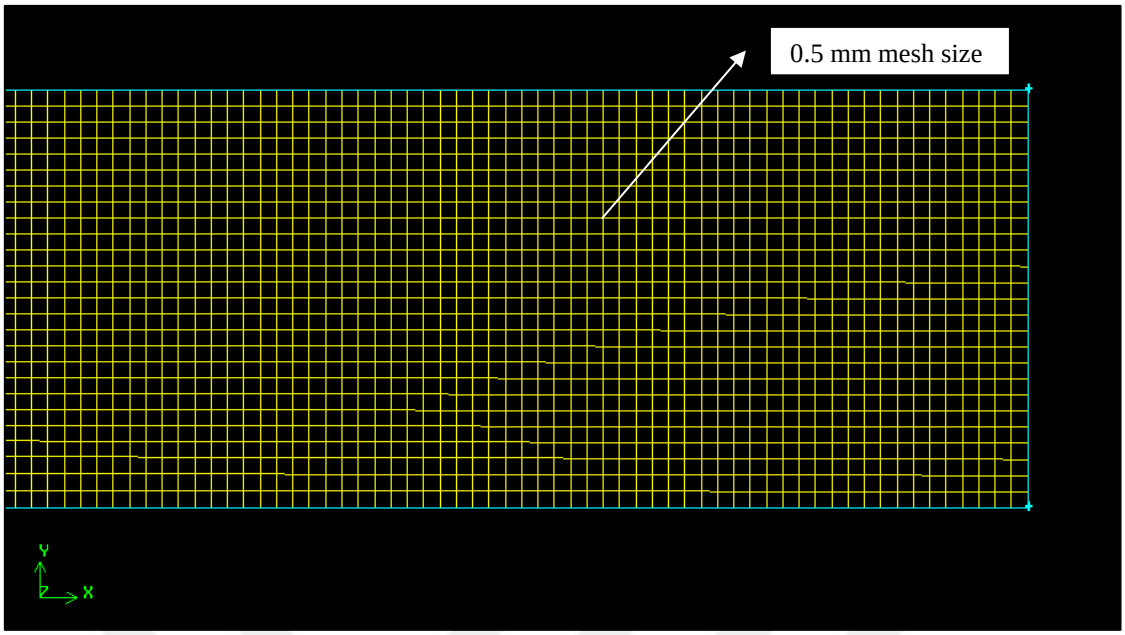

Figure 2.4. Gambit axisymmetric plane drawing and mesh of the ejector exit

The smallest dimension of the reference ejector model was 3.8 mm which is the nozzle diameter. The mesh size should be less than that size and also small enough to get approximate solution. It is also important that too small mesh size cause other problems like round off errors and requires much more time to reach convergence. In order to choose appropriate mesh size, mesh independency test has to be done. With the aim of determining mesh independency, 4 different mesh sizes were chosen as, 0.25 mm, 0.5 mm, 1 mm and 2 mm. CFD results for the 4 Nm^3/h nozzle inlet mass flow rate conditions related with the 4 different mesh sizes are shown in Table 2.1.

Table 2.1. Mesh independency test results for 4 different mesh sizes

Mesh Size	Number of Cells	Iteration	Solution Time	Residuals	CFD Results (Vacuum Pressure)
2 mm	725	131	10 s	$< 10^{-5}$	266 Pa
1 mm	2739	258	24 s	$< 10^{-5}$	266 Pa
0.5 mm	10602	912	2 m, 57 s	$< 10^{-5}$	267 Pa
0.25 mm	43624	3248	24 m, 36 s	$< 3x10^{-4}$	270 Pa

As shown in Table 2.1., 4 different mesh sizes which are considerable different in size from each other, giving quite similar results (vacuum pressure), which means mesh independency has been satisfied for a specified condition between 0.25 mm and the 2 mm mesh sizes.

It was also realized that, finer mesh sizes cause more iterations and more time to reach solution. For the mesh size of 2 mm, 131 iteration and 10 seconds were enough for reaching approximate solution with the residual magnitude of 10^{-5}. On the other hand, 3248 iterations and approximately 25 minutes with the residuals of less than $3x10^{-4}$ (no more improvement of residuals) were required for the solution of 0.25 mm mesh size model.

According to the mesh independency test results, it is logical to select minimum mesh size without any convergence problem and with acceptable time requirement for reaching the approximate solution. Because of that, 0.5 mm mesh size was selected for the improvement studies of ejector model with CFD model.

2.1.1.2. Boundary conditions

After the discretization of the model into appropriate finite elements, boundary types have to be assigned to inlet and outlets of the system. As shown in real model drawing (Figure 2.2.), there are four type of boundaries which are, motive gas inlet, exit of the ejector, wall of the nozzle and ejector and centerline of the ejector (for axisymmetric solution). Due to the ejector nozzle exit velocity (Mach number is bigger than 0.3), motive gas inlet was defined according to Fluent language as “mass flow inlet” which is appropriate for high speed compressible flows. Since the real model is operated for steady state conditions, any constant mass flow rate was assigned for the mass flow inlet boundary type which is the same for any other boundaries. Second boundary type is the exit of the ejector which was defined as the “pressure outlet” of the ejector. This boundary type can be used for both compressible and incompressible flows. The walls of the nozzle and ejector were defined as “wall” which determines the border of the analyzing surface. The last boundary type selected for the ejector model is the “axis” which represents the centerline of the ejector and nozzle in order to get solution in axisymmetric space. The pre-processing settings are summarized in Table 2.2.

Table 2.2. Pre-processing settings for ejector model

Model	Settings
Space	2D - Axisymmetric
Grid type	Quadrilateral
Mesh size	0.25mm, 0.5mm, 1mm, 2mm
Number of elements (respectively)	43624, 10602, 2739, 725
Boundary type – Motive gas inlet	Mass flow inlet
Boundary type – Ejector exit	Pressure outlet
Boundary type – Centerline of the ejector	Axis

After the discretization of the model with Gambit Software, Fluent Software was used for creating the system of algebraic equations with applying the governing differential equations to the finite elements and solving this equation set in order to get approximate solutions.

2.1.1.3. Solver

There are various options for obtaining CFD solutions which have to be selected according to the flow type (incompressible, compressible, turbulent, laminar, etc.). First of all, Fluent provides two different equation solvers, which are pressure based and density based equation solvers. Due to the better convergence performance with negligible accuracy loss, pressure based solver was selected as equation solver for CFD analysis.

Since the real model is axisymmetric, axisymmetric space was used in order to get solution with two dimensional model which has the advantages of less time consumption during solution and thus smaller mesh size can be used.

Due to the constant mass flow rate of inlet and outlet of the model, steady state solution was carried out which means solution was time independent.

2.1.1.4. Energy

Normally in incompressible inviscid adiabatic flow, there is no change in temperature of the fluid according to the Bernoulli equation. However, at high speed flows (Ma > 0.3), compressible effects dominate the flow behaviors. Beside, temperature of the fluid is also affected with that compressibility effect. Because of that, energy equations (means internal energy of the fluid which is not necessary for incompressible flow) are involved in the solution.

2.1.1.5. Viscous model

Due to the flow type of ejector nozzle which is high speed secondary round jet internal flow, RNG k-ϵ and Realizable k-ϵ viscous models can be selected. While these two models are similar in applications, Realizable k-ϵ model is better at convergence performance than RNG model which is the reason of the selection of Realizable k-ϵ viscous model. This model specifies the flow of internal flow which is not good at near wall flow (boundary layer), thus, standard wall function was selected for near wall treatment.

2.1.1.6. Material

Air is selected as working fluid for preliminary analysis. Since the flow is compressible, density of the fluid is not constant and determined with ideal gas relations.

2.1.1.7. Turbulence model

Turbulent intensity and hydraulic diameter has been used for the specification of the turbulence model and taken as 5% and inlet or outlet diameter of nozzle/ejector, respectively.

2.1.1.8. Pressure-velocity coupling

Due to the steady state turbulent flow behavior of the ejector flow, SIMPLE (Semi Implicit Method for Pressure Linked Equations) algorithm was selected for the pressure-velocity coupling relations.

2.1.1.9. Discretization

Discretization is generating a set of algebraic equations with governing partial differential equations. First order upwind method was selected where face value of the control volume is calculated from the center of the control volume (upwind) and is equal to the control volume center value (First order). Due to the satisfactory match of the preliminary CFD results with experimental results and better convergence behavior of first order solutions, second order upwind method was not needed for this study which is even supposed to be more accurate.

2.1.1.10. Convergence criteria

During the CFD analysis, numerical method has to be used in order to solve the system of algebraic equations. Estimated initial values are used (usually boundary values) for starting the iterative solution. For starting the second iteration, results from the first iteration have been used and the process is continuo with using previous results for the next iteration starting values up to the reaching negligible differences (residual) which is the point of approximate solution. It has to be realized that the appropriate convergence criterion is selected for residuals. If the residuals are not negligible enough, the results are not accurate enough. On the other hand, if the residuals are selected as excessively small, it takes more time to get solution without any considerable accuracy gain.

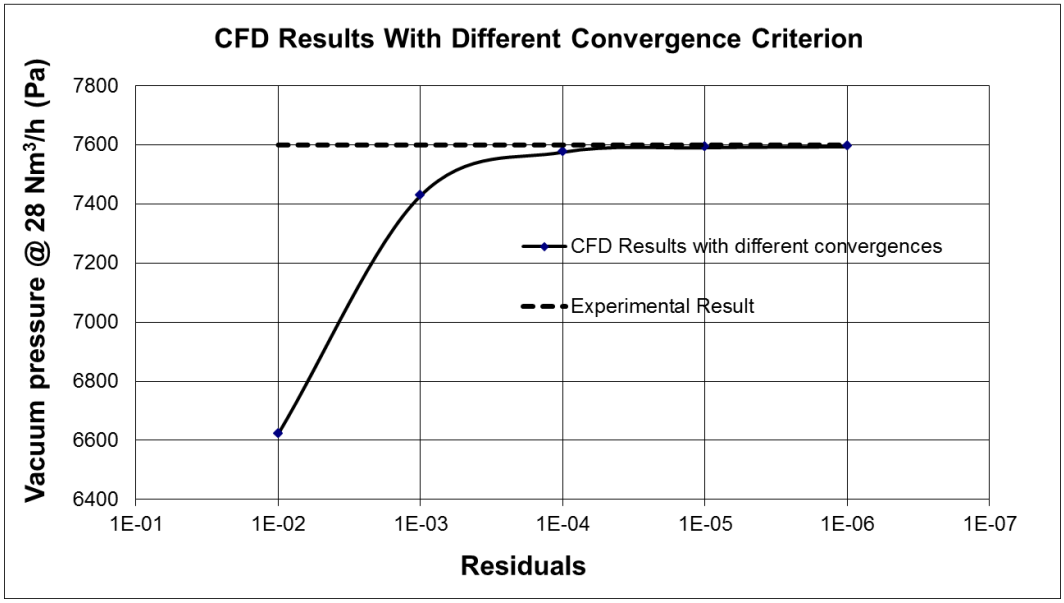

Figure 2.5. CFD results with different convergence criterions

As shown in Fig.2.5 obtained for the ejector analysis, as decreasing the magnitude of the residuals from 10^{-2} to 10^{-6}, CFD results are reaching to experimental value gradually. It was realized that for the residual magnitudes of 10^{-5} and 10^{-6}, the results were almost same and for the sake of less solution time for convergence, 10^{-5} was selected as the convergence criterion.

Table 2.3. Equation solver settings for ejector model

Model	**Settings**
Equation solver	Pressure based
Space	Axisymmetric
Time	Steady
Energy	Energy equations involved
Viscous	Realizable k-epsilon
Near wall treatment	Standard wall functions
Material	Ideal gas – air
Turbulence specification method	Intensity and hydraulic diameter
Turbulent intensity	5%
Hydraulic diameter	Nozzle or ejector diameter
Pressure – Velocity coupling	Simple (semi implicit method)
Discretization	First order upwind
Convergence criterion	10^{-5}

Equation solver settings of CFD model for ejector system is summarized in Table 2.3. After setting up the CFD model of any physical model, it has to be verified with the experimental data in order to be sure of accuracy level. Because, the main goal of using CFD model is making improvements with respect to reference physical model and these improvements has to be done with validated CFD model of reference physical model.

2.1.2. Experimental system for CFD model validation

Before the improvement studies of ejector design with CFD model, reference CFD model has to be verified with the experimental data in order to be sure if the accuracy level of the model is acceptable or not. Because, the main goal of using CFD model is making improvements with respect to reference ejector design and these improvements has to be done with validated model. For the verification of CFD model, reference ejector system was used as shown in Fig.2.6 and Fig.2.7. Reference ejector model is made up of transparent plexiglass material. Compressed air flow rate was measured with mass flow controller (mfc) then supplied to ejector nozzle. Ambient temperature level was measured with thermocouple and assumed as the feeding air temperature.

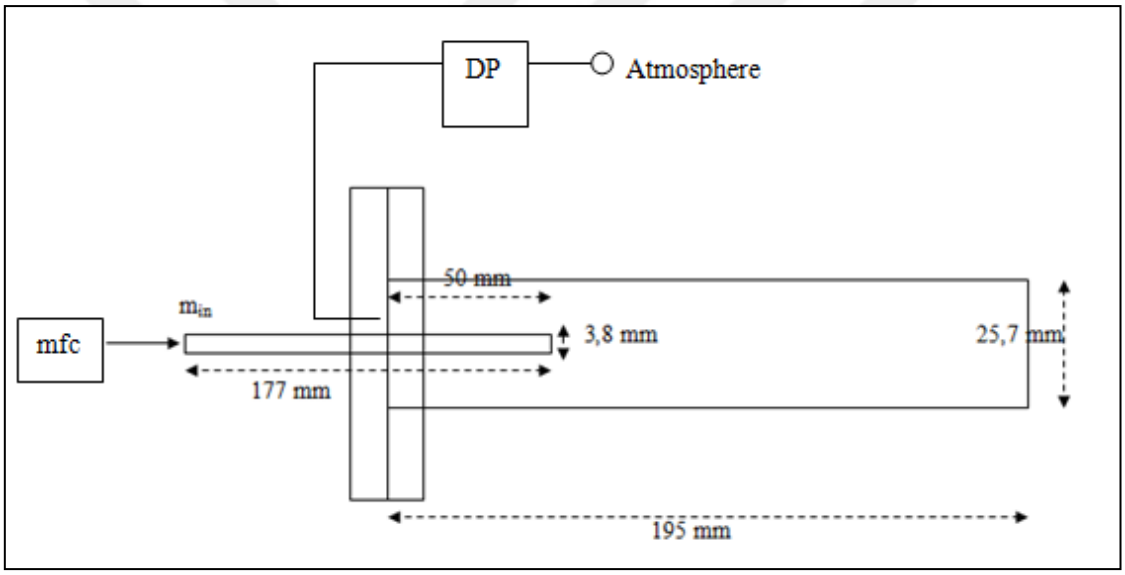

Figure 2.6. Reference Ejector System Drawing for CFD Calibration

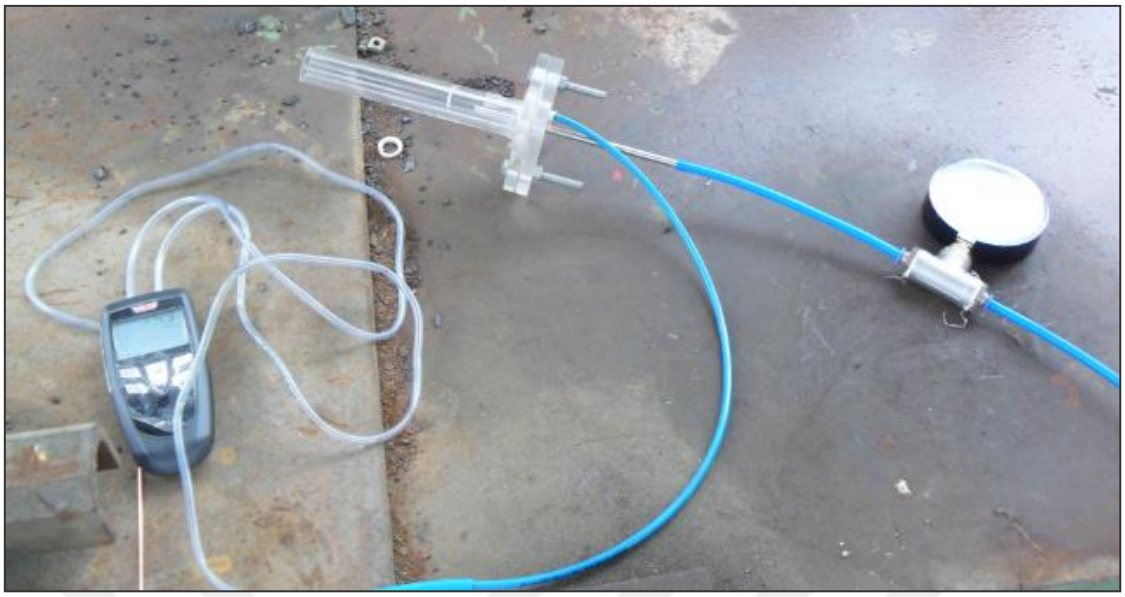

Figure 2.7. Reference Ejector System for CFD Calibration

Maximum vacuum pressure level caused by the entrainment effect of the ejector was selected as the comparison data between the CFD and the experimental results. Left side of the ejector was closed with blind flange in order to measure maximum vacuum pressure formed by the entrainment effect during the feed of compressed air to the nozzle. A differential pressure transmitter was used for measuring the vacuum pressure with respect to atmospheric pressure.

There are 2 pressure transmitter used during the experiments, which have different ranges (20 mbar and 1000 mbar) and resolutions (0.1 Pa and 1 mbar). Because of that, up to the 20 mbar vacuum level, high resolution pressure measuring device is used and from 20 mbar to the higher levels, low resolution device is used.

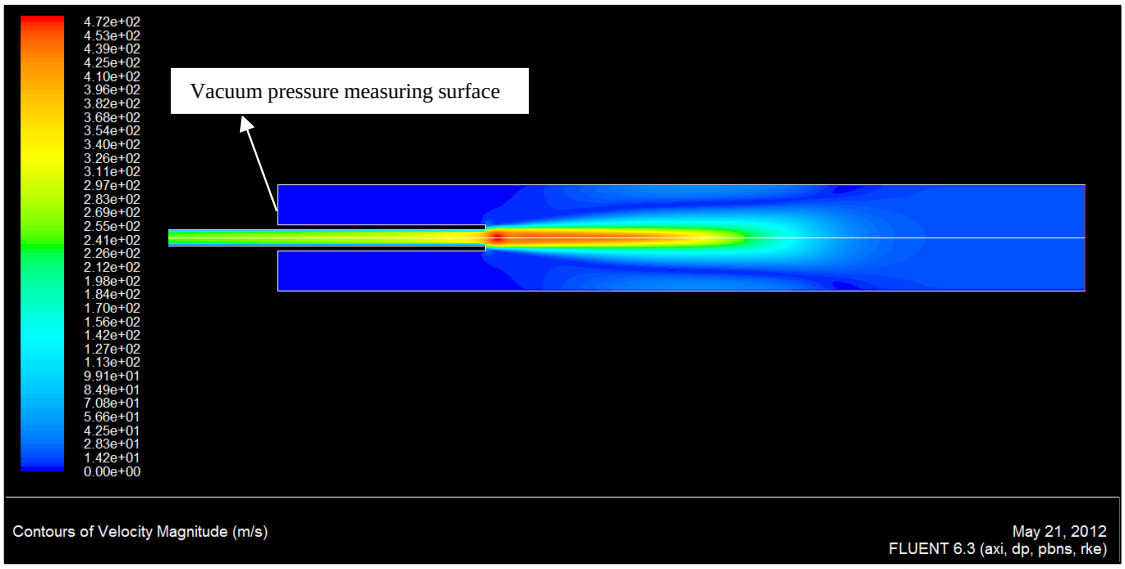

Figure 2.8. Fluent solution for velocity magnitude @ 28Nm^3/h

Typical ejector velocity magnitude distribution is shown in Fig.2.8 as an example. As shown in figure, left side of the model was closed and area weighted vacuum pressure was calculated with CFD model at that surface. Area weighted vacuum pressure was compared to the experimental results for validation.

2.2. CFD Model Analysis and Validation Methodology

2.2.1. CFD analysis matrix

Operational and geometric parameters which affect the ejector performance were determined and these parameters were considered as the CFD model parameters. Vacuum pressure occurred due to the entrainment effect was considered as the ejector performance which was considered as better when the static vacuum pressure level was higher. Operational and geometric parameters effects the ejector performance are listed in Table 2.4.

Table 2.4. Operational and geometric parameters investigated with CFD model

Motive gas flowrate (Nm^3/h)	Ejector tube lenght (mm)	Ejector tube diameter (mm)	Nozzle diameter (mm)	Motive gas temperature (K)	Induced gas temperature (K)	Induced gas static pressure (bara)
4	25	10	1	**300**	**300**	**1**
8	50	15	2	450	450	3
12	75	20	3	600	600	5
16	**100**	**25**	**3.8**	750	750	7
20	125	30	5	900	900	9
24	150	35			1050	
28	175	40			1200	

During the CFD analysis, each parameters effect was investigated separately with comparing the reference parameters results which are shown bolt in CFD matrix. When the induced gas temperature was analyzed, bolt values were fixed and the induced gas temperature values were investigated for each motive gas flowrate.

2.2.1.1. Performance criteria of ejector system

Ejector is used for generating pressure difference/barrier between CFB riser and the cyclone. It will be shown at subsequent sections that the vacuum pressure generated by the ejector was equal to the maximum pressure difference that can be getting with ejector at same conditions. Due to this reason, vacuum pressure generated by the ejector system was determined as the performance parameter for the ejector system.

2.2.1.2. Motive gas flowrate

The main parameter for CFD analysis is the motive gas flowrate. There were 7 different motive gas flowrates selected for CFD analysis from 4 Nm^3/h to 28 Nm^3/h with 4 Nm^3/h increments. The effect of motive gas flowrate on the ejector performance was not

investigated for only reference values but also for all parameters determined for the CFD analysis.

2.2.1.3. Ejector tube length

In order to determine the lower limit of ejector tube length, 7 different lengths from 25 mm to 175 mm were investigated with the reference parameters and 7 different motive gas flowrates. The relation of lower limit of ejector length and the nozzle exit gas velocity is also investigated.

2.2.1.4. Ejector tube diameter

Ejector tube inner diameter was another parameter investigated which is related to the cross-section area of the ejector tube. There were 7 different diameters investigated from 10 mm to 40 mm.

2.2.1.5. Ejector nozzle diameter

Motive gas exits from the ejector nozzle to the ejector tube section. If the nozzle exit diameter becomes lower, the speed of motive gas becomes higher for the same flowrate and higher kinetic energy. With the investigation of the effect of nozzle exit diameter from 1 mm to 5 mm, effect of motive gas exit velocity was also investigated for each motive gas flowrates.

2.2.1.6. Motive gas temperature

The main idea for the ejector system is converting kinetic energy of the motive gas to the pressure difference between ejector tube inlet end exits. In order to increase the kinetic energy of motive gas with constant mass flowrate, it would be practical to increase volume flowrate with the increase of motive gas temperature. With this study, 5 different temperatures were investigated from 300 K to 900 K in order to determine the effect of motive gas temperature.

2.2.1.7. Induced gas temperature

During the operation of ejector system at CFB reactor, inlet and the exit of the ejector tube is open in order to circulate solid bed material. Due to the pressure difference generated by the ejector at CFB system, some portion of syngas or flue gas can be entrained. In this study, effect of induced gas temperature on entrainment of gas was investigated from 300 K to 1200 K.

2.2.1.8. Induced gas static pressure

Ejector type solid circulation system can be used at pressurized CFB reactor. In order to the investigation of induced gas pressure which means reactor pressure, 5 different pressure values were analyzed from 1 bara to 9 bara.

2.2.2. CFD model validation methodology

The experimental system mentioned at section 2.1.2, was used for CFD model validation studies. The main idea of the validation study was the comparing the CFD results with the experimental results for 7 different motive gas flowrates (4 Nm^3/h to 28 Nm^3/h with 4 Nm^3/h increments). Experiments for CFD model validation was repeated two times in order to be sure that the results are consistent and the average of these results were used for the comparison with the CFD results. Additionally, CFD analysis of two mesh sizes (0.5 mm and 1 mm) were compared with experimental results in order to be sure if there is a difference related with the mesh size or not.

2.3. Experimental Cold Test Facility Design

The schematic of the cold model CFB system is shown in Fig.2.9 and the picture of model is shown in Fig.2.10. The model is made out of transparent plexiglass material. The system consists of CFB riser, cyclone separator, ejector at the downcomer, and return conduit to the riser. The riser is 7800 mm high. The riser and the downcomer have 94 mm and 34 mm inner diameter, respectively. An ejector with the tube diameter of 25.7 mm and nozzle diameter of 2 mm is located on the downcomer. There is a cyclone separator with 140 mm inner diameter. The cyclone and the riser are connected to each other with the downcomer where the ejector is mounted on. The downcomer is

connected to the riser with an angle of 45^0 where the recycled solid material is fed into the riser just above the dense bed.

An air blower was used for the supply of fluidization air which was controlled by the frequency controller (rpm control of blower motor). The flowrate of the fluidization air was measured with the orifice flow meter and adjusted by the rpm of the blower motor. Fluidization air passed through the windbox and the distributor plate to the riser. The distributor plate is made out of fabric material and it was supported by steel mesh.

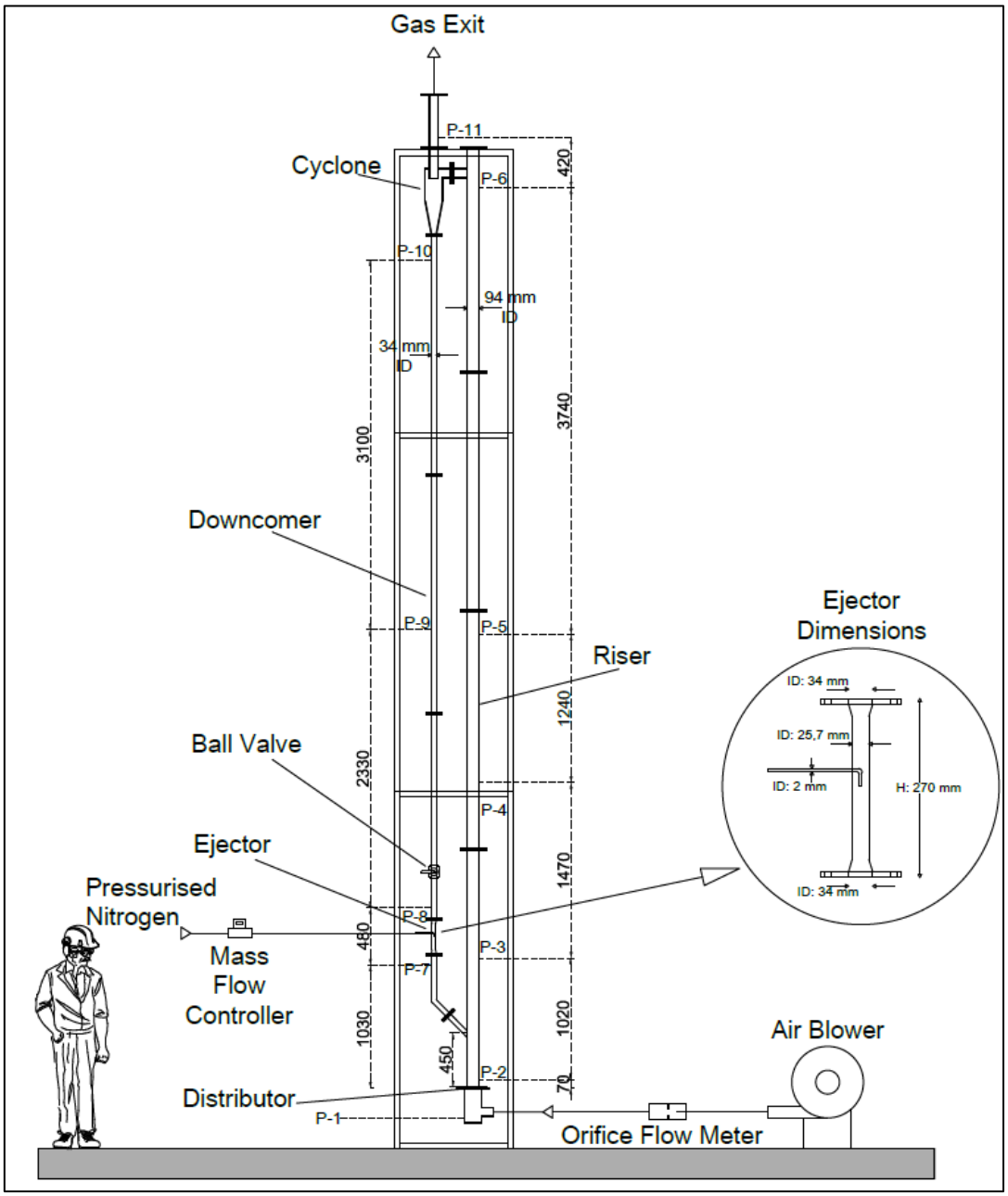

Figure 2.9. Experimental CFB Cold Model

There were eleven pressure ports mounted along the solids circulating loop to determine the pressure profile of the system. One pressure port was mounted on the windbox, 5 along the riser and 4 along the downcomer and the last one at the exit of the cyclone. A data logger was used to record pressure values of each port for a specified time interval.



Figure 2.10. Cold CFB model

There is a ball valve at the downcomer for measuring the solid circulation rate (Gs-kg/m^2.s) during the cold tests run. Pressurized nitrogen was used for the ejector motive gas supply. Its flowrate was adjusted by the mass flow controller (MFC) which is the combination of control valve and flowmeter.

2.3.1. Hydrodynamic calculations

In order to determine proper design and operational parameters of cold CFB system, hydrodynamic calculations should be done. Hydrodynamic calculations for cold CFB system design were done iteratively. The hydrodynamic calculation methodology is summarized in Fig.2.11. Pressure, temperature and working fluid were determined as constraints for the hydrodynamic calculations.

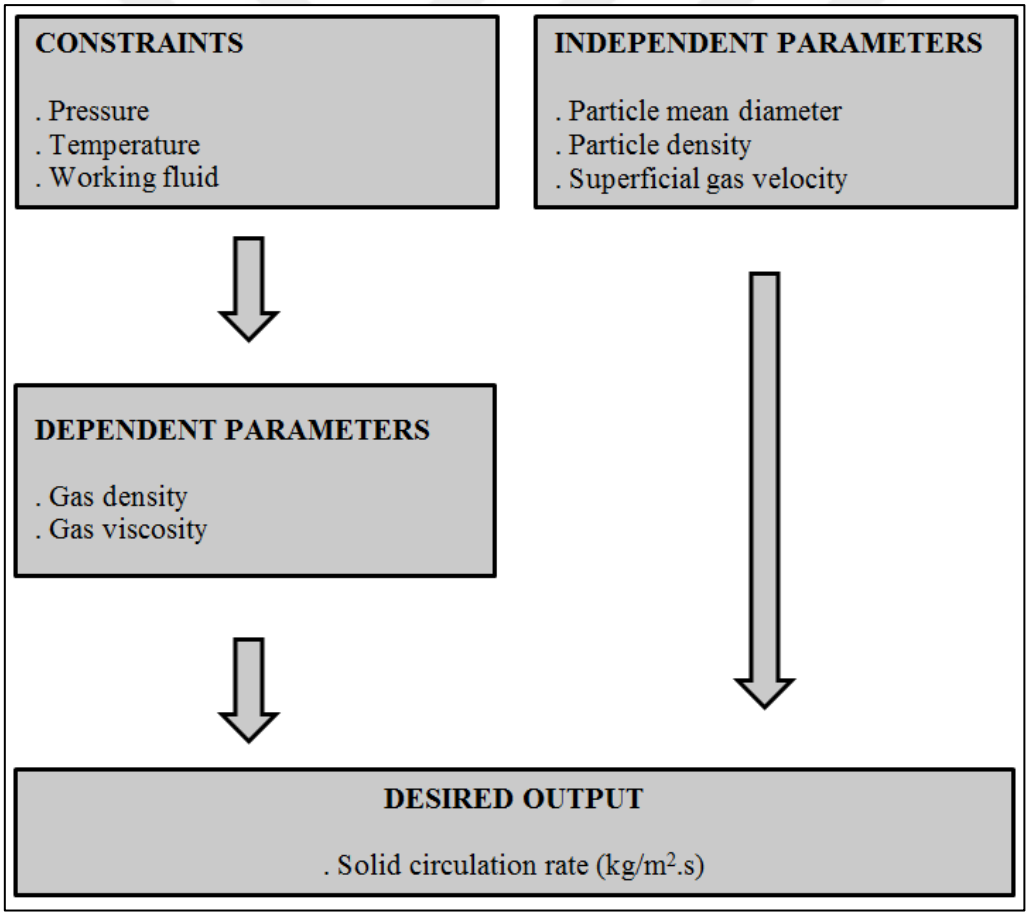

Figure 2.11. Hydrodynamic calculation procedure

Particle mean diameter, particle density and superficial gas velocity were assumed as independent parameters which were determined iteratively. Working fluid density and

viscosity are the dependent parameters depend on the working fluid, pressure and temperature. Solid circulation is desired output for the CFB hydrodynamic calculations.

There are two important dimensionless numbers which are Archimet and Reynolds numbers of solid particle. These two parameters are expressed with the equations given below (Eq. 2.1 and Eq. 2.2).

$$Re : [\rho_g.U_g.d_p] / \mu \quad (2.1)$$

Re: Reynolds number

ρ_g : Gas density

U_g : Superficial gas velocity

d_p : Particle diameter

μ : Gas dynamic viscosity

$$Ar: [\rho_g.(\rho_p - \rho_g).g.d_p^3] / \mu^2 \quad (2.2)$$

Ar: Archimedes number

ρ_p : Particle density

g: Gravitational acceleration

These two numbers were used for determining the terminal velocity of the solid particles. If the Reynolds number is higher than 0.4 and lower than 500 ($0.4 < Re < 500$), "intermediate law" is used for determining terminal velocity (Eq.2.3).

$$U_t: (Ar/7,5)^{0,666}.\mu/(\rho_g.d_p) \quad \text{(intermediate law)} \quad (2.3)$$

U_t: Terminal velocity of solid particle

With intermediate law equation, terminal velocity of the solid particle for the mean diameter was calculated. After determining the terminal velocity, void fraction inside the CFB riser was determined with the equation given below (Eq. 2.4).

$$\varepsilon = [((U_g - U_t)^2 . 6,81x10^5.\rho_g^{2,2}) / (2.g.D_r. \rho_p^{2,2}) + 1]^{-0,213} \quad (2.4)$$

ε: Void fraction

D_r: Reactor diameter

After determining the void fraction inside the CFB riser, solid circulation rate (Gs) can be calculated with equation given below (Eq. 2.5).

$$Gs = (U_g - U_t).(1 - \varepsilon). \rho_p \quad (2.5)$$

Gs: Solid circulation rate

If the calculated solid circulation rate is lower or higher than the desired value, independent parameters should be changed iteratively in order to get desired solid circulation rate.

2.3.2. Distributor plate

The distributor plate is made out of fabric material and it was supported by steel mesh. Fabric material is preferred due to the lower pressure drop and less solid transfer from dense bed to the windbox. Because the pores on the fabric material is very small and do not allow to fine particles transfer to windbox.

2.3.3. Riser

The dimensions of riser were selected as the same dimensions with the hot test facility. The riser is 7800 mm in high and 94 mm in inner diameter. Riser is made out of plexiglass material. There are 5 pressure measurement ports for measuring the CFB loop pressure profile. Riser is mounted on a modular aluminum platform.

2.3.4. Cyclone

Generally, empirical tables (Table 2.5) are used in industry for designing a cyclone. Inlet velocity determination of cyclone is the first step for cyclone design. Inlet velocity should be in the range of 20 to 40 m/s according to the industrial experience. After determining the inlet velocity, inlet area can be calculated. K and L are the inlet dimensions of the cyclone which is rectangular in shape. These two dimensions are reference dimensions for the empirical tables. Other cyclone dimensions (Figure 2.12) can be determined with the ratio of dimensions according to the tables.

Table 2.5. Empirical table for cyclone design [13]

Standard Proportion of Vertical Reverse-Flow Cyclones

Recommended Duty	$\frac{K}{D_c}$	$\frac{L}{D_c}$	$\frac{M}{D_c}$	$\frac{F}{D_c}$	$\frac{S}{D_c}$	$\frac{H}{D_c}$	$\frac{E}{D_c}$	N_h	$\frac{Q}{D_c^2}$	References
a. High throughput	0.75	0.375	0.75	0.875	1.5	4.0	0.375	7.2	4.58	Stairmand (1951)
b. High throughput	0.8	0.35	0.75	0.85	1.7	3.7	0.4	7.0	3.47	Swift (1969)
c. General purpose	0.5	0.25	0.5	0.6	1.75	3.75	0.4	7.6	1.86	Swift (1969)
d. General purpose	0.5	0.25	0.5	0.625	2.0	4.0	0.25	8.0	1.91	Lapple (1951)
e. High efficiency	0.44	0.21	0.4	0.5	1.4	3.9	0.4	9.2	1.37	Swift (1969)
f. High efficiency	0.5	0.22	0.5	0.5	1.5	4.0	0.375	5.4	1.53	Stairmand (1951)
General CFB	0.8	0.35	0.45	0.5–1.0	1.0	2.0	—	—	—	—

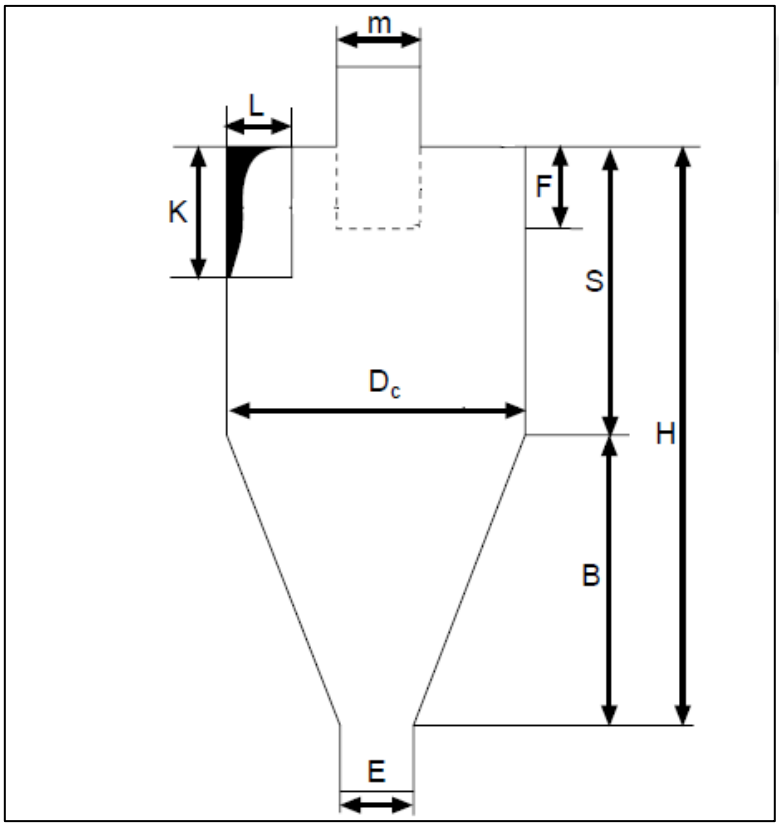

Figure 2.12. Cyclone dimensions [13]

In this study "General Purpose Lapple Cyclone" dimensions were used for cold test facility. According to the empirical ratios of cyclone design, cyclone of cold CFB test facility cyclone was manufactured from plexiglass transparent material. The dimensions of cyclone are shown in Fig.2.13.

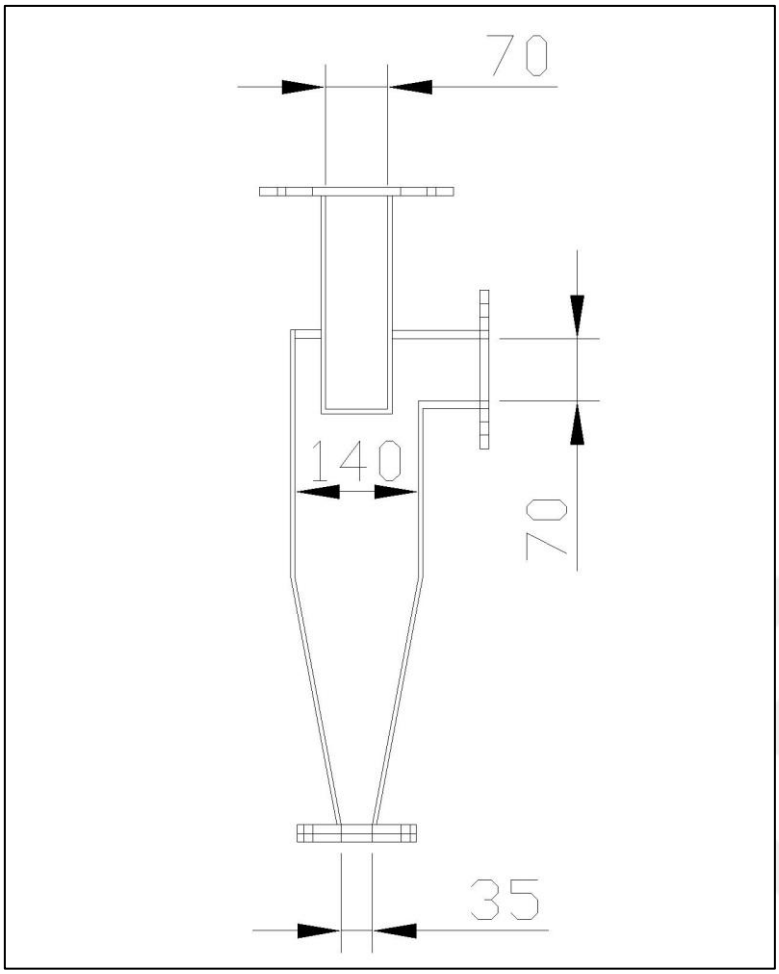

Figure 2.13. Cold CFB test facility cyclone dimensions

2.3.5. Downcomer

The inner diameter of downcomer of the CFB system is 34 mm which is close to the cyclone diameter at where the cyclone and downcomer are connected. Downcomer is also made out of transparent plexiglass material. There are 4 pressure measurement ports for measuring the pressure profile of CFB loop.

2.3.6. Air blower

4 kw air blower was used for primary air supply. The rpm of the blower was controlled by frequency converter. The blower is double stage high pressure blower. The maximum flowrate and pressure of the blower is 350 Nm^3/h and 250 mbar, respectively. The maximum flowrate of air during the cold tests was 150 Nm^3/h which corresponds to

6 m/s superficial gas velocity inside the riser. The capacity of the blower was sufficient for the cold tests.

2.3.7. Orifice flowmeter

In order to measure fluidization air flowrate, orifice plate flowmeter was used. Orifice flow meter was calibrated with pitot tube. In order to calibrate orifice flowmeter, pressure difference generated by the orifice flowmeter was measured with respect to air flow measured by the pitot tube. The relation between orifice pressure difference and volumetric flow is shown in Table 2.6 and Fig.2.14.

Table 2.6. Calibration data for orifice flowmeter

Orifice Delta P (Pa)	Measured Flow (Nm^3/h)	Calculated Flow (Nm^3/h)	Difference (%)
20	42	48	11.7
93	62	61	-1.5
218	87	83	-5.6
400	115	110	-4.4
932	167	169	1.1
1640	225	216	-3.8
2500	270	264	-2.3
2950	295	299	1.6

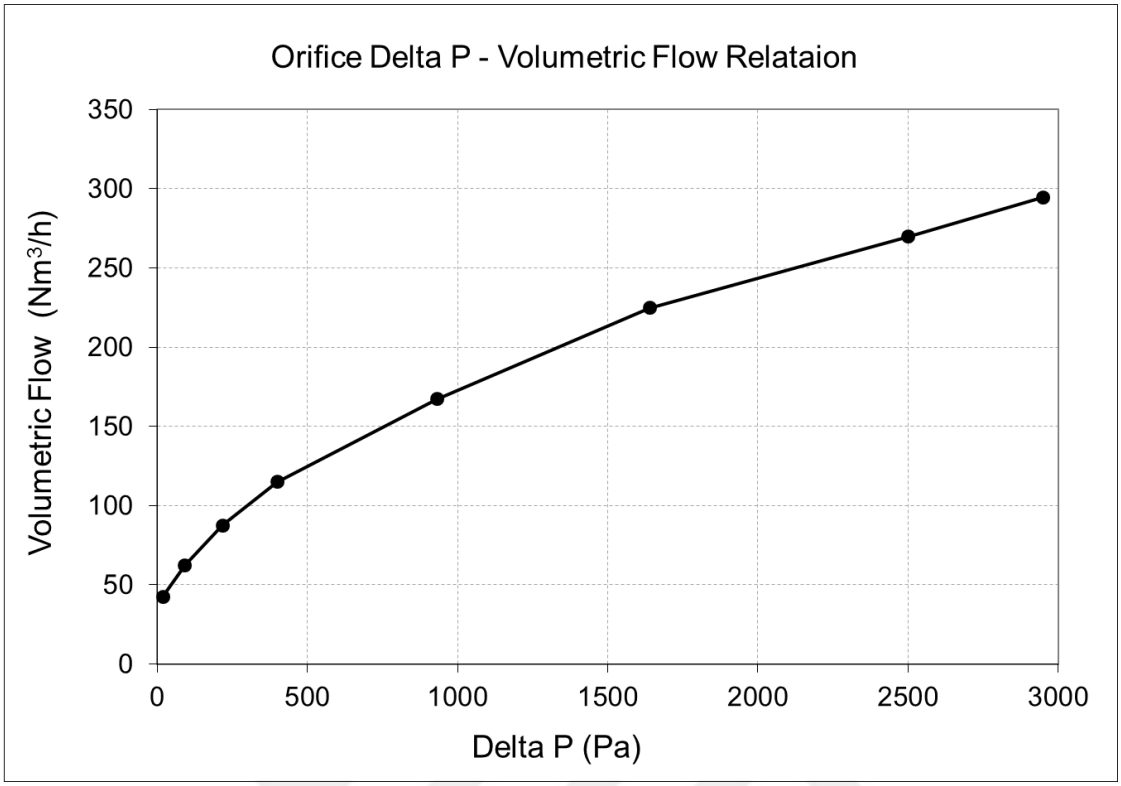

Figure 2.14. Orifice plate pressure difference and volumetric air flowrate relation

According to the relation of orifice pressure difference and the volumetric flow, an equation was generated in order to predict the volume flow. When the calculated flow is compared to the measured flow, the difference between calculated and the measured flow is acceptable.

2.3.8. Ejector motive gas

Pressurized nitrogen was used for the ejector motive gas supply. Due to the pressure fluctuations, air compressor was not used for pressurized gas supply. Nitrogen tube pressure is very high and during the experiments, pressure fluctuations were negligible.

2.3.9. Ejector motive gas flowmeter

Motive gas flowrate was adjusted by the mass flow controller (MFC) which is the combination of control valve and flowmeter. The range of mass flow controller is 0 – 100 lt/m. The resolution of mass flow meter is 0.1 Lt/m which is quite enough for sensitive analysis.

2.3.10. Bed material

Silica sand was used as bed material which has a weighted arithmetic mean diameter of 644 micron according to the sieve analysis and its size distribution is shown in Fig.2.15. Bulk and particle densities were 1450 kg/m^3 and 2545 kg/m^3, respectively. Properties of the sand particles used in CFB cold tests corresponded to the Group B particles according to the Geldart powder classification criteria [45].

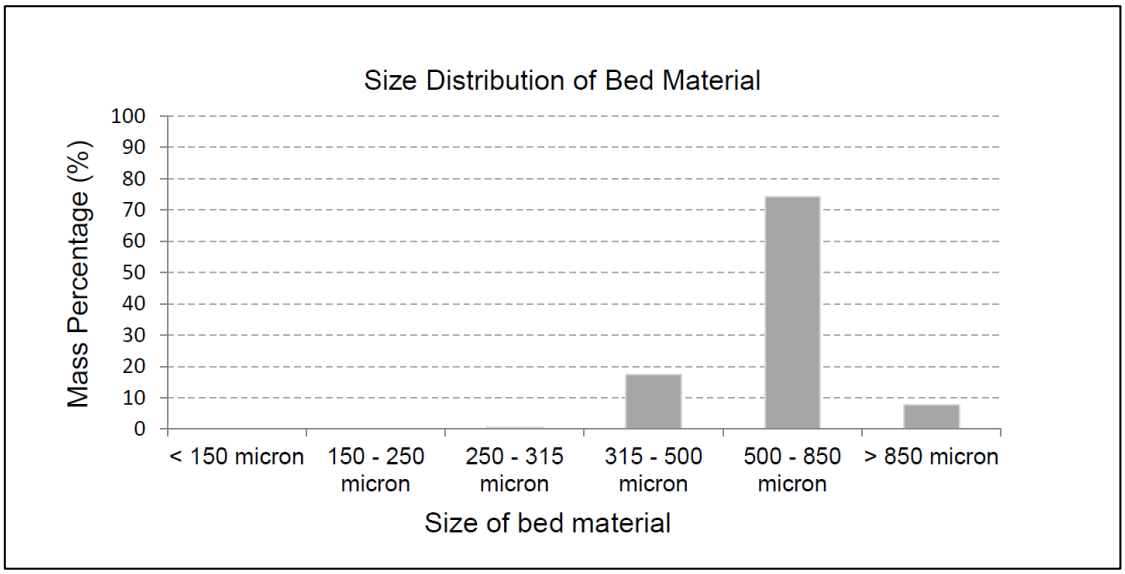

Figure 2.15. Bed material size distribution

2.3.11. Pressure measurement along the cfb loop

There were eleven pressure ports mounted along the solids circulating loop to determine the pressure profile of the system. One pressure port was mounted on the windbox, 5 along the riser and 4 along the downcomer and the last one at the exit of the cyclone. A data logger (Ahlborn-Almemo-2890-9) which has the accuracy of ± 0.5 % was used to record pressure values of each port for a specified time interval (60 second).

2.3.12. Ejector design

Ejector was made out of plexiglass transparent material. The dimensions of the ejector are shown in Fig.2.16. Nozzle material is stainless steel due to the higher working pressure. Inlet and exit of the ejector inside diameter is same with the downcomer. However, ejector tube section is 25.7 mm in inner diameter.

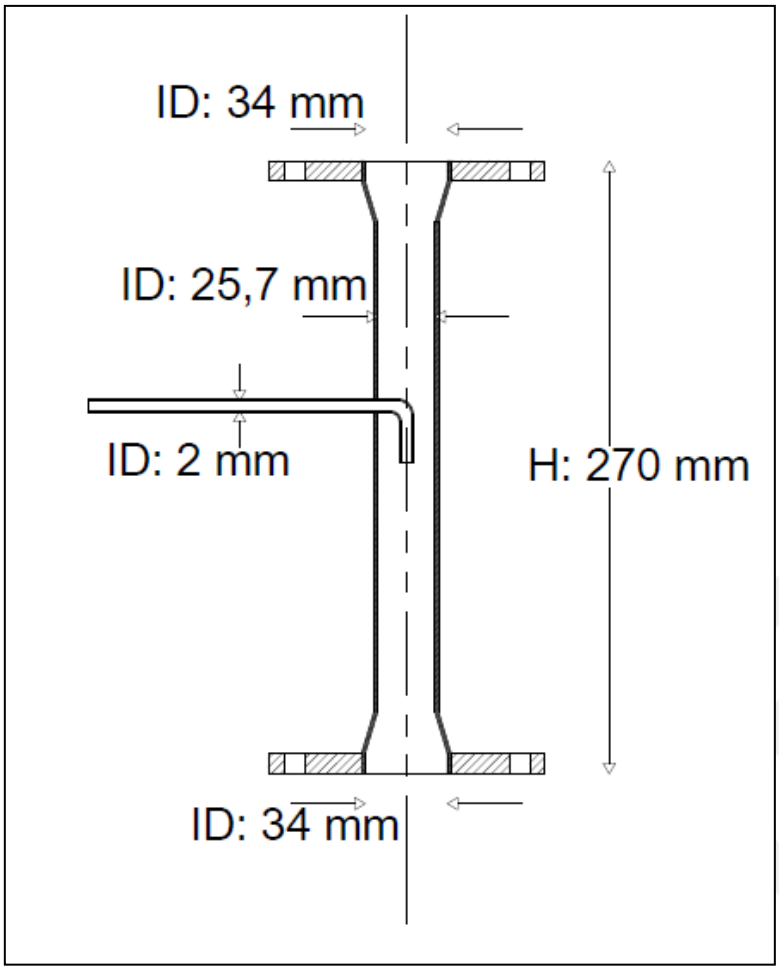

Figure 2.16. Ejector dimensions

The dimensions of ejector were selected according to the CFD analysis of ejector system which will be mentioned at subsequent sections. The inner diameter was selected as narrow as possible for generating maximum pressure difference and as big as possible for solid flow through ejector.

2.4. Experimental Cold Tests Methodology

2.4.1. Experimental matrix for cold tests

At first, the experimental system has been tried without any bed material with and without the ejector system. Then the effect of the ejector system on CFB with solid inventory has been investigated with and without ejector system.

In each experiment, 3 kg bed material (silica sand) was loaded to the riser which had the initial static bed height of approximately 330 mm. Air flowrate was gradually increased

in order to get a specified superficial gas velocity through the riser. A differential pressure measurement device was used in order to get vertical pressure profile along the riser and downcomer with eleven pressure measurement ports.

When the steady state circulation regime was reached, i.e. the pressure values along the circulation loop were stable, pressurized nitrogen was fed to the ejector with the specified gas flowrate which was adjusted automatically by mass flow controller.

Cold experiments were carried out according to the experimental matrix shown in Table 2.7. The effects of motive gas flowrate, cyclone efficiency, solid circulation rate, fluidized bed densities along the riser were investigated for 4, 5 and 6 m/s superficial gas velocities.

Table 2.7. Experimental matrix for CFB cold tests

Riser Superficial Gas Velocity (m/s)	**4**	**5**	**6**
Primer Air Flowrate (Nm^3/h)	x	x	x
Pressure profile along the CFB loop (mbar)	x	x	x
Ejector Motive Gas Flowrate (Lt/m)	x	x	x
Ejector Motive Gas Inlet Pressure (barg)	x	x	x
Particles Escape From Cyclone (kg/h)	x	x	x
Solid Circulation Rate (kg/h)	x	x	x
Gs at Riser ($kg/m^2.s$)	x	x	x
Gs at Downcomer ($kg/m^2.s$)	x	x	x
Gs at Ejector Tube (kg/m2.s)	x	x	x
Dense Bed Density - (kg/m^3)	x	x	x
Freeboard Density - (kg/m^3)	x	x	x

Required pressure difference generated by the ejector system was determined and pressure profile along the CFB loop was determined for each superficial gas velocities. Optimum CFB operation with ejector system was determined.

2.4.2. Measurement method for pressure profile

There were eleven pressure ports mounted along the solids circulating loop to determine the pressure profile of the system. A data logger was used to record pressure values of each port for a specified time interval. Due to the fluctuations inside the riser and downcomer, 30 measurements were taken in 60 seconds to obtain the mean values considered as the pressure value of these ports. The example of a pressure measurement is shown in Fig.2.17 which is the pressure measurement results for 6 m/s conditions.

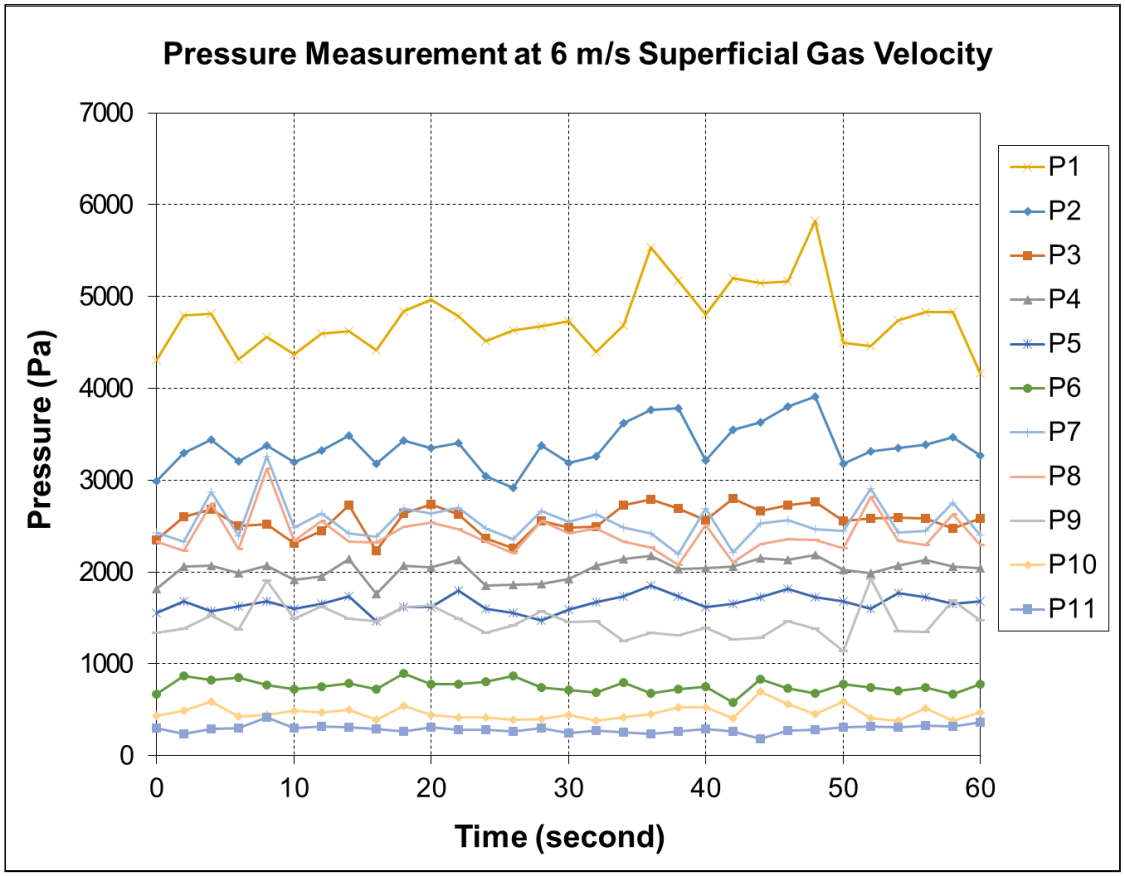

Figure 2.17. Pressure measurement at 6 m/s gas velocity

In order to create a pressure profile through the CFB loop, mean values of 30 pressure measurements were calculated for each pressure measurement point.

2.4.3. Determination of the solid circulation rate

For determining the Gs ($kg/m^2.s$) values in each run, the ball valve located at the downcomer was used. When the steady state conditions were reached inside the cold

model, the ball valve was suddenly closed and the time interval required for accumulating the bed material up to 200 mm above the ball valve, was measured. Mass of the accumulated bed material was calculated using the volume of this section and the bulk density of the bed material. It has to be taken into account that, there was a remarkable difference between the bulk density of the bed material accumulated above the ball valve and the measured bulk density of bed material before loading it to the riser. Bulk densities were 1450 kg/m3 and 1113 kg/m3 for the initial sand bulk density and the accumulated sand bulk density, respectively.

2.4.4. Determination of the cyclone efficiency

Cyclone performance was determined with the amount of solid particles escaped from the cyclone by comparing the amount of final and initial bed inventories. For each experiment, fresh sand was used in order to get similar size distribution of bed material. If the cold test is done with the sand used at previous tests, the size distribution is different because finer particles escaped from the cyclone and the mean diameter of sand become courser.

2.4.5. Determination of the dense bed and freeboard densities

The dense bed and freeboard densities of the riser were calculated with the pressure differences of related pressure ports. Difference between P6 and P3 pressure ports was used for calculating the freeboard density. Pressure ports of P3 and P2 were used for calculating the dense bed density. First 1 meter of the riser was assumed as dense bed region and the rest of the riser (6.5 m) up to the cyclone entrance was assumed as the freeboard.

2.5. Experimental Hot Test Facility Design (Gasifier)

A laboratory scale fluidized bed gasification system has been designed to study the effects of ejector system on CFB gasification reactor with selected Turkish coal. At first, simulation studies have been done for determining the mass&energy balance of the system. It was done with the Aspen-Hysys simulation program. The thermodynamic equilibrium conditions have been determined with specific assumptions about the gasification process. For specified fuel feeding capacity and specified thermodynamic

conditions, required air feeding capacities and possible syngas properties have been determined.

After determining the mass&energy balance and syngas properties, hydrodynamic calculations have been done in order to determine the required superficial gas velocity along the riser and the riser diameter with respect to specified fuel feeding capacity. According to hydrodynamic and chemical calculations, the system has the fuel feeding capacity of 18 kg/h with the riser diameter of 97 mm and 7000 mm in height. Specified temperature and pressure is 900 °C and atmospheric, respectively.

The CFB gasifier used for the hot experiments is shown in Fig.2.18. The system is made of 310 stainless steel. A control system is included for system equipment control (feeder motor control, valves, etc.) and data collection and storage (pressure, temperature, syngas composition, etc.). Mass flow controller is used for measuring and control the gasification agents flow rates. Electric heaters are used for heating of the reactor and maintain stable temperature profile along the gasifier reactor during steady state operation.



Figure 2.18. Hot CFB Gasifier

2.5.1. Fuel properties

Elemental analysis of selected Turkish coal is shown in Table 2.8. For determining the mass and energy balance of the gasifier, these values are used for simulation of the gasifier. With respect to the average of the Turkish coals which have the lower heating value (LHV) of 1600 kcal/kg, selected coal have respectively higher lower heating value.

Table 2.8. Elemental analysis of selected Turkish coal

C (%)	H (%)	O (%)	S (%)	N (%)	H_2O (%)	Ash (%)	LHV (kcal/kg)
45.2	2.84	11.5	1.16	0.94	13.75	24.61	3773

The size and the moisture content of the coal are set at desired value with coal preparation system which consists of drying, crashing and sieving units. The moisture content and the size of coal particles is %13.37±1 and 0.5-1 mm, respectively.

2.5.2. Gasifier energy and mass balance (ASPEN-HYSYS)

For making the hydrodynamic calculations of CFB reactor for a specified superficial gas velocity inside the riser, gas flow through the riser should be determined. In order to determine the required gas flow rate through the riser, iterative calculations were done to get the required coal and air feed to the reactor for a specified pressure and temperature levels. Aspen-Hysys process simulation program was used for calculating the thermodynamic equilibrium conditions of gasification reactions. With the simulation study, both the approximate gas composition and the real volumetric flow can be determined. The temperature of the reactor assumed as constraint and the other parameters were adjusted in order to get desired temperature value. The simulation flow diagram is shown in Fig.2.19.

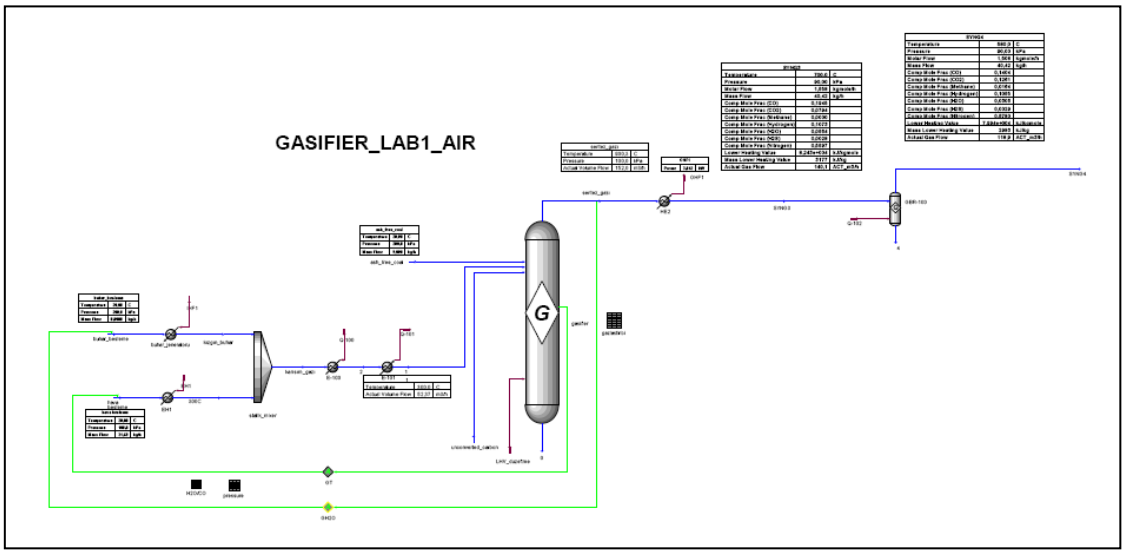

Figure 2.19. Simulation flow diagram of gasifier reactor

Gibbs reactor model was selected for determining the thermodynamic equilibrium conditions. At Gibbs reactor, there is no predefined reaction set; all possible reaction can take place. Input data for gasifier are, the amount of fuel and fuel composition as original basis, gasification agent, unconverted carbon ratios which is assumed as %5, heat losses of gasifier (%3 of total thermal load), and the desired pressure and temperature of the gasifier. By using input data, simulation program solve the equilibrium conditions. According to the equilibrium conditions, gas composition of syngas and physical/chemical properties was determined and the volumetric flow was determined in order to calculate superficial gas velocity at the upper part of the gasifier [46]. The design parameters determined with the simulation study is shown in Table 2.9.

Table 2.9. Mass&Energy Balance of Gasifier

Parameter	**Value**
Reactor temperature (°C)	900
Reactor pressure (barg)	0.1
Fuel feeding capacity (kg/h)	18.2
Required air flow rate (kg/h)	47.4
Thermal capacity (kWth)	78.4
Throughput (MWth/m^2)	17.9
Syngas flowrate (m^3/h)	112.7
Syngas flowrate (kg/h)	60.5
Gas flowrate at the bottom of reactor (m^3/s)	0.0368
Superficial gas velocity at the bottom of reactor (m/s)	6.0
Gas flowrate at the top of reactor (m^3/s)	0.0575
Superficial gas velocity at the top of reactor (m/s)	6.8
Equivalence ratio	0.46

Gas composition is also determined with simulation study which is shown in Table 2.10. According to the approximate molar fraction of the syngas, the physical properties were determined.

Table 2.10. Syngas composition result of simulation study (volumetric)

CO (%)	CO_2 (%)	CH_4 (%)	H_2 (%)	H_2O (%)	N_2 (%)	H_2S (ppm)	LHV (MJ/Nm^3)
16.5	10.6	0.6	11.5	3.8	57.0	2800	3.6

According to the gas properties and operational conditions, hydrodynamic calculations were done. Important parameters related to the hydrodynamic calculations which are density and viscosity of syngas was also determined with simulation study.

2.5.3. Hydrodynamic calculations

In order to determine proper design and operational parameters of hot CFB system, similar procedure with the cold system for calculating the hydrodynamic conditions were used. The hydrodynamic calculation methodology for hot CFB system is summarized in Fig.2.20.

Particle mean diameter, particle density, superficial gas velocity and reactor diameter were assumed as independent parameters which were determined iteratively. Working fluid density and viscosity are the dependent parameters which were determined with the simulation study. Solid circulation and fuel feeding capacity are desired output for the CFB hydrodynamic calculations.

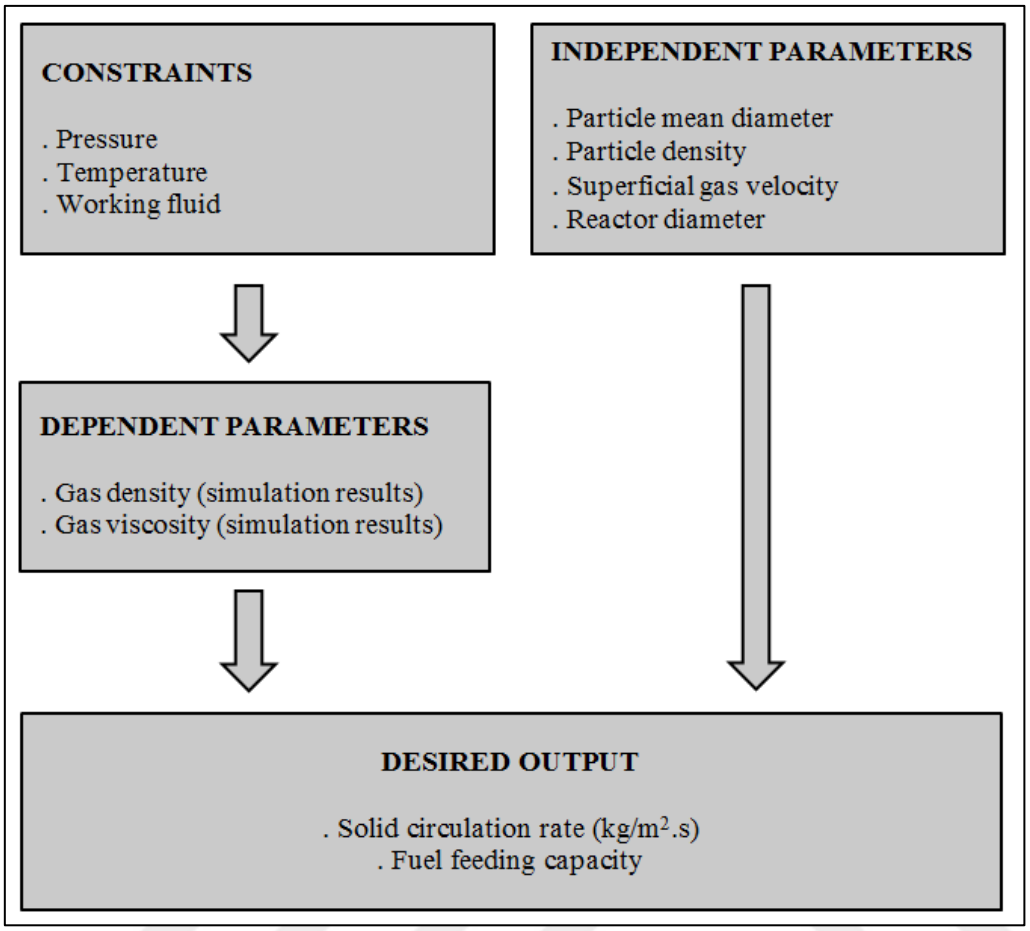

Figure 2.20. Hydrodynamic calculation procedure (hot system)

Density and viscosity values which are shown in Table 2.11, were used in order to calculate the Reynolds and Archimedes numbers with the equations shown below (Eq. 2.6 and Eq. 2.7).

Table 2.11. Density and viscosity values at gasifier bottom and top

	Gasifier bottom	**Gasifier top**
Viscosity (Pa.s)	5.142×10^{-5}	4.949×10^{-5}
Density (kg/m^3)	0.3233	0.2659

Re: $[\rho_g.U_g.d_p] / \mu$ (2.6)

Ar: $[\rho_g.(\rho_p - \rho_g).g.d_p^3] / \mu^2$ (2.7)

Reynolds and Archimedes numbers calculated with the equation 2.6 and 2.7 are shown below at Table 2.12. The physical properties of fluid at the bottom and top of the gasifier are significantly different from each other. In order to get average value of these parameters, calculations were done for gasifier bottom and the top conditions.

Table 2.12. Archimedes and Reynolds numbers at gasifier bottom and top

Gasifier bottom		**Gasifier top**	
Ar	Re	Ar	Re
219	17	194	15

These two numbers are used for determining the terminal velocity of the solid particles. If the Reynolds number is higher than 0.4 and lower than 500 ($0.4 < Re < 500$), "intermediate law" is used for determining terminal velocity (Eq. 2.8). The calculated terminal velocity values are shown in Table 2.13.

$$U_t: (Ar/7.5)^{0.666}.\mu/(\rho_g.d_p) \qquad \text{(intermediate law)} \qquad (2.8)$$

Table 2.13. Terminal velocity of the particles at gasifier bottom and top conditions

	Gasifier bottom	**Gasifier top**
Terminal velocity (m/s)	3.3	3.6

After determining the terminal velocity, void fraction inside the CFB riser was determined with the equation shown below (Eq. 2.9) and calculated values are shown in Table 2.14.

$$\varepsilon = [((U_g - U_t)^2 . 6.81x10^5.\rho_g^{2.2}) / (2.g.D.\rho_p^{2.2}) + 1]^{-0.213} \qquad (2.9)$$

Table 2.14. Void fraction of the reactor at gasifier bottom and top conditions

	Gasifier bottom	**Gasifier top**
Void fraction (m/s)	0.99763	0.99875

After determining the void fraction inside the CFB riser, solid circulation rate (Gs) can be calculated with equation shown below (Eq. 2.10) and the calculated values are shown in Table 2.15.

$$Gs = (U_g - U_t).(1 - \varepsilon). \rho_p \quad (2.10)$$

Table 2.15. Solid circulation rate of the reactor at gasifier bottom and top conditions

	Gasifier bottom	**Gasifier top**
Solid circulation rate (kg/m2.s)	4.8	12.6

If the calculated solid circulation rate is lower or higher than the desired value, independent parameters should be changed iteratively in order to get desired solid circulation rate.

2.5.4. Distributor plate

The distributor plate is made out of stainless steel and it was mounted between two flanges. There are 715 holes with the diameter of 1 mm. The holes are inclined with an angle of 45° in order to minimize the back flow of solid material.



Figure 2.21. Distributor plate of hot system

Gas velocity through the holes is 40 m/s for 6 m/s superficial gas velocity through the riser. Distributor plate is shown in Fig.2.21.

2.5.5. Riser

The dimensions of riser are approximately same with the cold test facility. The riser is 7000 mm in high (7800 mm for cold system) and 97 mm in inner diameter (94 mm for cold system). Riser is made out of stainless steel which has the thickness of 8.56 mm. There are 5 pressure measurement ports for measuring the CFB loop pressure profile.

2.5.6. Cyclone

Cyclone dimensions are same with the cold test facility (General Purpose Lapple Cyclone). It is made out of stainless steel and thickness of cyclone is 8.56 mm.

2.5.7. Downcomer

The inner diameter of downcomer of the CFB system is 38.1 mm (34 mm for cold system). Downcomer is also made out of stainless steel. Due to the temperature difference between riser and downcomer which was approximately 150 °C during the operation, there is elastic steel pipe for the compensation of relative thermal expansion of downcomer. There are 4 pressure measurement ports for measuring the pressure profile of CFB loop.

2.5.8. Fluidization agent

Air was used as the gasification agent. Air compressor was used for pressurized air supply. The compressor has capacity of 600 Nm^3/h at 7.5 barg. There was also dryer unit at the exit of the compressor in order to extract moisture content of air and dried air was fed to the reactor.

2.5.9. Fluidization agent flowmeter

In order to measure fluidization air flowrate, orifice plate flowmeter was used. Flowmeter model is Autrol-APT3100 which has the flow range of 0 Nm^3/h to 50 Nm^3/h

and the connection size is 1” (DN25). The accuracy of the flow transmitter is %0.075 at 20 °C which was quite accurate for experimental study.

2.5.10. Ejector motive gas

Similar to the cold test facility, pressurized nitrogen was used for the ejector motive gas supply. There is combustible syngas inside the reactor and ejector region. Due to the uncontrolled combustion risk at ejector nozzle exit, air was not used as ejector motive gas.

2.5.11. Bed material

Silica sand was used as bed material which has a weighted arithmetic mean diameter of 644 micron according to the sieve analysis. Bulk and particle densities were 1450 kg/m^3 and 2545 kg/m^3, respectively.

2.5.12. Control system

Gasifier system was controlled and monitored with PLC (Programmable logic controller) system. There were pressure measurement sensors, temperature transmitters and flow control and measurement devices in order to control the operation. Fuel feeding and electric heaters were also controlled with PLC system. Mainly system was controlled manually instead of automatic control. The main control parameter was temperature of the gasifier reactor. It was controlled by the air or fuel feeding rates.

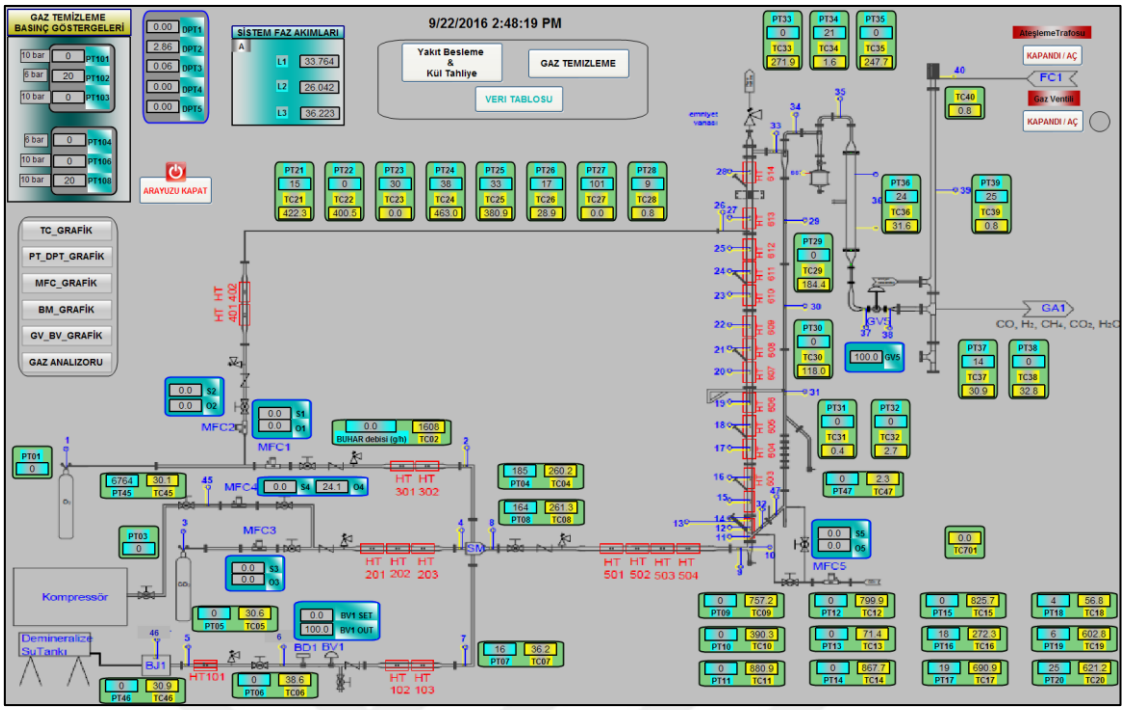

Figure 2.22. Control screen of PLC system

Some subsystems such as flow control valves and electric heaters are automatically controlled automatically according to the set values. First page of PLC control screens is shown in Fig.2.22.

2.5.13. Fuel feeding system

Screw feeder was used for feeding the coal to the reactor. Screw feeder was derived by electric motor which was controlled by the frequency control. Screw feeder was tested with coal at various speed of electric motor in order to determine the feeding rates at corresponding frequency of electric motor. With these calibration data, empirical equation was derived (Eq. 2.11) in order to predict the feeding rate during the experiments.

$$y = 0.0485x^3 - 5.5481x^2 + 867.19x - 1092.9 \ (R^2: 0.9998) \qquad (2.11)$$

y: coal feeding rate (gram/h)

x: frequency of electric motor (0 – 50)

Calibration of screw feeder feeding rates was tested 3 times in order to verify the feeding rate equation with very little fluctuations. It should be take into account that feeding calibration is valid for only selected coal which has specific physical properties like size, density and void fraction. If another coal is selected for gasification experiments, fuel feeding calibration should be done for that coal type.

2.5.14. Gas analyzing system

There was gas analyzing port at the exit of cyclone. During the gasification experiments, syngas was collected with the teflon bag from gas analyzing port and analyzed by the gas analyzer. Gas analyzer model is ABB–AO2040 which is infrared analyzer.

2.6. Experimental Hot Test Methodology

2.6.1. Experimental method for hot tests

In hot gasification experiment, 3 kg bed material (silica sand) was loaded to the riser which had the initial static bed height of approximately 304 mm. Air flowrate was gradually increased in order to get 1 m/s superficial gas velocity inside the riser at initial conditions (20 °C) which corresponds to 4 m/s superficial gas velocity at steady state gasification conditions (850 °C). In other words, reactor hydrodynamic regime was bubbling at the beginning and then it turned out CFB regime with the increase of temperature at same air flowrate. In order to heat up the reactor to the ignition temperature of coal, electric heater was used. There are 7 heaters for preheating the fluidization air and 14 heaters on the reactor for adjusting the temperature of the riser. With these electric heaters, fluidized bed temperature is increased to 350 °C which was the practical limit of ignition of coal particles. After reaching bed temperature of 350 °C, coal was started to feed and combustion reactions started and the temperature increased very rapidly to 850 °C. After reaching steady state condition for combustion process, fuel feeding rate was approximately increased 3 times in order to get gasification conditions at constant air flowrate. The temperature slightly increased during this process than decreased to its initial value. After reaching steady state

gasification conditions, fine tuning of temperature was done with adjusting the fuel flowrate.

2.6.2. Measurement method for pressure profile

Similar to the cold test facility, there were eleven pressure ports mounted along the solids circulating loop to determine the pressure profile of the system. The locations of pressure measurement ports were same with cold system. One pressure port was mounted on the windbox, 5 along the riser, 4 along the downcomer and one at the exit of the cyclone. A data logger (Ahlborn-Almemo-2890-9) which has the accuracy of ± 0.5 % was used to record pressure values of each port for a specified time interval (30 measurements in 60 second).

3. RESULTS AND DISCUSSION

3.1. CFD Analysis of Ejector System

3.1.1. CFD model validation results

In order to validation of the CFD model, 7 different mass flow rate of ejector nozzle were investigated for reference ejector design with 0.5 mm and 1 mm mesh size. Results are shown in Table 3.1 and Fig.3.1. The maximum deviations of the CFD result from the experimental result were -4.6% and -5.0% for 4 Nm^3/h motive gas feed condition for 0.5 mm and 1 mm mesh sizes, respectively. The averages of the absolute deviations of the all vacuum levels were 1.26% and 2.46% for 0.5 mm and 1 mm mesh sizes, respectively.

Table 3.1. CFD validation results for 7 different operating conditions

V (Nm^3/h)	P_{vacuum} (mbar) Experimental results	P_{vacuum} (mbar) Fluent results with 0.5 mm mesh	% Deviation @ 0.5 mm mesh	P_{vacuum} (mbar) Fluent results with 1 mm mesh	% Deviation @ 1 mm mesh
4	2.8	2.7	-4.6%	2.7	-5.0%
8	10.2	10.2	0.2%	10.2	-0.1%
12	21	21.6	2.6%	21.5	2.1%
16	35	35.0	0.0%	34.6	-1.1%
20	49	48.8	-0.4%	47.9	-2.3%
24	63	62.4	-0.9%	60.8	-3.5%
28	76	75.9	-0.1%	73.6	-3.1%

It was also realized that the mesh independency was valid for the all flowrates and both results of the mesh sizes were acceptable for the deviation levels. However, due to the acceptable computation time and the more accurate results, 0.5 mm mesh size model is selected as the validated model.

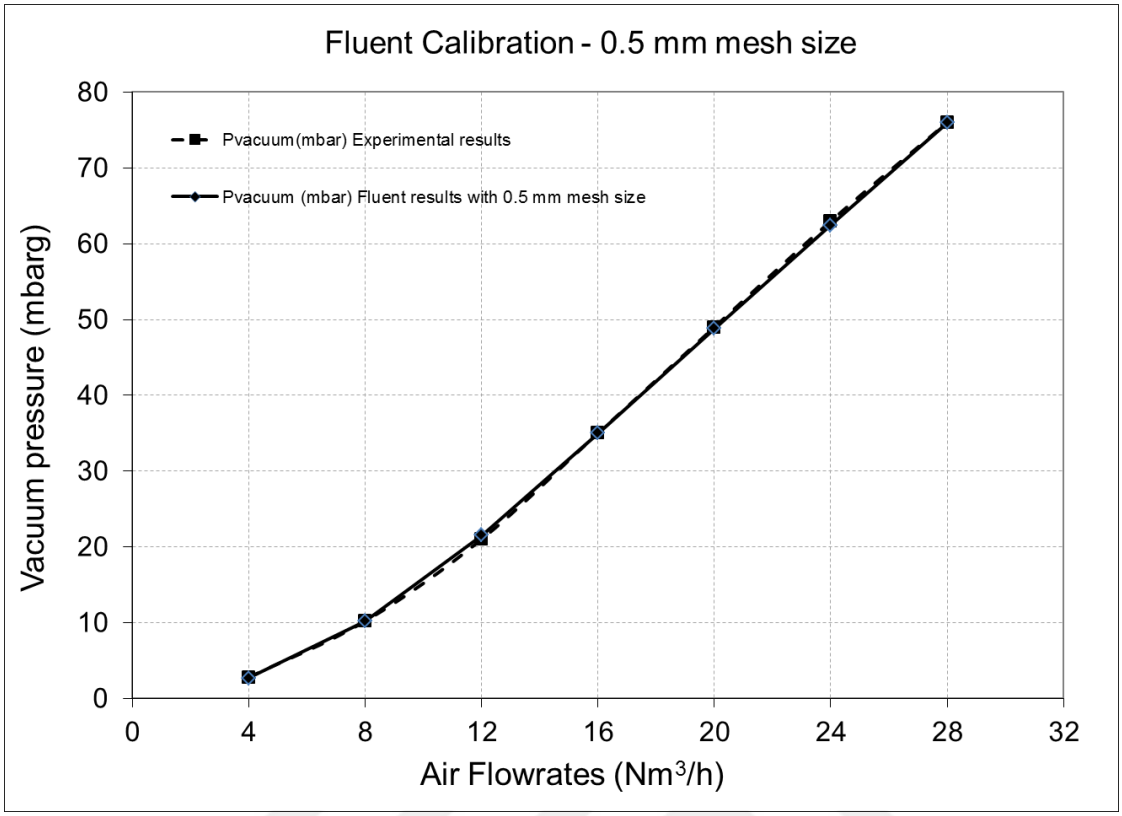

Figure 3.1. Experimental and Fluent Results (0.5 mm mesh size)

It can be concluded that the CFD model can be accurate enough for improving the ejector design, because as shown from the results, the maximum deviations of Fluent results were acceptable. The next step of this study was improving the ejector performance in terms of selected performance criteria with validated CFD model.

3.1.2. Flow characteristics of ejector model

In order to show the characteristics of flow of ejector system, some properties related with the conditions through the axis and side wall of the ejector at 7 different operating conditions are given in Fig.3.2 to 3.7 according to the CFD solution. Detailed information related with the flow characteristics are given at subsequent sections.

3.1.2.1. Velocity magnitude along the axis of the ejector

At Fig.3.2, velocity magnitudes along the axis of the ejector are shown. The maximum value was observed at the exit of the ejector nozzle at the distance of 0.177 m from the inlet of the nozzle. The maximum velocity magnitudes are 115 m/s and 472 m/s for the

motive gas flow rate of 4 Nm^3/h and 28 Nm^3/h, respectively. The other velocity magnitudes are in between these two levels. The air velocity is slow down after the exit of the nozzle due to the bigger cross-section area of the ejector and becomes fully developed flow just before the exit of the ejector tube.

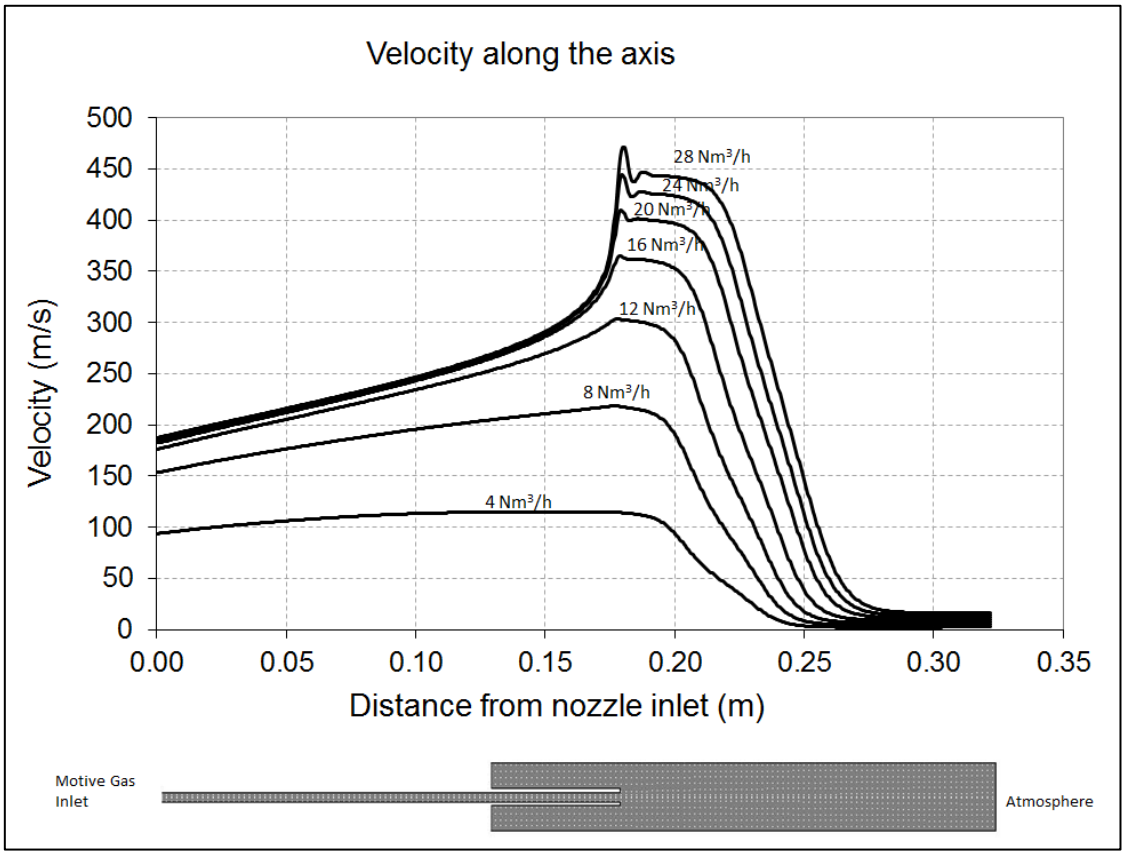

Figure 3.2. Velocity magnitude along the axis of the ejector

3.1.2.2. Mach number along the axis of the ejector

At Fig.3.3, Mach numbers along the axis of the ejector are shown. Similar to the velocity magnitude profiles, the maximum value is observed at the exit of the ejector nozzle. The maximum Mach numbers are 0.33 and 1.68 for the motive gas flow rate of 4 Nm^3/h and 28 Nm^3/h, respectively. Since the Mach number is not only depending on the velocity of fluid, but also depending on speed of sound, it's increase is not directly proportional to the velocity because speed of sound depends on other thermodynamic properties such as C_p, C_v and temperature of the fluid.

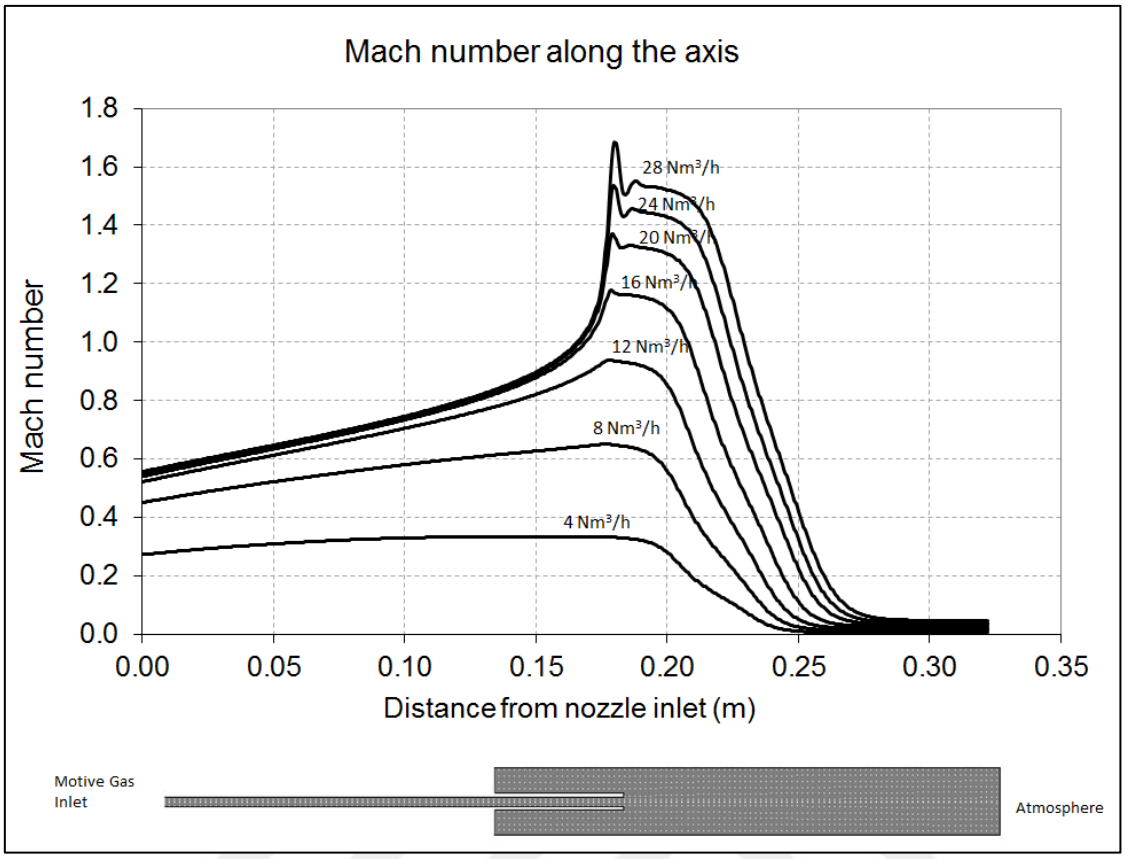

Figure 3.3. Mach Number along the axis of the ejector

3.1.2.3. Static pressure along the axis of the ejector

At Fig.3.4, static pressures along the axis of the ejector are shown. As increasing the flowrate of air, required inlet pressure level is increasing. The inlet pressures are 7.1 kpa and 261.7 kpa for the 4 Nm^3/h and 28 Nm^3/h air flowrates, respectively.

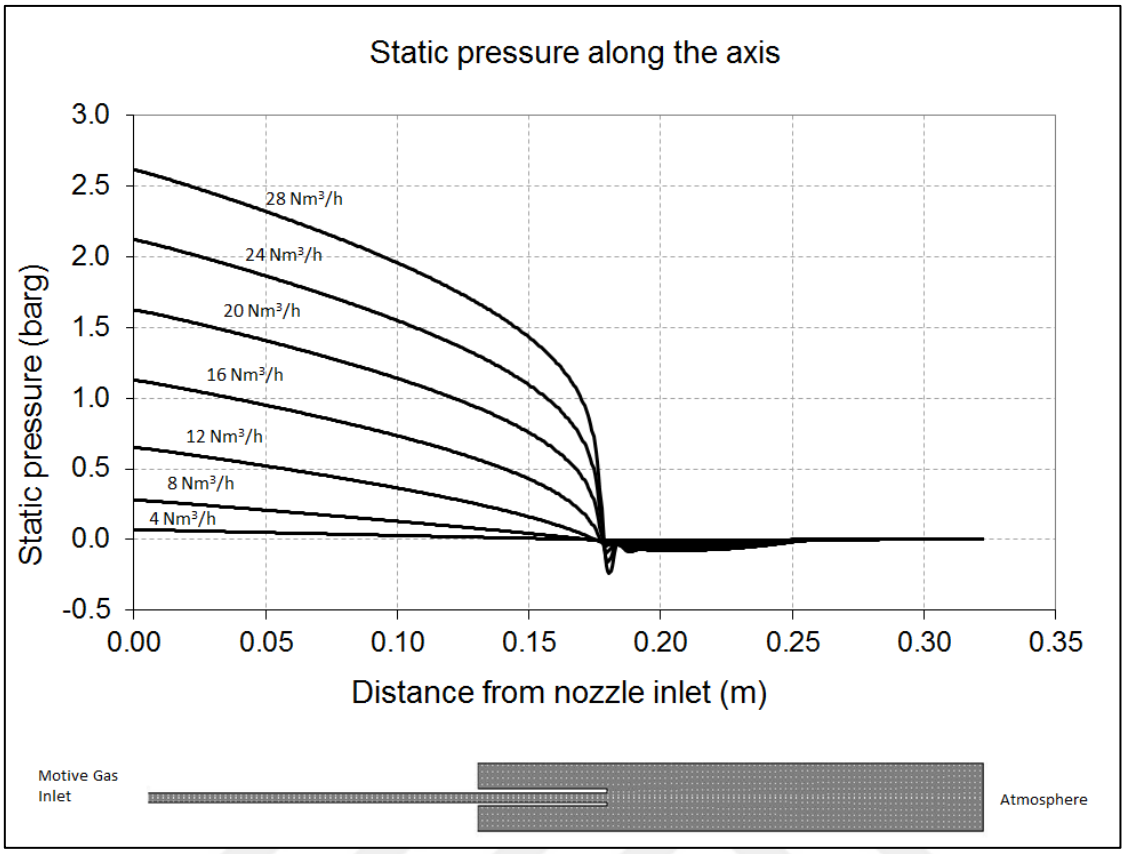

Figure 3.4. Static pressure along the axis of the ejector

3.1.2.4. Static temperature change along the axis of the ejector

At Fig.3.5, static temperature changes along the axis of the ejector are shown which has the minimum value of approximately 295 K for the 4 Nm^3/h flowrate and 195 K for the 28 Nm^3/h at the exit of the ejector nozzle. The temperature of the air is decreasing along the nozzle due to the compressible flow effect because the Mach number is higher than the practical limit of incompressible flow (0.3) at the exit of the nozzle for all 7 different conditions. According to the thermodynamic relations, some part of the enthalpy of the air is converted to the velocity during the acceleration of the flow through the nozzle and the temperature of the air which is related to the enthalpy, is decreased. Just after the exit of the nozzle at the position of 0.177 m, temperature is again increasing due to the decrease of velocity and reaching approximately its initial value at the exit of the ejector tube.

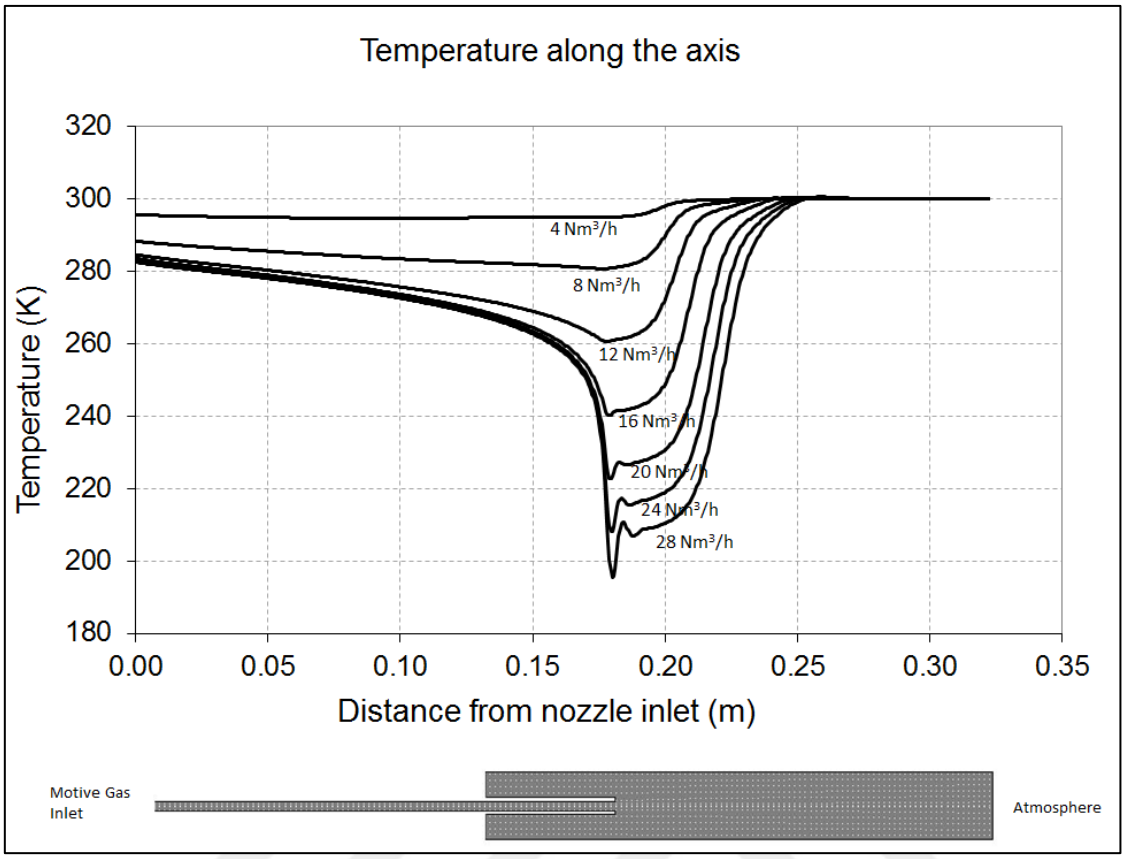

Figure 3.5. Static temperature change along the axis of the ejector

3.1.2.5. Static pressure along the inside wall of the ejector

At Fig.3.6, static pressure values at the inside wall of the ejector are shown which represents the pressure difference generated by the ejector. This figure shows also maximum vacuum level occurred at closed side at the ejector which is constant up to the distance of approximately 0.19 m that is just a little bit beyond the nozzle exit. After the position of 0.19 m, static vacuum pressure decreases continuously and reaches to atmospheric pressure at the position of 0.27 m.

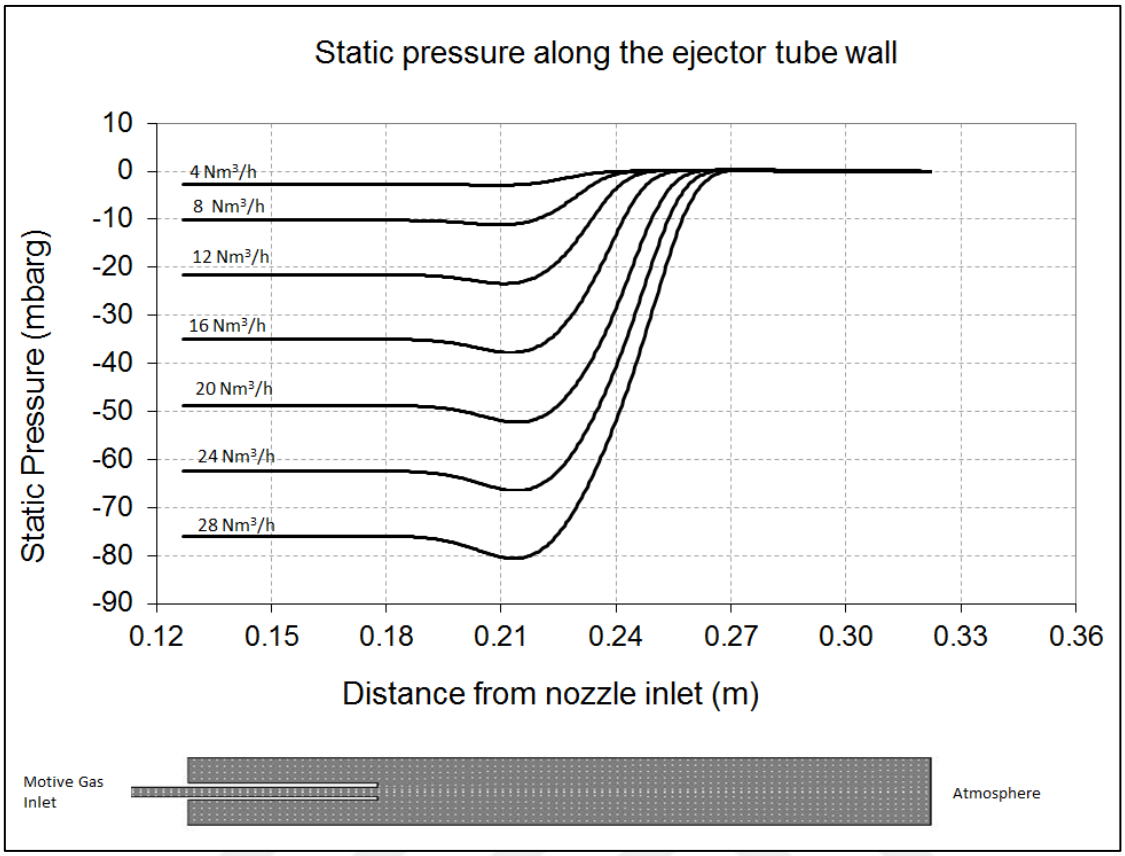

Figure 3.6. Static pressure along the inside wall of the ejector

3.1.2.6. Density along the axis of the ejector

At Fig.3.7, density changes along the axis of the ejector are shown. At the inlet of the ejector nozzle, the pressure level is maximum and it decreases gradually to the exit of the nozzle because, acceleration of the fluid causes to the decrease of the static pressure and it lowers the density of the fluid. In contrast with the other thermodynamic properties, densities at the nozzle exit are not much different from each other. The densities at the nozzle exit are 1.2 kg/m^3 and 2 kg/m^3 for the motive gas flow rate of 4 Nm^3/h and 28 Nm^3/h, respectively.

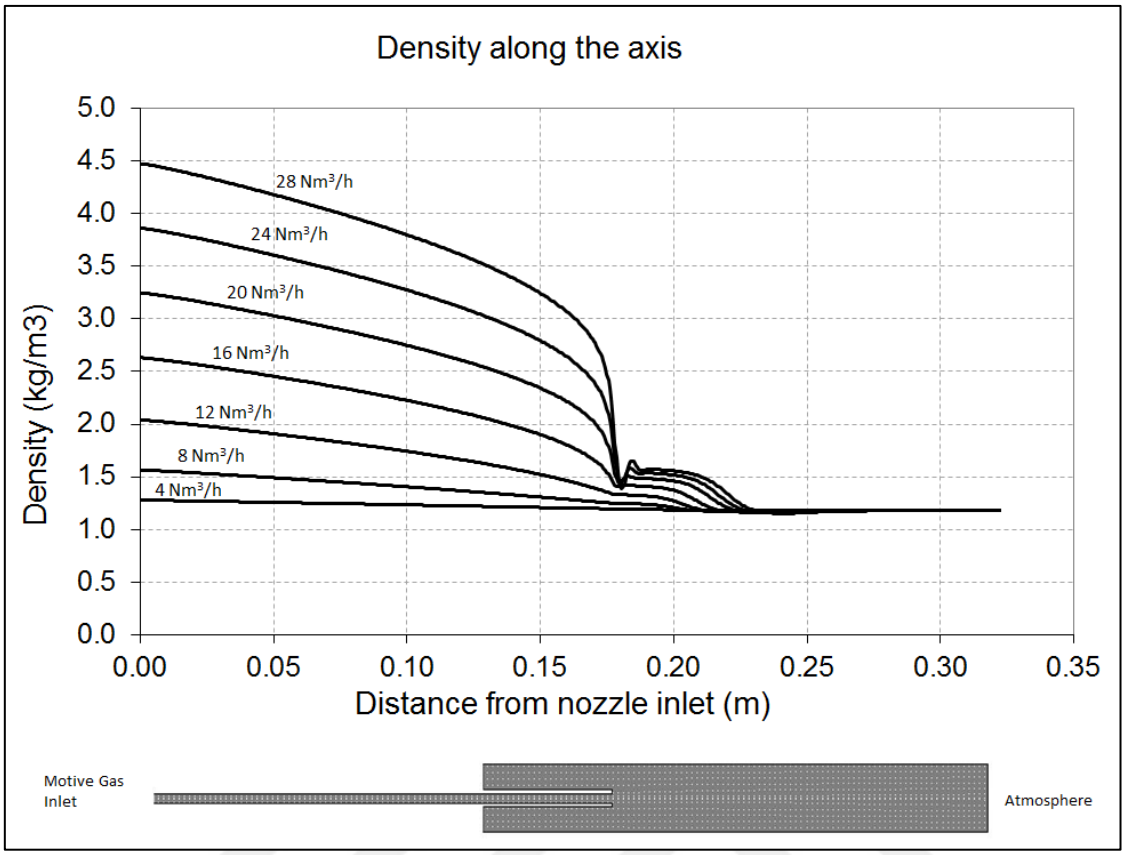

Figure 3.7. Density along the axis of the ejector

3.1.2.7. Thermodynamic properties through the axis

Changes of related thermodynamic properties along the axis and side wall are summarized at Table 3.2. As increasing the flowrate of the motive air from 4 Nm^3/h to 28 Nm^3/h, vacuum pressure level is increasing from 2.7 mbar to 75.9 mbar. Required nozzle inlet pressure is also increasing from 7.1 kpa to 261.7 kpa.

Table 3.2. Thermodynamic Properties through the Axis with 7 Different Flow Rates

V (Nm^3/h)	P_{vacuum} (mbar) Fluent results	Static Pressure (kPa) @ Nozzle Inlet	Velocity Magnitude (m/s) @ Nozzle Exit	Mach Number @ Nozzle Exit	Temperature (K) @ Nozzle Exit	Density (kg/m^3) @ Nozzle Exit
4	2.7	7.1	115.0	0.33	295.0	1.2
8	10.2	28.0	219.0	0.65	281.0	1.2
12	21.6	65.2	304.0	0.94	260.0	1.3
16	35.0	112.8	365.0	1.18	240.0	1.4
20	48.8	162.6	410.0	1.37	223.0	1.7
24	62.4	212.2	444.0	1.54	208.0	1.8
28	75.9	261.7	472.0	1.68	195.0	2.0

Velocity magnitude at nozzle exit is increasing from 115 m/s to 472 m/s and Mach number is also increasing from 0.33 to 1.68. Temperature is decreasing from 295 K to 195 K with compressible flow effect. Density is increasing at nozzle exit from 1.2 kg/m^3 to 2.0 kg/m^3 with the decrease of temperature and slightly increase of static pressure (-0.2 kpag to 34.9 kpag) at the exit of nozzle.

3.1.3. CFD model validation with positive pressure conditions

Previous investigation was carried out for the vacuum pressure effect of the ejector. There is also positive pressure effect. In order to investigate this effect, ejector nozzle was placed as shown in Fig.3.8. Compressed air flow rate was measured with mass flow controller (mfc) then supplied to ejector nozzle. A differential pressure transmitter was used for measuring the positive pressure with respect to atmospheric pressure. Experimental and fluent results for 7 different flow rates are shown in Table 3.3 and Fig.3.9.

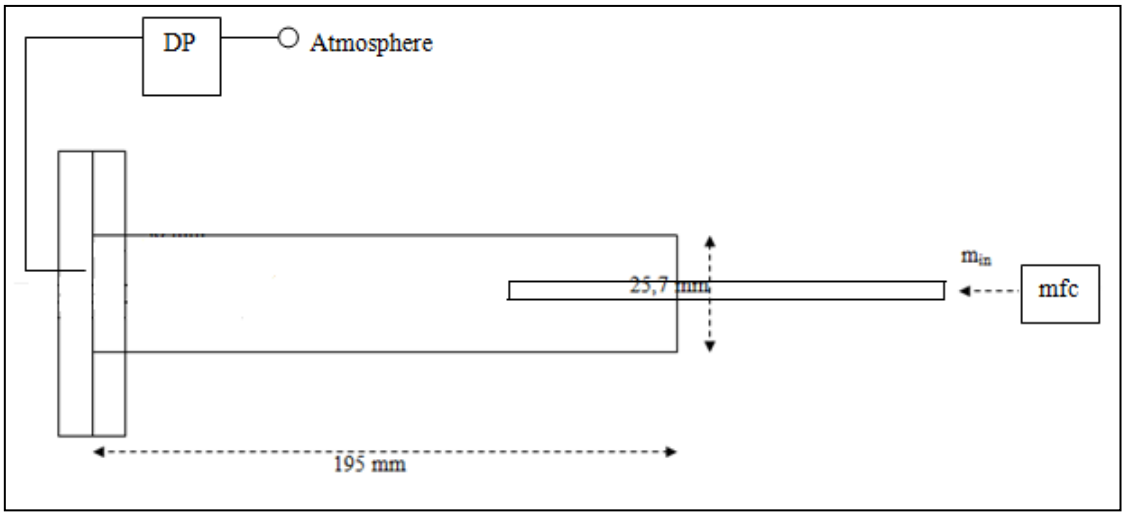

Figure 3.8. Apparatus for Positive Pressure Effect Investigation

Similar to the previous experiments carryout out for vacuum effect, 7 different flow rates between 4 Nm^3/h to 28 Nm^3/h were investigated. As seen from the table, maximum deviations of CFD results from the experimental results for 0.5 mm and 1 mm mesh size solutions are -4.5% and -6.6%, respectively. The average of the absolute deviation of the all positive pressure levels are 3.13% and 4.37% for 0.5 mm and 1 mm mesh sizes, respectively. It is also quite acceptable for analyzing real conditions with CFD model without considerable accuracy loss.

Table 3.3. CFD validation results for 7 different operating conditions (positive pressure)

V (Nm^3/h)	P_{vacuum} (mbar) Experimental results	$P_{positive}$ (mbar) experimental results	$P_{positive}$ (mbar) Fluent results with 0.5 mm mesh	Deviation % @0.5 mm mesh	$P_{positive}$ (mbar) Fluent results with 1 mm mesh	Deviation % @1 mm mesh
4	2.8	3	2.9	-4.3%	2.9	-5.0%
8	10.2	11	10.8	-1.5%	10.8	-1.9%
12	21	23	22.7	-1.2%	22.6	-1.7%
16	35	38	36.9	-2.8%	36.6	-3.8%
20	49	54	51.8	-4.1%	51.0	-5.6%
24	63	70	66.9	-4.5%	65.4	-6.6%
28	76	85	82.0	-3.5%	79.9	-6.0%

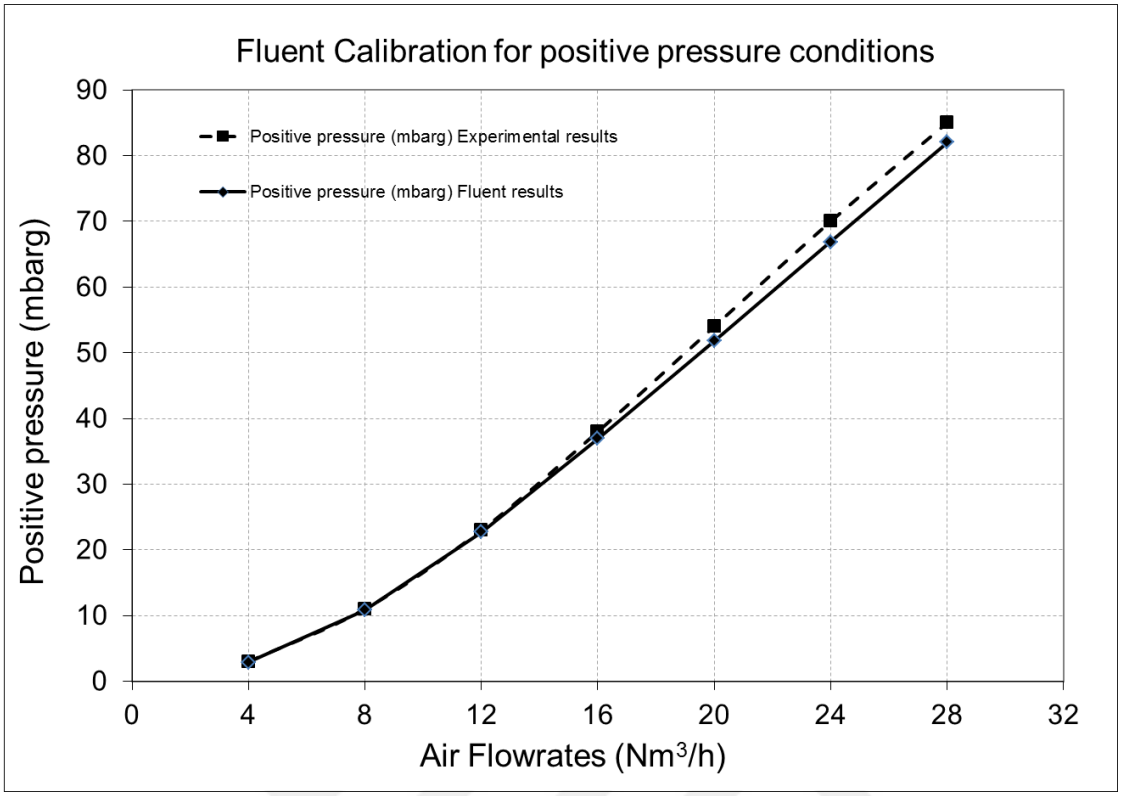

Figure 3.9. Experimental and Fluent Results for Positive Pressure (0.5 mm mesh size)

It was also realized that, for both experimental and CFD results, there was considerable difference between the magnitude of the vacuum pressure effect and the positive pressure effect of the ejector. As seen from the Table 3.3, according to the experimental data, vacuum pressure level is 76 mbar and the positive pressure is 85 mbar for the flow rate of 28 Nm^3/h conditions. This situation will be evaluated at subsequent section in detail.

3.1.4. Ejector analysis with CFD (both side open)

Previous investigations were carried out for analyzing the maximum vacuum pressure and positive pressure effect of the ejector. In order to do that, left side of the ejector tube was closed. At this study, both side of the ejector was opened in order to investigate the entrainment effect and looking for the point where the maximum vacuum or positive pressure levels were reached.

Fan (air blower) operation analogy can be made for these situations. If there is no restriction at the inlet and outlet of a fan, it provides the maximum air flow rate. If there

is a restriction at the inlet of the fan, it provides less flow rate and higher vacuum level at the inlet. The maximum vacuum level is reached when the inlet of the fan is completely closed. This is same for the positive pressure level as the maximum positive pressure is reached when the outlet of the fan is closed.

With fan analogy point of view, ejector was investigated for maximum vacuum and positive pressure levels. At this section, some induced air flow is allowed to flow with specific restriction (back pressure) at the outlet of the ejector.

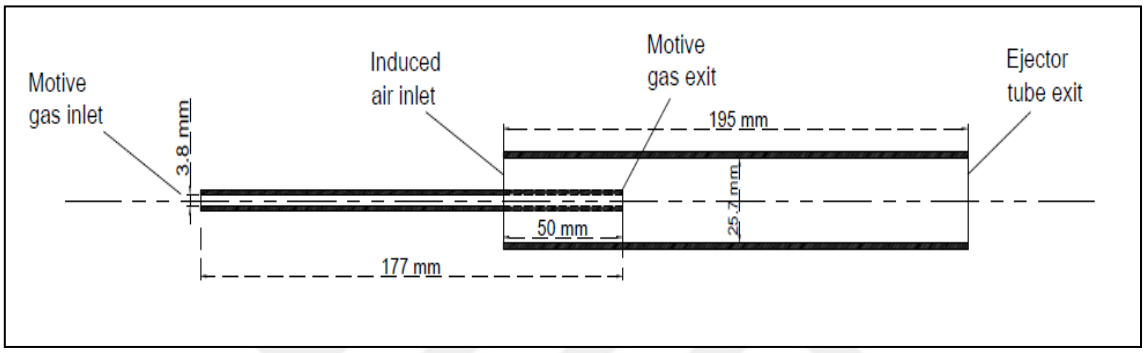

Figure 3.10. Ejector Model (both side open) for Entrainment Analysis with CFD Model

Ejector model drawing for entrainment analysis with CFD model is shown in Fig.3.10. As shown in figure, both side (left anf right) of the ejector is open and left side is induced air entrance and right side is the outlet of the total flow (motive and induced) where back pressure is applied.

At first CFD test, for zero back pressure and 28 Nm3/h air flow rate conditions, it was realized that ejector length is not enough for reaching the fully developed flow at the exit of the ejector as shown in Fig.3.11, (shown with dashed circle). At that situation, induced air flow rate is 137.8 Nm^3/h.

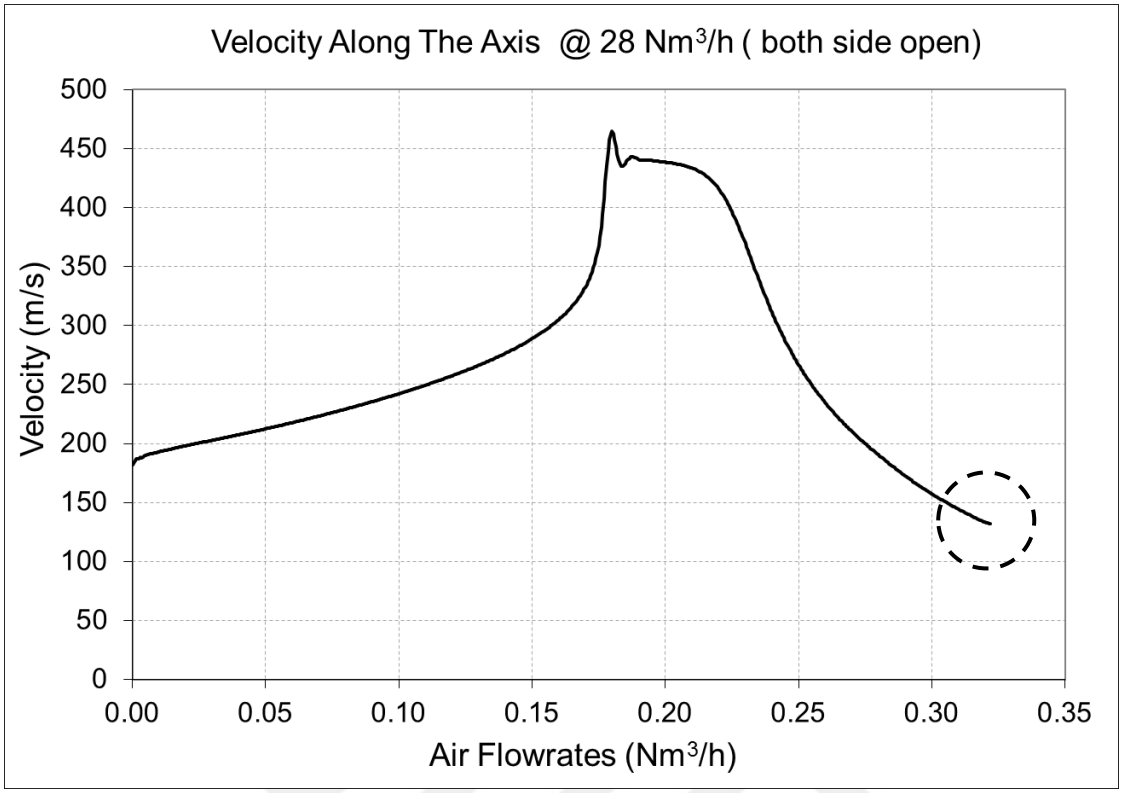

Figure 3.11. Velocity Profile Along the Axis of the Ejector (both side open–zero back pressure)

In order to make flow fully developed at the exit of the ejector and investigate the effect of ejector length to vacuum effect, new ejector was modeled which was 100 mm longer than the original one. The velocity profile with new ejector is shown in Fig.3.12.

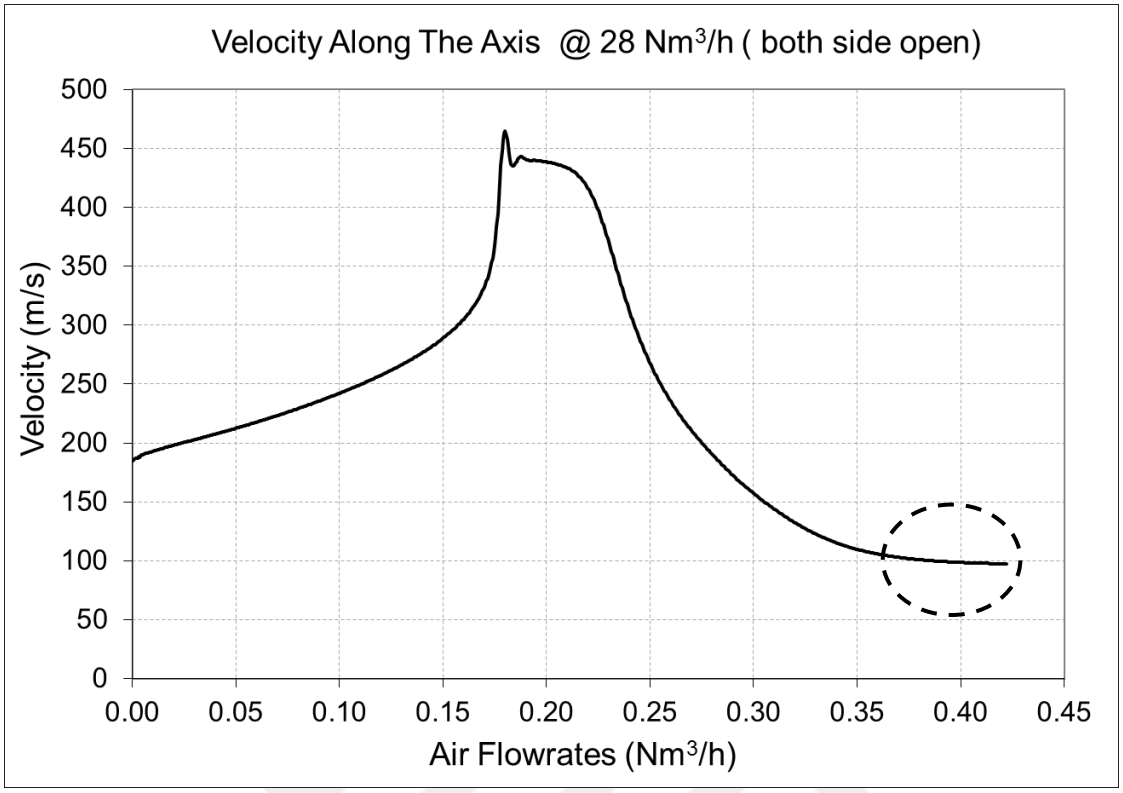

Figure 3.12. Velocity Profile Along the Axis of the Ejector (295 mm ejector length)

As shown with dashed circle, fully developed flow was reached with new ejector. However, induced air flow rate becomes 137.0 Nm^3/h. It was realized that the induced air flow rate was not sensitive to the length of the ejector or the ejector exit flow conditions, that was fully developed or not. The slightly decrease of the induced air flow rate can be explained with the additional restriction caused by the friction of the inner surface of the longer ejector.

Due to the negligible effect of ejector length on the performance, it was not required to lengthen the ejector and the entrained effect of the ejector was investigated with the reference model which is 195 mm in length.

In order to investigate the ejector behavior with various motive air flow rate and various back pressure levels applied to the ejector exit, 35 CFD test was executed for 7 different motive gas flow rates as shown in Table 3.4 and Fig.3.13.

Table 3.4. Induced air flow rates with various motive air flow rates and back pressures

Motive Air - 4 Nm^3/h					
Back Pressure (mbar)	0	0,7	1,4	2,1	2,8
Induced Air (Nm^3/h)	26.7	19.4	14.1	5.2	-3.4
Motive Air - 8 Nm^3/h					
Back Pressure (mbar)	0	3	6	9	12
Induced Air (Nm^3/h)	53.1	41.8	28.5	9.9	-19.1
Motive Air - 12 Nm^3/h					
Back Pressure (mbar)	0	6	12	18	24
Induced Air (Nm^3/h)	77.0	61.6	43.5	18.8	-21.9
Motive Air - 16 Nm^3/h					
Back Pressure (mbar)	0	9	18	27	36
Induced Air (Nm^3/h)	97.4	79.8	59.1	32	-12.2
Motive Air - 20 Nm^3/h					
Back Pressure (mbar)	0	13	26	39	52
Induced Air (Nm^3/h)	113.5	92.4	67.2	33.1	-22.8
Motive Air - 24 Nm^3/h					
Back Pressure (mbar)	0	16	32	48	64
Induced Air (Nm^3/h)	126.6	104.4	77.8	42.1	-14.2
Motive Air - 28 Nm^3/h					
Back Pressure (mbar)	0	20	40	60	80
Induced Air (Nm^3/h)	137.8	113.0	82.9	41.8	-22.9

As shown data in Table 3.4, first tests for 7 different motive gas flow rates were with zero back pressure conditions. This value is the maximum achievable induced gas flow rate. Maximum induced air flow rate was achieved as 137.8 Nm^3/h with 28 Nm^3/h motive air and minimum induced air flow rate is 26.7 Nm^3/h with 4 Nm^3/h motive air flow rate with no back pressure applied to the exit of the ejector.

After the first tests, back pressure was applied to the exit of the ejector and increased gradually with different incremental ratios for each motive air flow rates which were 20 mbar and 0.7 mbar for 28 Nm^3/h and 4 Nm^3/h motive gas flow rates, respectively.

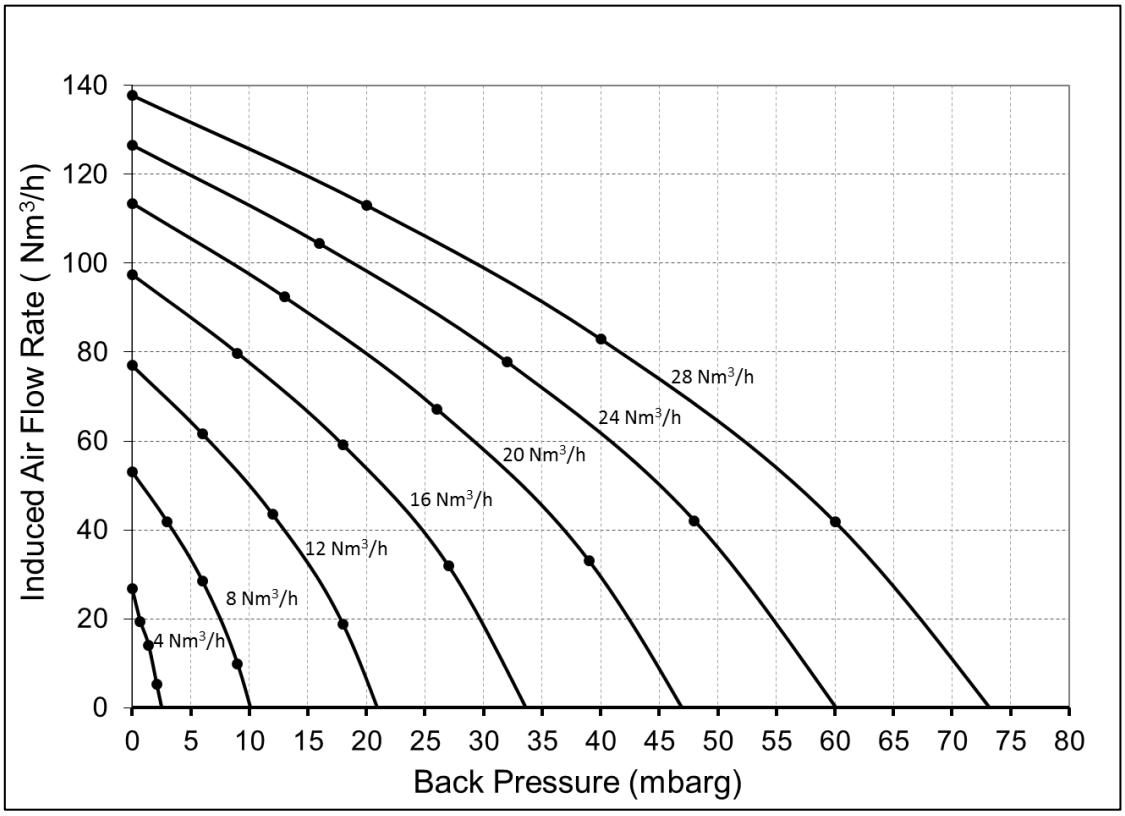

Figure 3.13. Motive Air Flow Rate & Back Pressure Chart

3.1.4.1. Comparison of maximum vacuum pressure & back pressure without induced flow

With using the data shown in Table 3.4, induced air flow rate, motive air flow rate and back pressure chart was formed as shown in Fig.3.13. Just like the fan analogy mentioned previously, the induced air flow rates were decreasing with the increase of back pressure levels. It was also realized that the back pressure levels where zero

induced flow rate was observed, was approximately same with the maximum vacuum pressure levels observed at the previous maximum vacuum pressure tests where the left side of the ejector (induced air entrance in this study) was completely closed. Comparison of the results of the maximum vacuum pressure investigation and back pressure levels where zero induced flow is shown in Table 3.5.

Table 3.5. Comparison of Maximum Vacuum Pressure & Back Pressure with No Induced Flow

Motive Air Flow Rate (Nm3/h)	Maximum Vacuum Pressure With Closed Entrance (mbar)	Back Pressure With No Induced Air Flow Rate (mbar)
4	2.7	2.5
8	10.2	10.1
12	21.6	20.9
16	35.0	33.6
20	48.8	46.9
24	62.4	60.1
28	75.9	73.2

According to the results, it is logical to assume maximum vacuum pressure represents the back pressure level where zero induced gas flow rate conditions are occurred. This assumption made CFD analysis easier with regard to required solution time. Because, it was realized that analysis of both side open ejector CFD analysis require much more time than the one side open ejector.

3.1.4.2. Comparison of maximum positive pressure & back pressure with reverse flow

There is also another similarity for the positive pressure condition where the motive gas was fed to the ejector tube from the right side of the ejector. It was realized during the back pressure analysis for both side open ejector, when the reverse flow inside the

ejector was same with the flow rate of motive gas flow, required back pressure level was approximately same with the positive pressure value for one side closed ejector. This is because the similar condition due to the reverse flow during the one side closed ejector. Comparison of the results of the maximum positive pressure investigation and back pressure levels is shown in Table 3.6.

Table 3.6. Comparison of Maximum Positive Pressure & Back Pressure with Reverse Flow (equal to motive gas flowrate)

Motive Air Flow Rate (Nm3/h)	Maximum Positive Pressure With Closed Exit (mbar)	Back Pressure With Rverse Flow Equal to Motive Gas Flow Rate (mbar)
4	2.9	2.9
8	10.8	10.8
12	22.7	22.6
16	36.9	36.7
20	51.8	51.5
24	66.9	66.5
28	82.0	81.4

3.1.4.3. Entrainment ratio

Entrainment ratio that is defined as the ratio of induced gas to the motive gas flow rate was also investigated with zero back pressure conditions. Results are shown in Table 3.7 and Fig.3.14. It was realized that the entrainment ratio was decreasing with the increase of motive air flow rate.

Table 3.7. Entrainment Ratios for Both Side Open Ejector at Zero Back Pressure Conditions

V (Nm^3/h)	Entrainment Ratio, m_i/m_m, P_{back} = 0 mbar
4	6.7
8	6.6
12	6.4
16	6.1
20	5.7
24	5.3
28	4.9

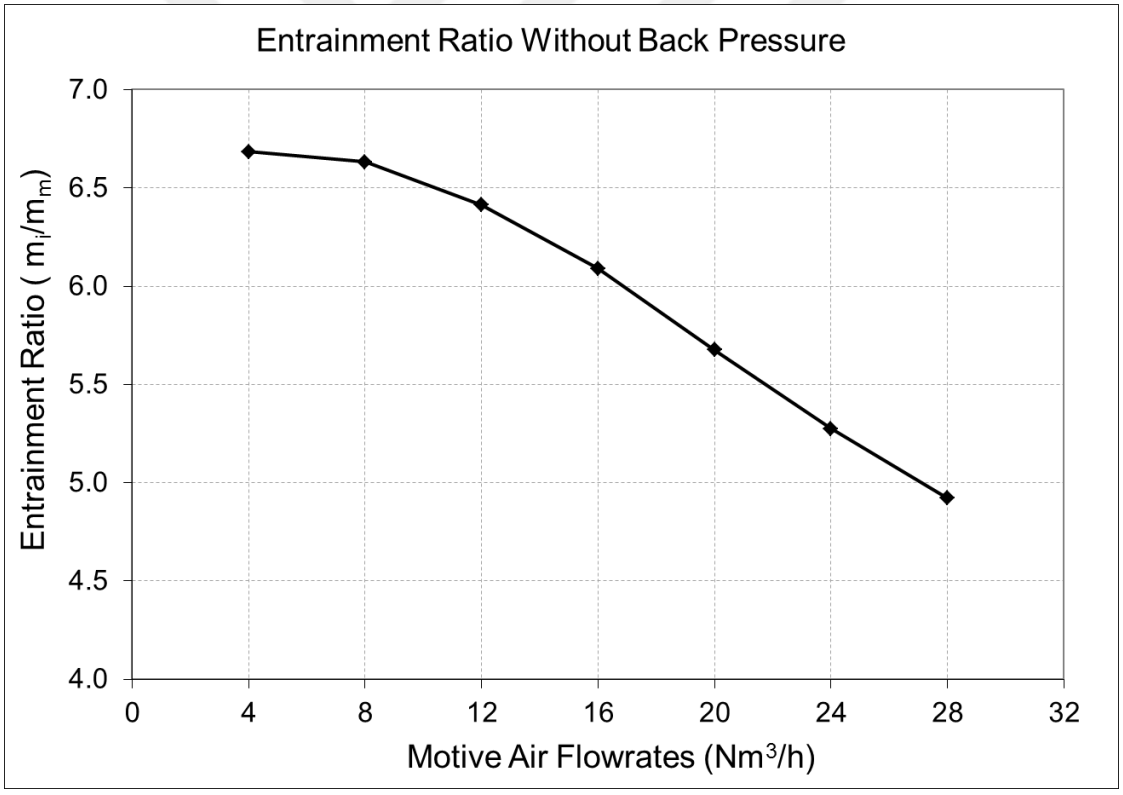

Figure 3.14. Entrainment Ratios for Different Motive Air Flow Rates with Zero Back Pressure

The decrease of the entrainment ratios is explained by the difference between the motive gas velocity and the induced gas velocity [47]. It was realized that, when the

difference between the motive gas and induced gas velocity increases, the efficiency of the ejector decreases i.e. the entrainment ratio decreases.

3.1.5. Flow profiles of motive gas through the ejector tube

Flow profile of motive gas obtained by the CFD analyses is shown in Fig.3.15. Due to the shear forces caused by the high speed motive gas flow at the nozzle exit, there are severe vortices occurred inside the ejector tube which is torus in shape. This flow profile is important for the conditions investigated experimental study. In experimental studies for higher solid flux (Case II), solid column formation was observed just above the nozzle exit and this situation was explained with resistance to the solid flow caused by the severe vortices.

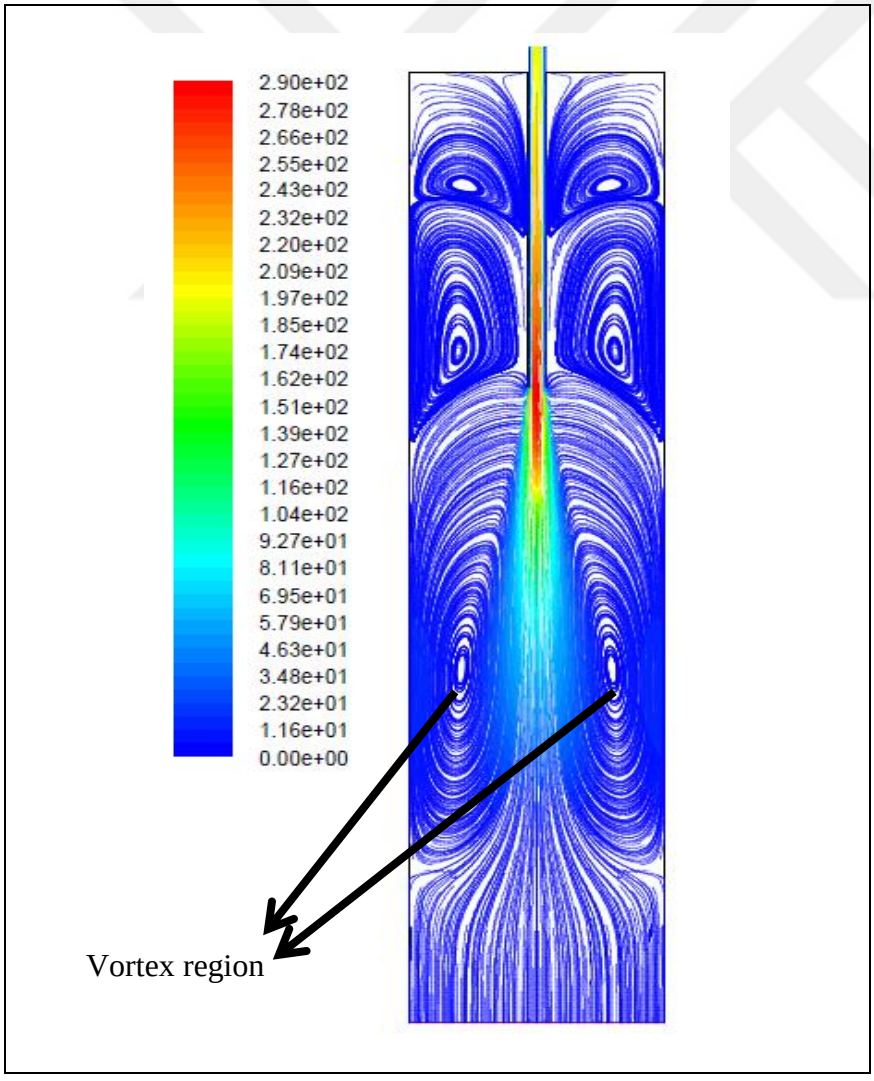

Figure 3.15. Flow profile of motive gas (colors represent velocity magnitude)

3.1.6. CFD results for different operational and geometric ejector design parameters

In order to improve ejector performance, CFD model was used. Operational and geometric parameters which affect the ejector performance were determined and these parameters were considered as the CFD model parameters. Vacuum pressure occurred due to the entrainment effect was considered as the ejector performance which was considered as better when the static vacuum pressure level generated by the ejector was higher.

3.1.6.1. Ejector type: Central nozzle vs. Radial nozzles

There are two types of ejector investigated with CFD model which are central and radial ejectors. At central ejector, there is one nozzle located at the center of the ejector tube and it is parallel to the vertical axis. At radial ejector, there are multiple nozzles located at the ejector tube wall and inclined at an angle of 30° with the vertical axis. The CFD results for both ejector types at 7 different motive gas flowrates are shown in Table 3.8.

Table 3.8. CFD results of ejector types for different motive gas flowrates

Motive gas flowrate (Nm^3/h)	P_{vacuum} (mbar) - Central Nozzle	P_{vacuum} (mbar) - Radial Nozzles
4	2.8	2.5
8	10.2	10.0
12	21.0	21.0
16	35.0	35.0
20	49.0	48.0
24	63.0	61.0
28	76.0	73.0

According to the CFD results, vacuum pressure generated by the ejectors is very close to each other. Central ejector is slightly higher than the radial ejector as shown in Fig.3.16.

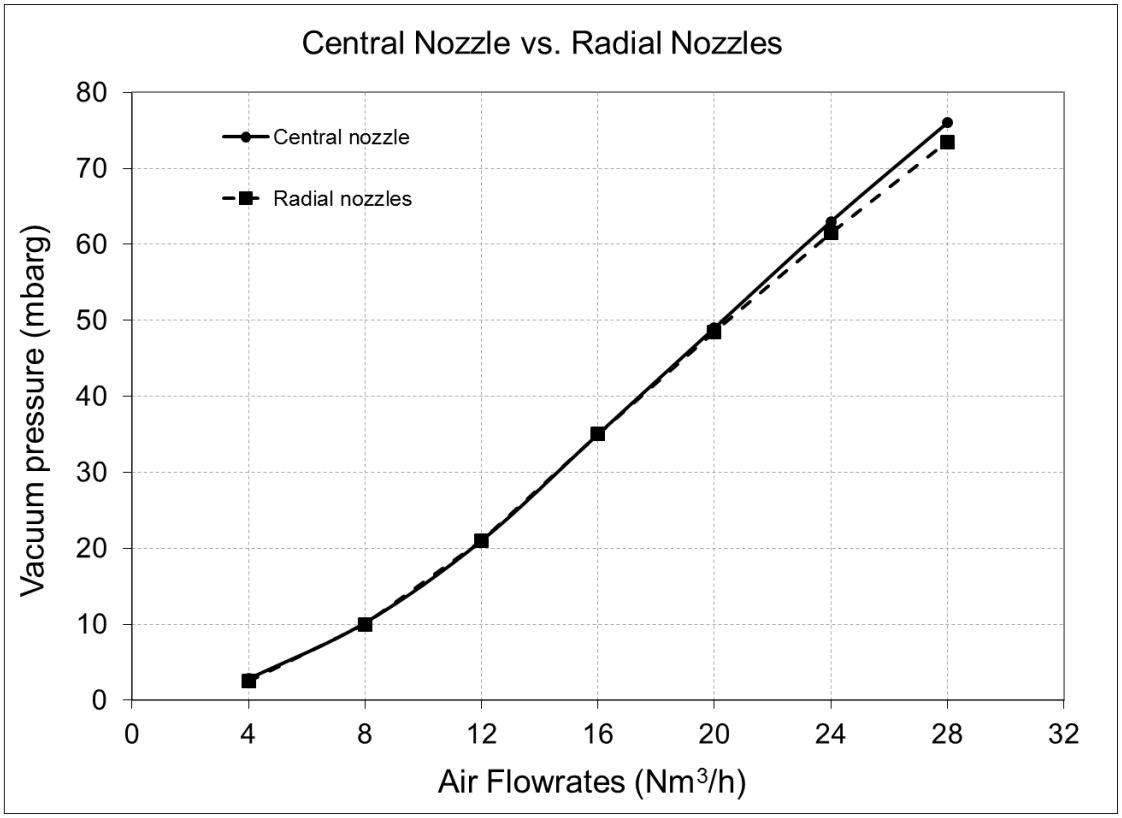

Figure 3.16. Comparison of ejector types performance

It should be taken into account that the total cross-section area of the ejector nozzle exit of both type ejector are same which means the exit velocities of motive gas are same. Even though the performance of both ejectors are very close to each other, radial type ejector have drawback related to the particle flow. Due to the inclined nozzles of radial ejector, particles passing through the ejector tube can hit the wall of ejector tube and may cause wear at ejector tube wall.

3.1.6.2. Effect of ejector length

Ejector tube length is defined as the distance between the ejector nozzle exit and the ejector tube exit. CFD results show that, there is a limiting ejector length above which ejector performance does not change considerably and below which it drops steeply.

This length depends on ejector nozzle exit velocity. Hence, the limiting ejector length increases with increasing flow rate. The results are shown in Table 3.9 and Fig.3.17.

Table 3.9. Ejector tube length effect on ejector performance

Vacuum Pressure (mbar)		**Ejector Length (mm)**						
		25	**50**	**75**	**100**	**125**	**150**	**175**
Motive Air (Nm^3/h)	**4**	0.0	1.3	2.7	2.7	2.7	2.7	2.7
	8	0.1	4.1	10.2	10.2	10.2	10.2	10.2
	12	0.1	6.5	21.3	21.6	21.6	21.6	21.5
	16	0.1	7.3	33.3	35.1	35.0	35.0	35.0
	20	0.1	7.3	41.3	48.9	48.8	48.8	48.8
	24	0.1	8.4	48.2	62.5	62.4	62.4	62.4
	28	0.1	9.7	54.1	76.0	76.0	75.9	75.8

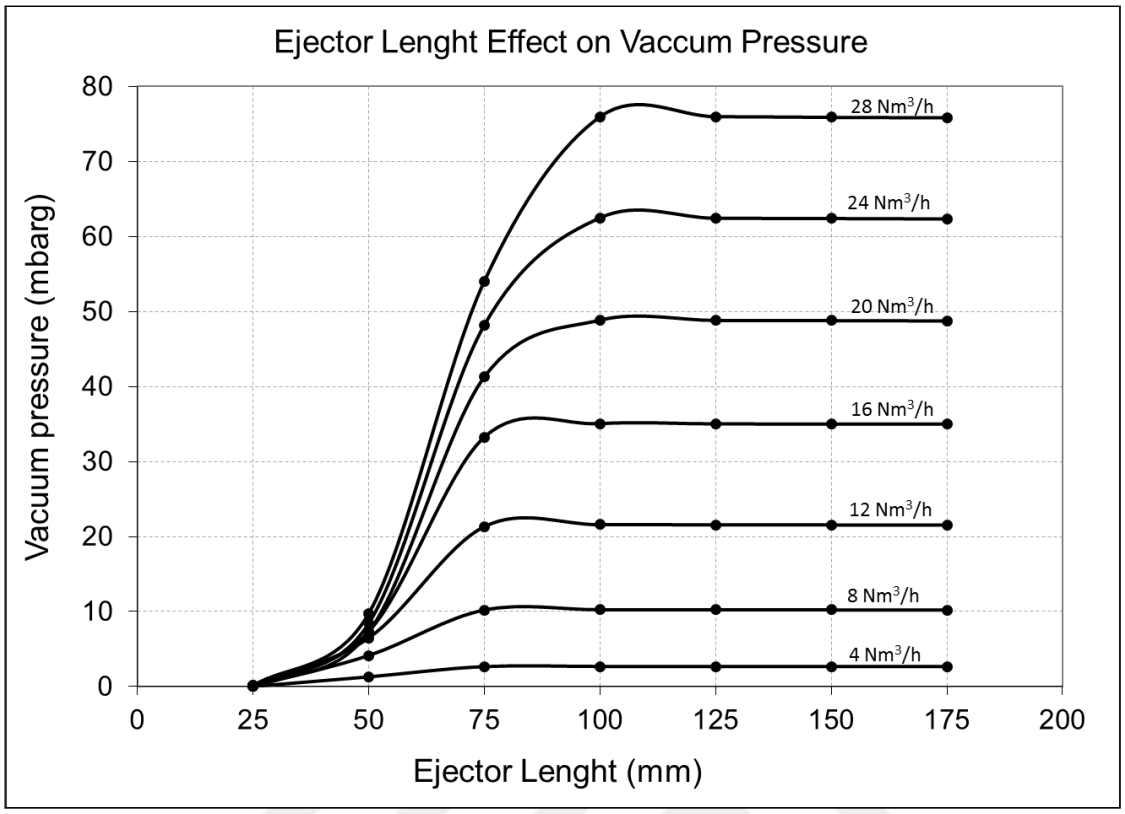

Figure 3.17. Ejector tube length effect on ejector performance

Above the ejector tube length of 100 mm for all motive gas flowrates, ejector performance does not change with the change of ejector length. For lower motive gas flowrates (4 – 16 Nm^3/h) this limit is 75 mm. It could be concluded that there is a lower limit of ejector tube length which depends on the ejector motive gas flowrate or ejector nozzle exit velocity. Above this lower limit of length, the performance does not change significantly.

3.1.6.3. Effect of motive gas flowrate

CFD results show that the vacuum level of ejector system is almost linearly proportional to the motive gas flow rate as shown in Table 3.10 and Fig.3.18. The calculated ejector nozzle exit gas velocities indicate that all flow rates of motive gas are in compressible region (Mach number > 0.3). Due to the effect of compressibility, the effect of flow rate of motive gas becomes linearly proportional.

Table 3.10. Motive gas flowrate effect on ejector performance

V (Nm^3/h)	P_{vacuum} (mbar)
4	2.7
8	10.2
12	21.6
16	35.0
20	48.8
24	62.4
28	75.9

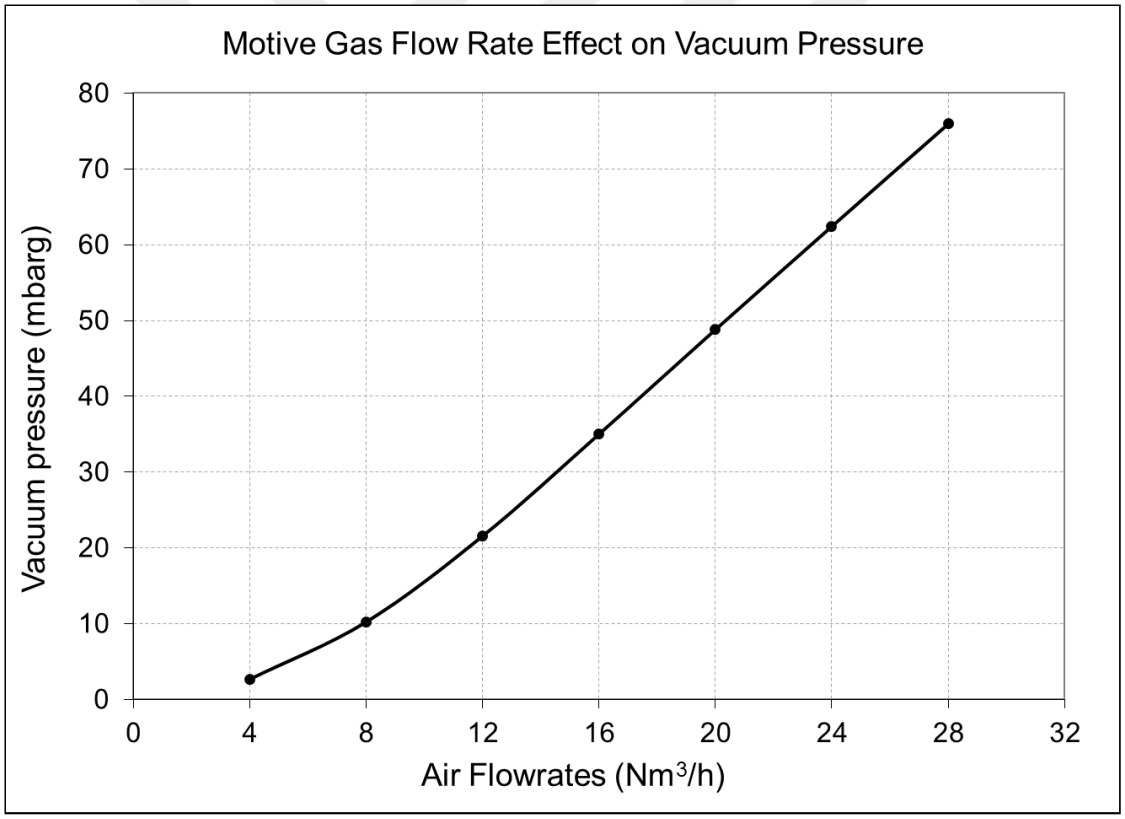

Figure 3.18. Motive gas flowrate effect on ejector performance

In fact, the vacuum pressure generated by the ejector is linearly depends on the momentum flux ($kg/m.s^2$) of motive gas at ejector nozzle exit. This relation is going to be explained at subsequent sections (Section 3.2).

3.1.6.4. Effect of nozzle diameter

Nozzle diameter effect on vacuum pressure generated by the ejector was investigated for 5 different nozzle diameters for 1 mm to 5 mm. The results of CFD study show that exit velocity i.e. momentum of the motive gas decreases with the increase of nozzle diameter. The decrease of momentum results in the decrease of vacuum pressure as shown in Table 3.11 and Fig. 3.19.

Table 3.11. Vacuum pressures for different nozzle diameters

Vacuum Pressure (mbar)		**Nozzle Diameter (mm)**				
		1 mm	**2 mm**	**3 mm**	**3.8 mm**	**5 mm**
Motive Air (Nm^3/h)	**4**	12.3	8.2	4.2	2.7	1.5
	8	26.3	21.9	15.2	10.2	6.0
	12	40.5	35.5	28.9	21.6	13.3
	16	54.9	49.0	42.6	35.0	22.9
	20	69.3	62.4	56.1	48.8	34.6
	24	83.6	75.9	69.5	62.4	47.6
	28	97.8	89.4	82.8	75.9	61.3

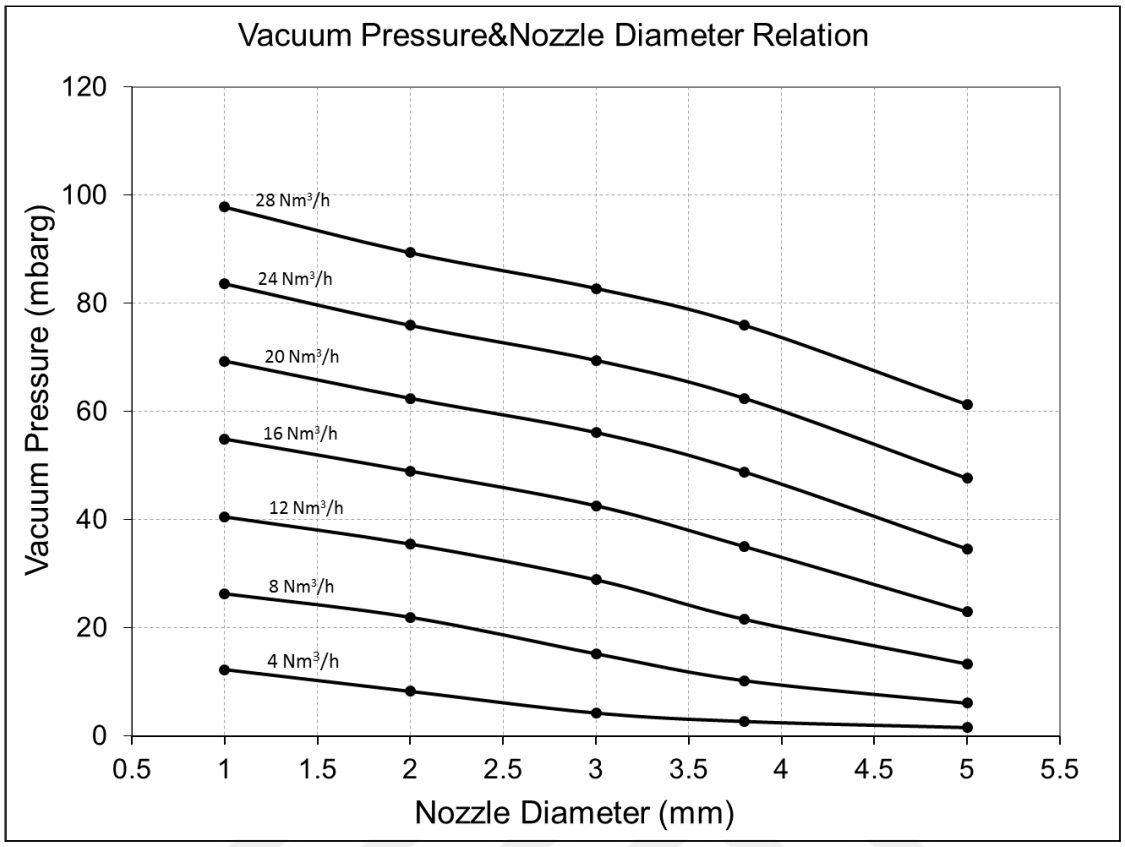

Figure 3.19. Vacuum pressures for different nozzle diameters

It can be concluded that the smallest nozzle diameter is the best for increasing the ejector performance. However, the nozzle inlet pressure of the motive gas also has to be taken into account. The motive gas inlet pressure change with the change of nozzle diameter is shown in Table 3.12 and Fig.3.20.

Table 3.12. Nozzle inlet pressure change with nozzle diameter

Nozzle Inlet Pressure (bar)		Nozzle Diameter (mm)				
		1	**2**	**3**	**3.8**	**5**
Motive Air (Nm^3/h)	**4**	10.1	1.4	0.2	0.1	0.02
	8	20.3	3.6	0.9	0.3	0.1
	12	30.1	5.7	1.7	0.7	0.2
	16	39.8	7.8	2.6	1.1	0.3
	20	49.4	9.8	3.4	1.6	0.5
	24	58.9	11.9	4.3	2.1	0.7
	28	68.4	13.9	5.1	2.6	1.0

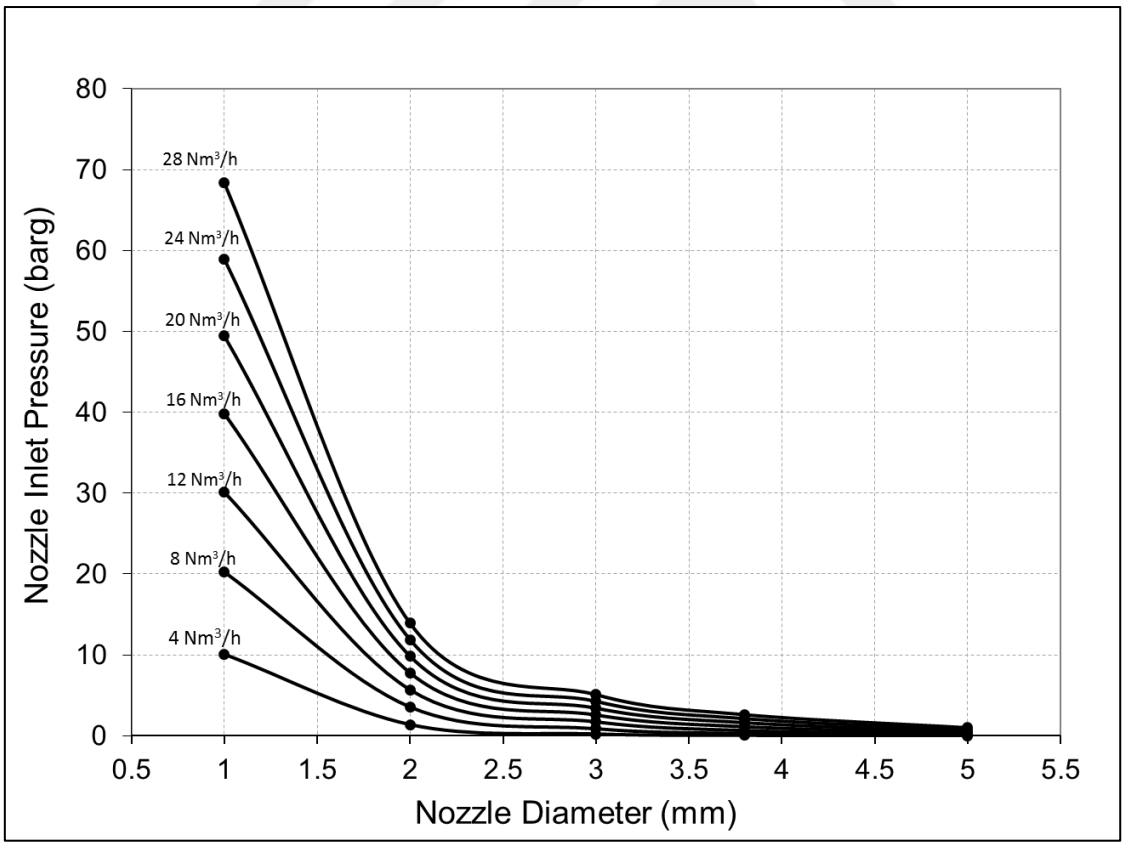

Figure 3.20. Nozzle inlet pressure change with nozzle diameter

For 28 Nm^3/h motive gas flowrate condition, the vacuum pressures are 61.3 mbar and 97.8 mbar for 5 mm and 1 mm nozzle diameters, respectively. However, the motive gas supply pressures are 1.0 barg and 68.4 barg for 5 mm and 1 mm nozzle diameters, respectively. In other words, 60% increase of ejector performance prerequisites 68 times increase of the supply pressure of motive gas. These results show that vacuum level and motive gas supply pressure have to be taken into account together in order to determine the optimum nozzle diameter.

3.1.6.5. Effect of ejector tube diameter

Vacuum pressure generated by the ejector is decreasing nonlinearly with the increase of ejector tube diameter and the rates of changes are very sensitive to the ejector tube diameter changes as shown in Table 3.13 and Fig.3.21. These results show that the vacuum pressure is approximately inversely proportional to the square of the ejector tube diameter i.e. ejector tube cross-section area.

Table 3.13. Vacuum pressures for different ejector tube diameters

Vacuum Pressure (mbar)		**Ejector Diameter (mm)**				
		15	**20**	**25.7**	**30**	**35**
Motive Air (Nm^3/h)	**4**	7.4	4.3	2.7	2.0	1.5
	8	28.8	16.7	10.2	7.6	5.6
	12	61.5	35.3	21.6	15.9	11.7
	16	100.1	57.4	35.0	25.8	19.0
	20	138.4	79.7	48.8	36.0	26.5
	24	175.4	101.7	62.4	46.1	34.0
	28	211.0	123.2	75.9	56.1	41.4

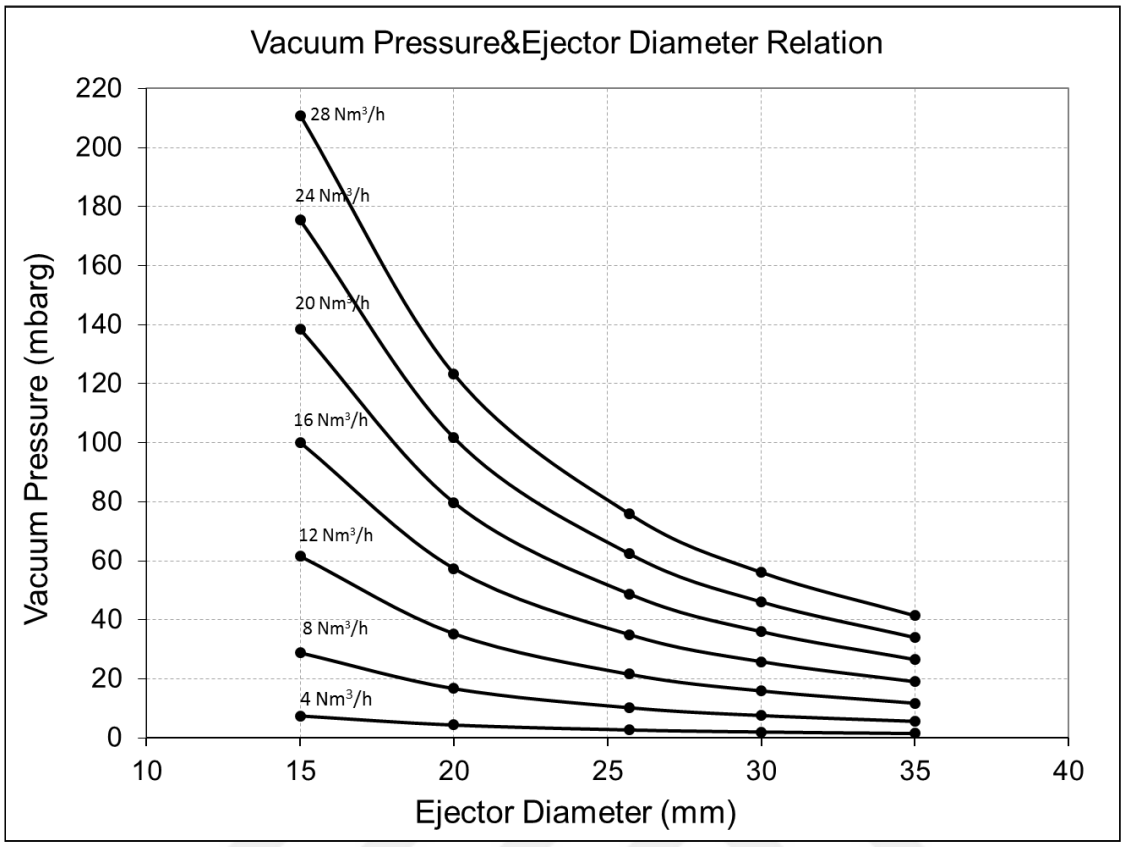

Figure 3.21. Vacuum pressures for different ejector tube diameters

It can be concluded that the smaller ejector tube diameter is better. However, the process, that ejector is applied should be taken into account. At this study, solid particles pass through the ejector tube and the ejector tube diameter should be smaller for higher ejector performance and bigger for smooth particle flow without any blockage.

3.1.6.6. Effect of induced gas static pressure

Induced gas static pressure is defined as the pressure of process where the ejector is applied. In this study, ejector is used for solid circulation at CFB system and CFB systems may be pressurized depending on the process product or application. In this section, effect of process pressure on the vacuum pressure generated by the ejector was investigated.

Table 3.14. Vacuum pressures for different induced gas pressures

Vacuum Pressure (mbar)		Induced Gas Pressure (bara)				
		1	**3**	**5**	**7**	**9**
Motive Air (Nm^3/h)	**4**	2.7	0.9	0.5	0.4	0.3
	8	10.2	3.6	2.2	1.6	1.2
	12	21.6	8.1	4.9	3.5	2.7
	16	35.0	14.2	8.7	6.2	4.9
	20	48.8	21.9	13.5	9.7	7.6
	24	62.4	30.9	19.2	13.9	10.9
	28	75.9	41.2	26.0	18.8	14.7

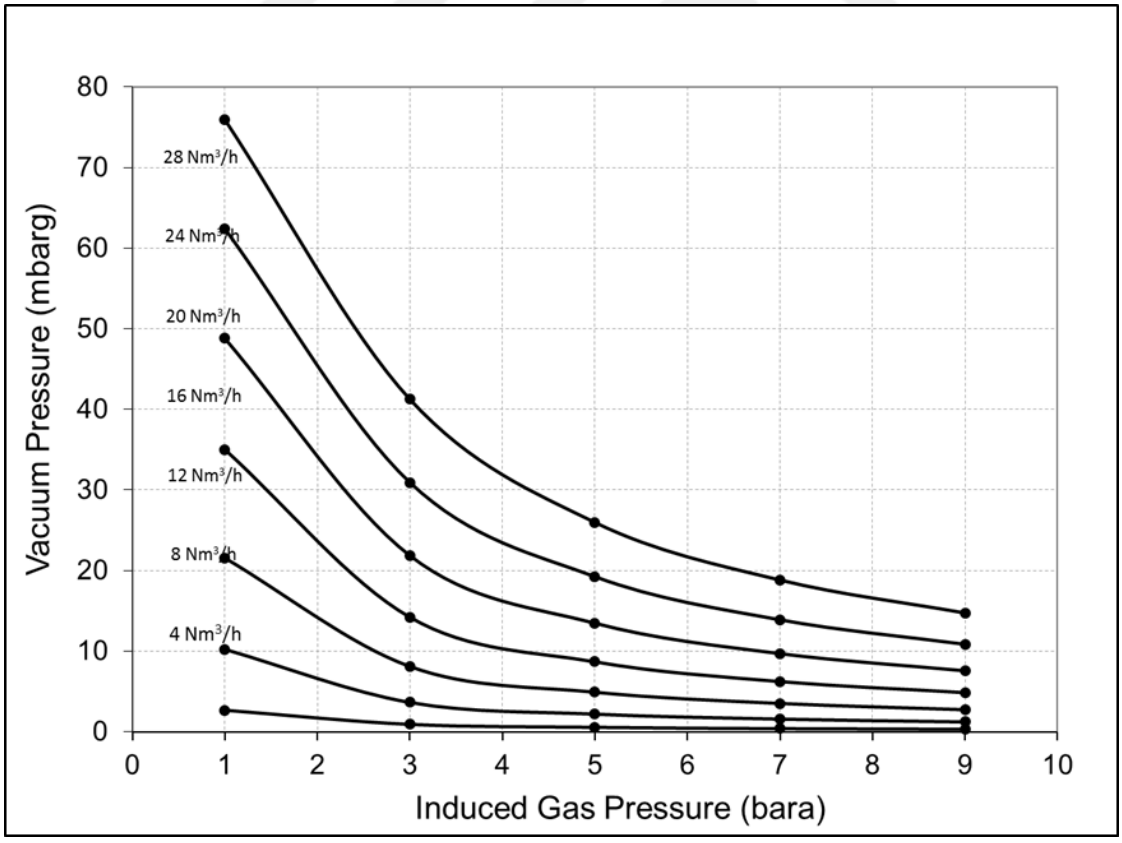

Figure 3.22. Vacuum pressures for different induced gas pressures

It was concluded that the vacuum pressure generated by the ejector is directly proportional to the momentum of the motive gas at the exit of the ejector nozzle exit. When the pressure of induced gas or process pressure is higher, the volumetric flow of motive gas for constant mass flowrate becomes lower and velocity or momentum of motive gas at the exit of ejector nozzle exit becomes lower. Due to the lower momentum of motive gas, vacuum pressure generated by the ejector becomes lower, as shown in Table 3.14 and Fig.3.22.

3.1.6.7. Effect of induced gas temperature

Temperature of the downcomer or circulating bed material is about 800-900 °C at CFB reactors (combustion/gasification), which means the ejector system located at downcomer will inevitably exposed to high temperature. In order to analyze the temperature effect on the ejector operation, 7 different temperature level (300 K to 1200 K) are investigated for 28 Nm^3/h motive gas flowrate and 5 different back pressure level (0, 40, 60, 80 mbar). At previous studies, ejector tube inlet was closed and the vacuum level was observed as the performance parameter. In this section, ejector tube inlet is opened and induced gas flows through the ejector tube by means of vacuum effect of the ejector. Relationship of the induced gas flowrate with the induced gas temperature at 28 Nm^3/h motive gas flowrate is shown in Fig.3.23.

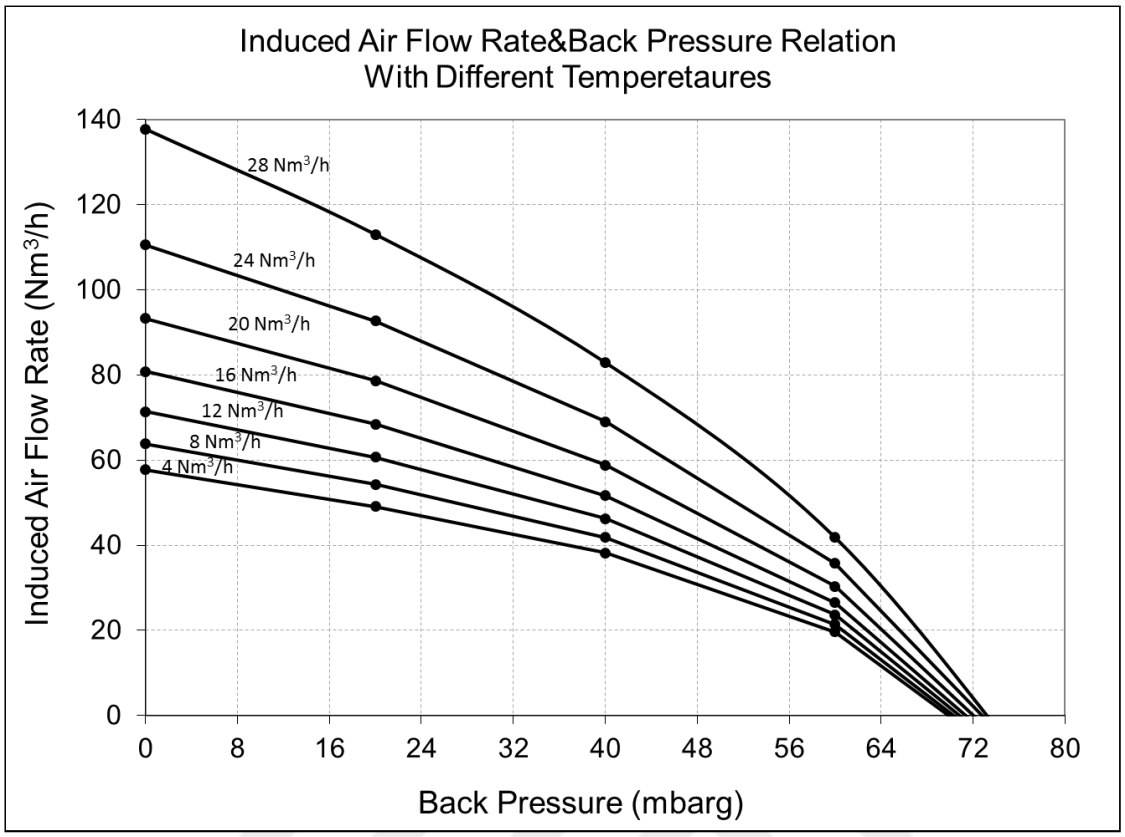

Figure 3.23. Induced air flowrate for different temperatures and back pressures

On the basis of the CFD results, it was obtained that induced gas flowrate decreases with increasing induced gas temperature. However, for each temperature, the maximum back pressure level is approximately same (72 mbar) which is close to the vacuum pressure (75.9 mbar) obtained at previous studies.

3.1.6.7. Effect of motive gas temperature

It was shown that the increase of the nozzle gas exit velocity causes the increase of the vacuum pressure generated by the ejector. If the temperature of the motive gas is increased, the volumetric flowrate of the gas is also increased and the speed of the nozzle gas exit is increased as well.

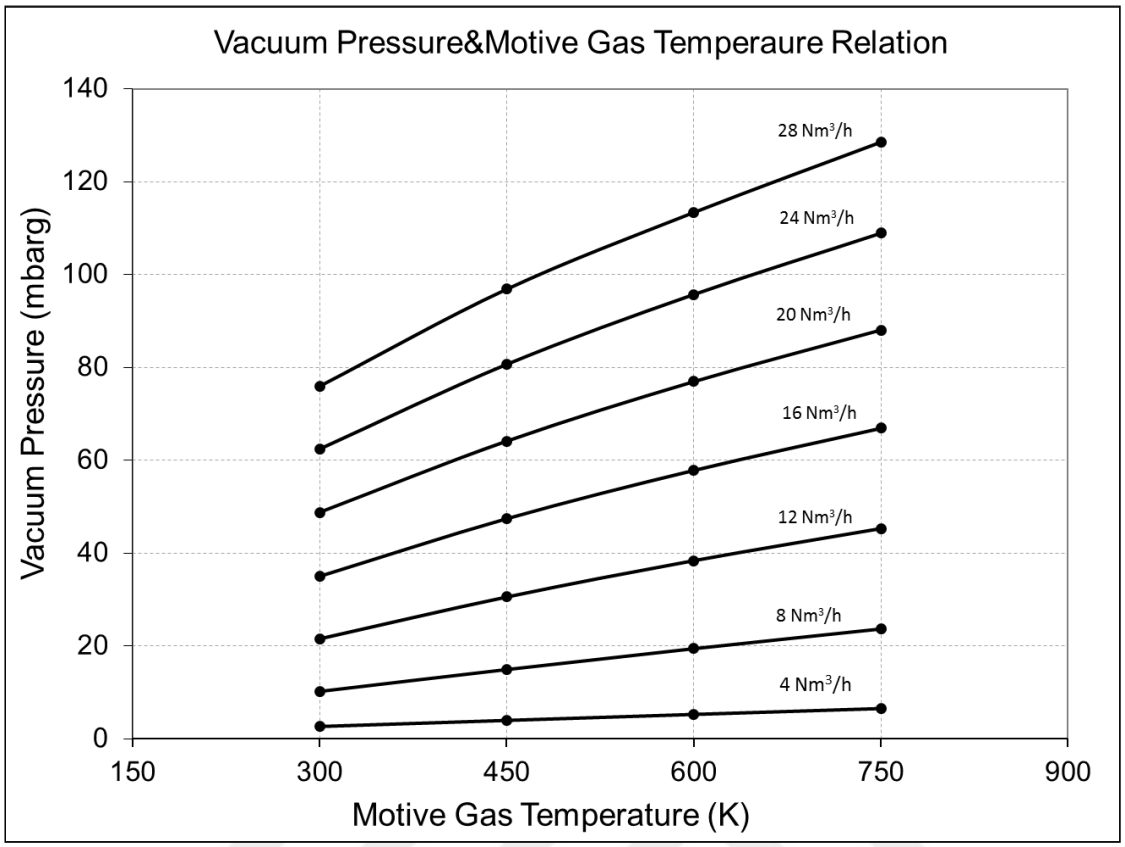

Figure 3.24. Vacuum pressures for different motive gas temperatures

In order to analyze the temperature effect of the motive gas on the ejector operation, 4 different temperature levels (300 K, 450 K, 600 K and 750 K) were investigated for 7 different motive gas flowrates. Fig.3.24 shows the relationship of the vacuum pressure with the motive gas temperature. According to the CFD results, the vacuum pressure almost linearly increases with increasing motive gas temperature. This can be explained with the increase of motive gas volumetric flowrate i.e. nozzle exit velocity with the increase of temperature.

3.2. Semi Empirical Correlation for Ejector Design

3.2.1. Vacuum pressure & motive gas momentum relation

A semi-empirical correlation was developed by using CFD results. The correlation is based on the relation between motive gas momentum flux with respect to ejector tube cross-section area and the vacuum pressure generated by the ejector system (Table 3.15). To show the relation between momentum flux and the vacuum pressure, both

parameters were transformed to the dimensionless parameter with dividing the values to the smallest ones. When the dimensionless values are compared with each other, the percentages of difference are very small and the rates of change of dimensionless values are very close to each other.

Table 3.15. Vacuum pressure & motive gas momentum relation

V (Nm^3/h)	Momentum Flux ($kg/m.s^2$)	Momentum Flux (Dimensionless)	P_{vacuum} (Pa)	P_{vacuum} (Dimensionless)	Difference (%)
4	308	1.0	267	1.0	-
8	1173	3.8	1022	3.8	0.5
12	2443	7.9	2155	8.1	1.7
16	3911	12.7	3501	13.1	3.2
20	5491	17.8	4880	18.3	2.5
24	7136	23.2	6242	23.4	0.9
28	8851	28.7	7594	28.4	-1.0

The strong relation of dimensionless vacuum pressure and the dimensionless momentum flux of the motive gas can be expressed with only equation 3.1, given below.

$$P_{vacuum} = C_D . \frac{\dot{m}.V_e}{A_D} \quad (3.1)$$

P_{vacuum} : Vacuum pressure generated by the ejector

C_D :Ejector tube diameter correction factor

$\dot{m}$: Motive gas mass flowrate (kg/s)

V_e :Motive gas nozzle exit velocity (m/s)

A_D :Ejector tube cross-section area (m^2)

where P_{vacuum} is vacuum pressure in Pascal, C_D is correction factor related to the ejector diameter which is almost constant for this situation, $\dot{m}$ is the mass flow rate of motive air in kg/s, V_e is the motive air nozzle exit velocity in m/s and A_D is the ejector

tube cross-section area in m^2. At this point, ejector nozzle exit gas velocity (V_e) needs to be determined with known input parameters using basic thermodynamic relations in order to find out maximum vacuum pressure of ejector. V_e can be expressed with the equations below.

$$V_e = \frac{\dot{V}_e}{A_d} \tag{3.2}$$

V_e Motive gas nozzle exit velocity (m/s)

$\dot{V}_e$ Volumetric flow rate of the motive gas at the exit condition of the ejector nozzle (m^3/s)

A_d Ejector nozzle cross-section area (m^2)

$$\dot{V}_e = \frac{\dot{m}.R.T_e}{P_e} \tag{3.3}$$

$\dot{V}_e$ Volumetric flow rate of the motive gas at the exit condition of the ejector nozzle (m^3/s)

R Specific gas constant (j/kg.K)

T_e Temperature of the motive gas at the exit of the ejector nozzle (K)

P_e Motive gas nozzle exit static pressure (Pa)

$$V_e = \frac{\dot{m}.R.T_e}{A_d.P_e} \tag{3.4}$$

where $\dot{V}_e$ is the volumetric flow rate of the motive gas at the exit condition of the ejector nozzle in m^3/s, A_d is the cross-section area of the ejector nozzle exit in m^2, R is the specific gas constant in J/kg.K which is assumed as constant, T_e is the temperature of the motive gas at the exit condition of the ejector nozzle in K, P_e is the static pressure of the motive gas at the exit condition of the ejector nozzle in Pa which was assumed equal to the atmospheric pressure because the boundary condition of the exit of the ejector tube was defined as atmospheric pressure in CFD studies. At this point, T_e need to be determined with the known input parameters and it can be expressed with equations below.

$$(T_a - T_e).C_p = \frac{V_e^2}{2} \tag{3.5}$$

T_a Temperature of the motive gas at the inlet of the ejector nozzle (K)

C_p Specific heat of motive gas (J/kg.K)

$$\frac{\left(\frac{\dot{m}.R}{A_d.P_e}\right)^2}{2.C_p}.T_e^2 + T_e - T_a = 0 \quad (3.6)$$

$$T_e = C_p.\left(\frac{A_d.P_e}{\dot{m}.R}\right)^2.\left(-1 + \sqrt{1 + 2.\left(\frac{\dot{m}.R}{A_d.P_e}\right)^2.\frac{T_a}{C_p}}\right) \quad (3.7)$$

where T_a is the temperature of the motive gas at the inlet of the ejector nozzle in K, C_p is the specific heat of motive gas which is assumed as constant. Equation (3.5) expresses the relation between kinetic energy and the temperature difference of motive gas which is expressed as second order polynomial equation. Mathematically, second order polynomial equations have 2 solutions, however, for the equation (3.6), one of the solutions is always less than 0 which is thermodynamically impossible because T_e is in Kelvin. Therefore, there is only one physical solution for T_e which is expressed with equation (3.7). When the equation (3.7) is substituted to the equation (3.4), the nozzle exit velocity (V_e) can be expressed with equation (3.8) given below which is composed of 8 known input parameters ($A_d, A_D, \dot{m}, P_e, T_a, k, R, C_p$).

$$V_e = \left(\frac{A_d.P_e.C_p}{\dot{m}.R}\right).\left(-1 + \sqrt{1 + 2.\left(\frac{\dot{m}.R}{A_d.P_e}\right)^2.\frac{T_a}{C_p}}\right) \quad (3.8)$$

Equation (3.8) is substituted to the equation (3.1) in order to express the maximum vacuum pressure (P_{vacuum}) in terms of design and thermodynamic properties. New equation can be expressed with equation (3.9), given below.

$$P_{vacuum} = C_D.\left(\frac{A_d.P_e.C_p}{A_D.R}\right).\left(-1 + \sqrt{1 + 2.\left(\frac{\dot{m}.R}{A_d.P_e}\right)^2.\frac{T_a}{C_p}}\right) \quad (3.9)$$

When equation (3.9) is applied for the conditions investigated with CFD model, C_D - correction factor is expressed with the empirical equation given below (Eq. 3.10).

$$C_D = 1.2215.D^{0.0613} \quad (3.10)$$

where D is ejector tube diameter in m. The new equation for the maximum vacuum pressure is given below (3.11).

$$P_{vacuum} = 1.2215.D^{0.0613}.\left(\frac{A_d.P_e.C_p}{A_D.R}\right).\left(-1+\sqrt{1+2.\left(\frac{\dot{m}.R}{A_d.P_e}\right)^2.\frac{T_a}{C_p}}\right) \quad (3.11)$$

3.2.2. Conditions for the comparison of semi-empirical correlation and CFD results

When equation (3.11) was applied for the conditions investigated with CFD model which are shown in Table 3.16, it was realized that the equation was valid for the condition of Mach number (Ma) less than 1. The maximum error between semi-empirical correlation and the CFD results was 2.1% for the condition of Ma less than 1. If the equation (3.11) is applied to the higher Ma numbers from 1 to the 8 (which is the case for the CFD results), the error increases and the maximum error is observed at Mach number 8.08 as 28.6 %.

Table 3.16. Conditions for the Comparison of Semi-empirical Correlation and CFD Results

Motive gas flowrate (Nm^3/h)	Motive gas mass flowrate (kg/s)	Nozzle diameter (mm)	Ejector diameter (mm)	Motive gas temperature (K)
4	0.00138889	1	10	300
8	0.00277778	2	15	450
12	0.00416667	3	20	600
16	0.00555556	3.8	25.7	750
20	0.00694444	5	30	
24	0.00833333		35	
28	0.00972222			

3.2.3. Mach number correction factor

In order to make equation (3.11) more accurate at higher Mach numbers, correction factor (C_{M_a}) depending on the Ma is used and P_{vacuum} can be expressed with equation (3.12) given below.

$$\boldsymbol{P_{vacuum} = C_{M_a}.(1.2215.D^{0.0613}).\left(\frac{A_d.P_e.C_p}{A_D.R}\right).\left(-1+\sqrt{1+2.\left(\frac{\dot{m}.R}{A_d.P_e}\right)^2.\frac{T_a}{C_p}}\right)} \quad (3.12)$$

C_{Ma} Mach number correction factor

D Ejector tube diameter (m)

C_{M_a} was generated with using the ratio of CFD data to the results of equation (3.11) as shown in Fig.3.25. C_{M_a} is approximately 1 when the Ma number is less than 1. Further increase of Ma number from 1 to 4, causes the decrease of correction factor and reaches the value of 0.72. For the Ma number values of 4 to 8, correction factor is approximately constant at a value of 0.72.

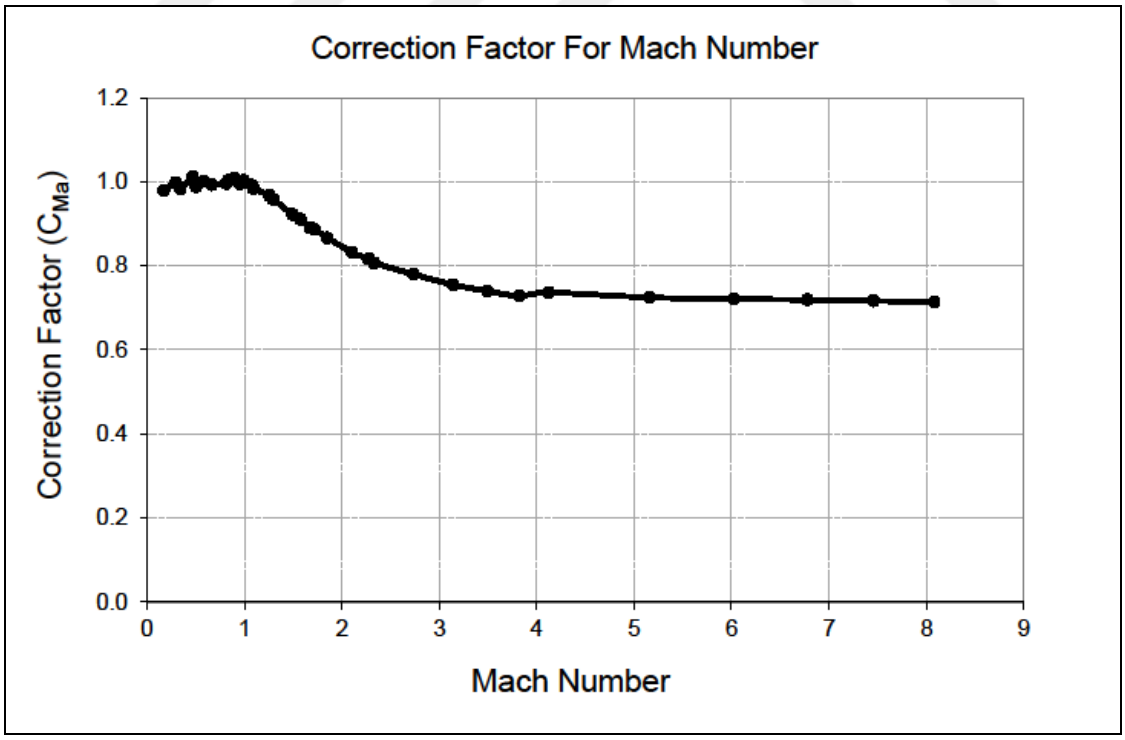

Figure 3.25. Correction factors for different Mach numbers

According to the comparison of the CFD data and the results obtained by the semi-empirical correlation (Eq.11), correction factors (C_{M_a}) for different Ma ranges are given below.

1 > Ma > 0 , $C_{M_a} = 1$ (3.13)

4 > Ma > 1 , $C_{M_a} = 1.013.{M_a}^{-0.254}$ (3.14)

8 > Ma > 4 , $C_{M_a} = 0.72$ (3.15)

Ma Mach number

When equation (12) is applied with the appropriate condition of Mach number (Equation 13, 14, 15) for the conditions investigated with CFD model which are shown in Table 3.16, the maximum and the average (absolute deviation) error for all results of semi-empirical correlation are 3.6 %and 0.88 %, respectively.

3.2.4. Derivation of Mach number

In order to predict the vacuum pressure generated by the ejector by using the semi-empirical correlations (Eq. 12, 13, 14 and 15), Mach number has to be calculated with known input parameters ($A_d, A_D, \dot{m}, P_e, T_a, k, R, C_p$). Ma number is the ratio of the velocity and the speed of sound as given below.

$$M_a = \frac{V_e}{C} \quad (3.16)$$

C Speed of sound

where V_e is the nozzle exit gas velocity (m/s) which is determined with the equation (8) and C is the speed of sound (m/s) at nozzle exit conditions. According to the thermodynamic relations, C (speed of sound) is expressed with the equation given below.

$$C = \sqrt{k.R.T_e} \quad (3.17)$$

k Specific heat ratio

where T_e is the nozzle exit gas temperature (K) which is determined with the equation (10), R is the specific gas constant (J/kg.K) and k is the specific heat ratio in J/kg.K. When the equation (7) is substituted to the equation (16), C can be expressed with the equation given below.

$$C = \sqrt{k.R.\left(C_p.\left(\frac{A_d.P_e}{\dot{m}.R}\right)^2.\left(-1+\sqrt{1+2.\left(\frac{\dot{m}.R}{A_d.P_e}\right)^2.\frac{T_a}{C_p}}\right)\right)} \quad (3.18)$$

In order to get Mach number with 7 input parameters ($A_d, \dot{m}, P_e, T_a, k, R, C_p$), equation (8) and equation (18) are substituted to the equation (16) which is given below.

$$M_a = \left(\frac{1}{\sqrt{k.R}}.\sqrt{C_p.\left(-1+\sqrt{1+2.\left(\frac{\dot{m}.R}{A_d.P_e}\right)^2.\frac{T_a}{C_p}}\right)}\right) \quad (3.19)$$

At this point, semi-empirical correlation for the maximum vacuum pressure that can be achieved with an ejector is expressed as a function of nozzle diameter, ejector tube diameter, motive gas mass flow rate, ambient pressure, inlet temperature, specific heat ratio, specific gas constant and specific heat of motive gas, as shown below.

$$P_{vacuum} = f\ (A_d, A_D, \dot{m}, P_e, T_a, k, R, C_p\ ) \quad (3.20)$$

3.2.5. Comparison of semi-empirical correlation with CFD results

The results show that the semi-empirical correlation for estimating the maximum vacuum pressure that can be achieved with an ejector is used instead of CFD analysis in order to get quick results with negligible loss of accuracy (average deviation and standard deviation of all errors are, 0.88% and 0.79%, respectively), if the limits of operating conditions are in between the values described at previous sections.

3.3. Cold Model Experimental Results

3.3.1. Effect of ejector system at CFB without solid bed inventory

In order to understand the effect of the ejector system at CFB experimental model, experiments were first carried out without solid bed inventory. Five different superficial gas velocities (2, 3, 4, 5, 6 m/s) were selected for the operation without ejector. Empty cold model without ejector was run with air in order to obtain the reference pressure profile and to distinguish the effect of the ejector. As shown in Fig.3.26, the pressure difference between the downcomer and the riser gradually increased with the increase of the flow rate of air (i.e. superficial gas velocity). The cyclone pressure drop which is important for determining the required pressure difference formed by the ejector system also increased as expected. For proper operation of CFB systems, a pressure barrier (loop seal or ejector) is necessary to overcome the sum of the pressure drop at riser and the cyclone. In the without ejector mode, the absence of pressure resistance at the downcomer resulted in pressure values gradually decreasing from bottom of the downcomer to cyclone (From P-7 to P-11). Some part of the air passed through the downcomer to the cyclone as well.

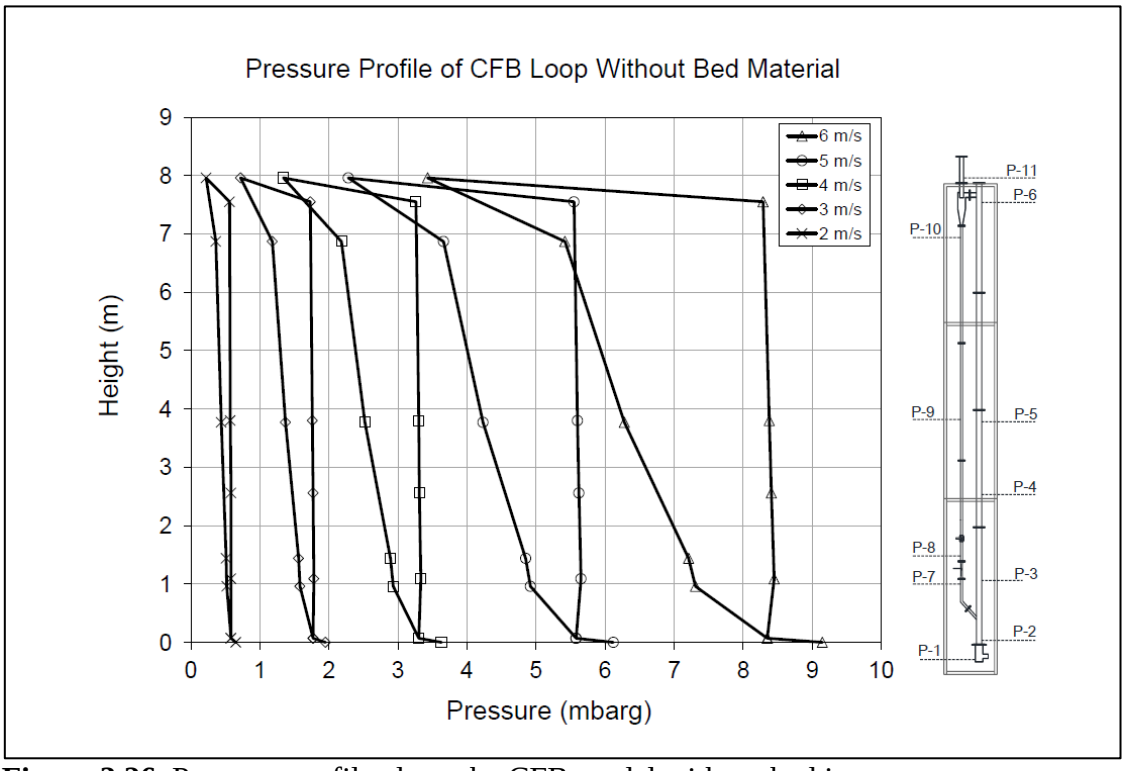

Figure 3.26. Pressure profile along the CFB model without bed inventory

For further experiments, the ejector system was used to determine the required pressure difference (barrier) at the downcomer. Fig.3.27 presents the results for 5 m/s superficial gas velocity for 5 different motive gas flow rates (1.2 - 6.0 Nm^3/h). The slope of the downcomer pressure profile was negative and the P-7 pressure measurement point value was less than the point P-2 value for 0 Nm^3/h and 1.2 Nm^3/h motive gas flowrates. For 2.4 Nm^3/h motive gas flowrate at ejector system, P-2 and P-7 values were the same but cyclone pressure profile was positive (P11>P10) which means there was no reverse flow and some part of the air was re-circulated. Reverse gas flow from riser to downcomer was stopped and gas was being re-circulated at a point between 1.2 Nm^3/h and 2.4 Nm3/h motive gas flowrates. For the conditions of 3.6, 4.8 and 6.0 Nm^3/h motive gas flowrates, the slope of the pressure profile was positive and P-7 values were higher than the P-2 values. In this condition, some part of the air was re-circulated from the cyclone to the riser through the downcomer.

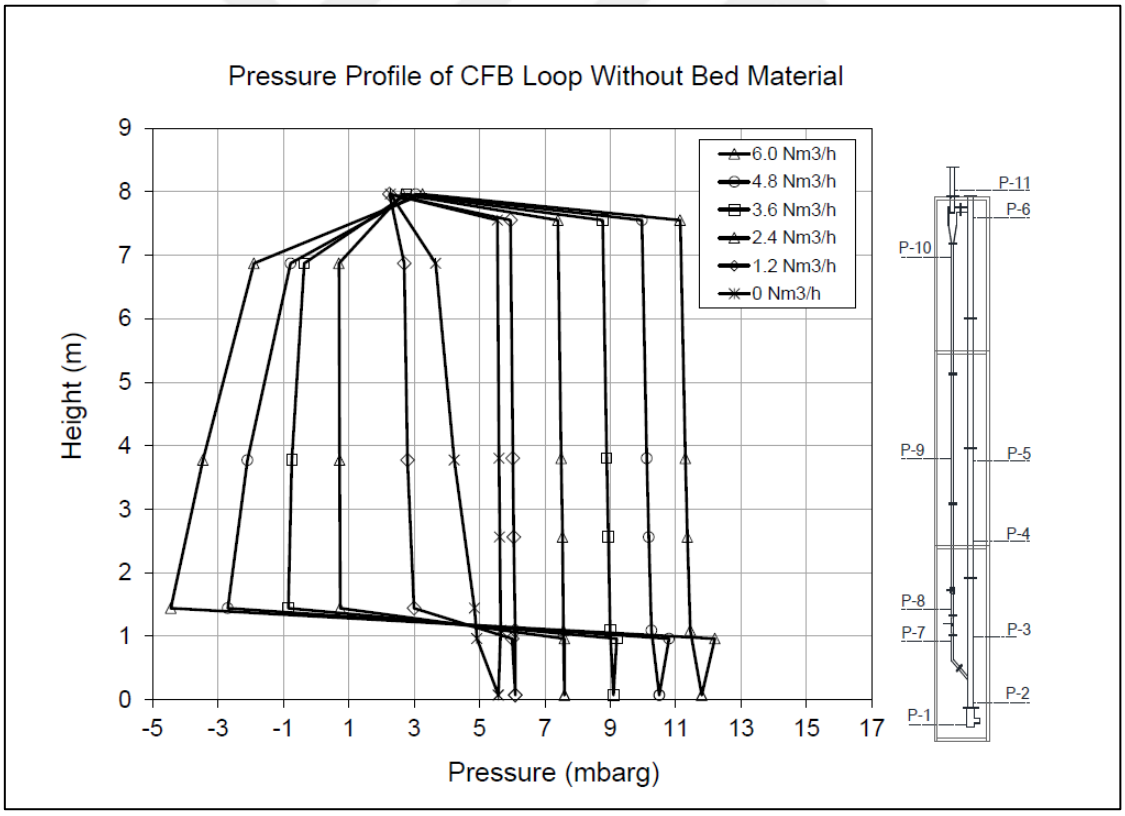

Figure 3.27. Pressure profile with ejector and without bed inventory

3.3.2. Effect of ejector system at CFB with solid bed inventory

3.3.2.1. Experimental results of CFB cold model without ejector system

Experiments were carried out with bed material and without ejector system for 3 different superficial gas velocities (4, 5, 6 m/s). Main experimental parameters are listed in Table 3.17. The experimentally obtained pressure profiles of CFB loop for various superficial velocities are shown in Fig.3.28. The solid flux through the riser was 0.05 kg/m^2.s for 4 m/s superficial gas velocity indicating not circulating regime. The pressure profile of the same system in Fig.3.28 shows that the main pressure drop of the riser occurring at the lower 1 meter of the riser corresponds to 98% of the total riser pressure drop. The main amount of the bed inventory was located at the lower 1 meter of the riser. Hence, the corresponding regime was not circulating fluidized bed [13] and it was only suitable for the ejector application with no solid accumulation through the downcomer due to the very low solid circulation rate.

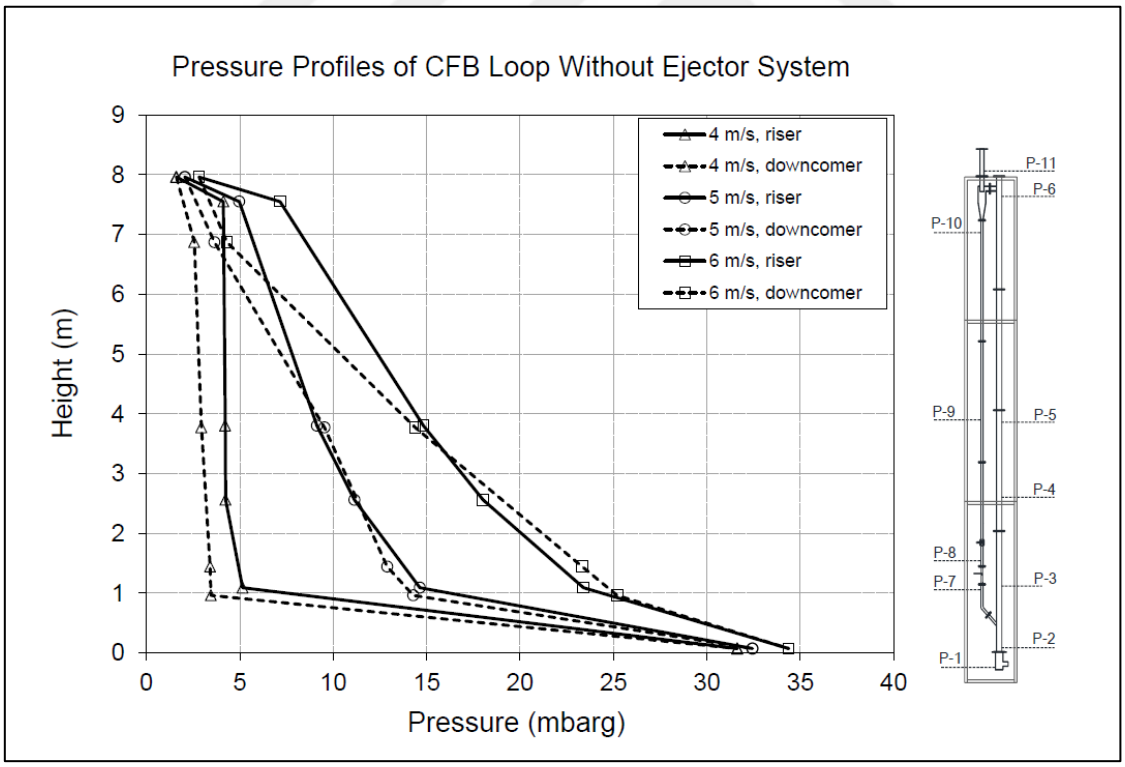

Figure 3.28. Pressure profile of CFB loop without ejector system

For solid circulation rates at 5 and 6 m/s gas velocity, solid flux at the riser was 2.80 and 5.71 kg/m^2.s, respectively, indicating circulating fluidized bed regime (1 – 10 kg/m^2.s)

[13]. The solid distribution through the riser was more homogenous for 5 m/s compared to 4 m/s case and became much more homogenous at 6 m/s superficial gas velocity. The dense bed and freeboard densities of the riser calculated with the pressure differences of related pressure ports are in line with these results. The deepest 1 meter of the riser was assumed as dense bed region and the rest of the riser (6.5 m) up to the cyclone entrance was assumed as the freeboard. According to the densities predicted by the related pressure differences (P6-P3 for the freeboard and P3-P2 for the dense bed), dense bed densities were decreasing with the increase of the superficial gas velocity. Meanwhile, freeboard densities were increasing with the increase of the superficial velocity. The differences between the densities of the freeboard and the dense bed region were decreasing and the riser solid material distribution was getting more homogenous.

Another important parameter investigated with these experiments was cyclone performance. Cyclone performance was determined with the amount of solid particles escaped from the cyclone by comparing the amount of final and initial bed inventories for each experiment (Table 3.17).

Table 3.17. Experimental Parameters without Ejector System

Superficial Gas Velocity	**4 m/s**	**5 m/s**	**6 m/s**
Air Flow Rate (Nm^3/h)	100	125	150
Duration of Experiment (minute)	60	60	60
Mean Particle Size (micron)	644	644	644
Initial Bed Inventory (kg)	3.00	3.00	3.00
Final Bed Inventory (kg)	2.71	2.61	2.63
Solid Particles Escape from Cyclone (kg/h)	0.29	0.39	0.37
Solid Circulation Rate (kg/h)	1.1	69.9	142.6
Solid Flux at Riser - Gs ($kg/m^2.s$)	0.05	2.80	5.71
Solid Flux at Downcomer - Gs ($kg/m^2.s$)	0.35	21.40	43.65
Dense bed Density (kg/m^3)	265	178	110
Freeboard Density (kg/m^3)	2	15	26
P8 - P9 when the ball valve is closed (mbar)	7.10	13.20	19.37

Fig.3.28 indicates the reverse flow of gases from the riser to the cyclone through the downcomer. The pressure line of the downcomer was very close to the pressure line of the riser and there was no sudden pressure change (pressure barrier) along the downcomer. In other words, primary air flow was split into two streams. The main stream flowed through the riser and the other stream flowed through the downcomer.

In order to simulate the pressure barrier and to determine the required pressure difference to prevent reverse flow through the downcomer, ball valve located at the downcomer between P-8 and P-9 pressure ports was closed for a short period of time (2 minute). The difference between P-8 and P-9 pressure values was measured. The required pressure differences were 7.10 mbar, 13.20 mbar and 19.37 mbar for the superficial gas velocities of 4, 5 and 6 m/s, respectively (Table 3.17). These pressure differences were initial guesses to be tried with ejector system applications.

3.3.2.2. Experimental results of CFB cold model with ejector system

The ejector system was used and the pressure profile was investigated for 3 different superficial gas velocities (4, 5, 6 m/s). Main experimental results are listed in Table 3.18. Duration of experiments, bed material type and the amount of initial bed inventory were held constant with the previous experiments carried out without ejector system.

Table 3.18. Experimental Parameters with Ejector System

Superficial Gas Velocity	**4 m/s**	**5 m/s**	**6 m/s**
Air Flow Rate (Nm^3/h)	100	125	150
Duration of Experiment (minute)	60	60	60
Mean Particle Size (micron)	644	644	644
Solid Column Formation Above Ejector	-	+	+
Motive Gas Flow Rate (Nm^3/h)	3.84	3.27	2.76
Motive Gas Pressure at Nozzle Inlet (barg)	2.6	2.0	1.5
Initial Bed Inventory (kg)	3.00	3.00	3.00
Final Bed İnventory (kg)	2.82	2.84	2.87
Solid Particles Escape from Cyclone (kg/h)	0.18	0.16	0.13

Solid Circulation Rate (kg/h)	1.9	88.7	165.3
Solid Flux at Riser - Gs ($kg/m^2.s$)	0.08	3.55	6.62
Solid Flux at Downcomer - Gs ($kg/m^2.s$)	0.59	27.15	50.59
Solid Flux at Ejector Tube - Gs ($kg/m^2.s$)	1.04	47.51	88.55
Dense bed Density (kg/m^3)	240	142	53
Freeboard Density (kg/m^3)	6	21	37

The required pressure differences determined with the without ejector experiments were sought to be achieved with ejector system. For 4 m/s condition, the minimum required pressure difference was 7.10 mbar. In order to determine the required motive gas flowrate to achieve the desired pressure difference, the ball valve was closed and the motive gas flowrate was increased gradually up to a level of 8.10 mbar which was 1.00 mbar more than the required level (7.10 mbar) to assure sufficient pressure difference. The 8.10 mbar pressure difference was achieved with the 3.84 Nm^3/h motive gas flowrate. The pressure profile of the CFB loop for the 4 m/s condition with and without ejector system is shown in Fig.3.29. The pressure jump was observed at downcomer between P-7 and P-8 pressure ports as 8.22 mbar, which was almost negligible (0.47 mbar) for the experiment without ejector system. The solid flux through the riser, dense bed densities and freeboard densities were almost the same with the experiment carried out for without ejector system at 4 m/s condition.

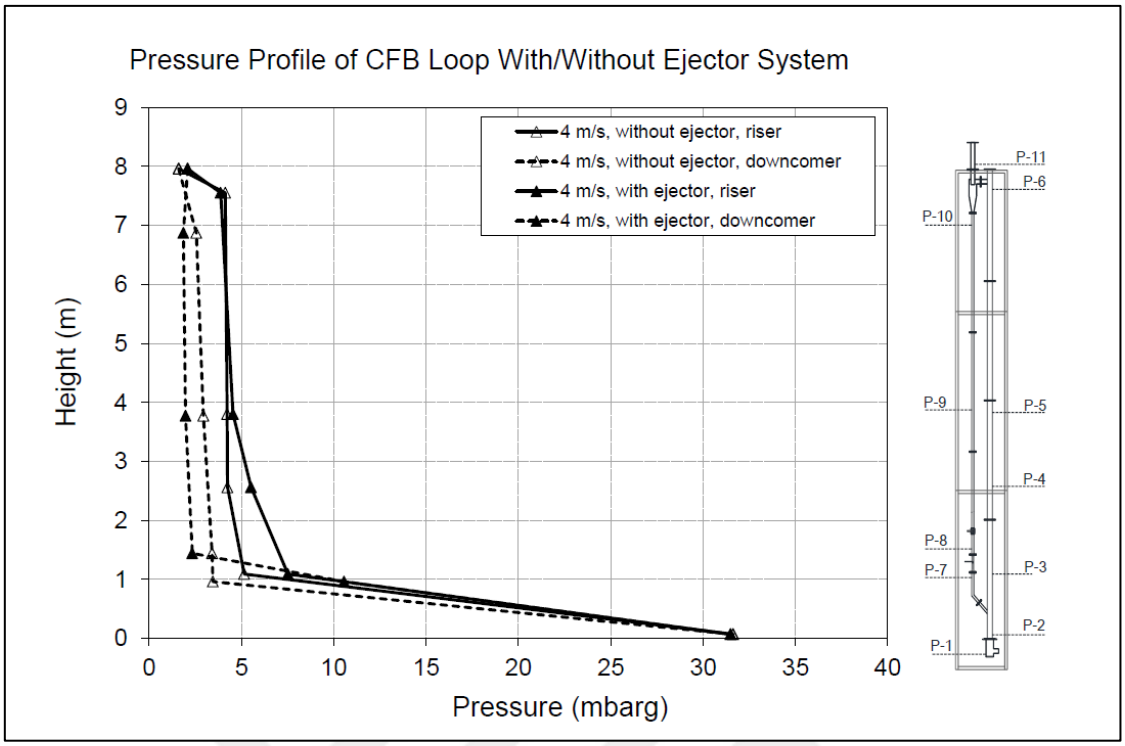

Figure 3.29. Pressure profile of CFB loop with/without ejector system for 4 ms

For 5 m/s condition, the required pressure difference was determined as at least 13.20 mbar. In contrast to the 4 m/s condition the solid circulation rate was enough for solid accumulation just above the ejector nozzle exit (Figure 3.30).

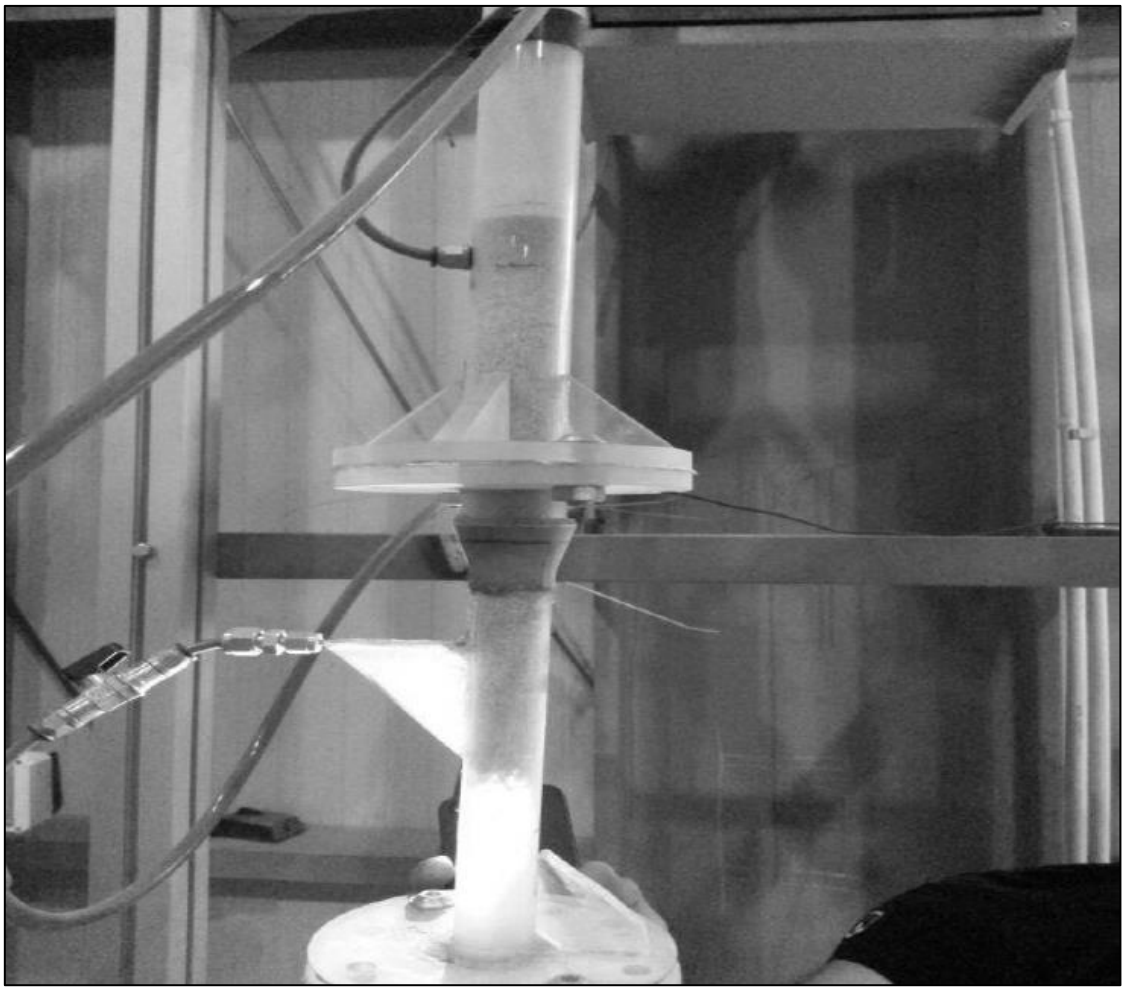

Figure 3.30. Solid column formation

In that case, solid particles captured by the cyclone fell down to the upper surface of the solid column, meanwhile, some amount of particles fell down from the bottom region of the solid column (vortex region). The solid column height was approximately constant (~300 mm) with little fluctuations. The flowrate of the particles passing through the vortex region of the ejector was controlled adjusting of the motive gas flowrate. Due to the solid column, the required motive gas flowrate was less than the 4 m/s condition even though the required corresponding pressure difference is higher (13.20 mbar). The pressure profile of the CFB loop for the 5 m/s condition with and without ejector system is shown in Fig.3.31.

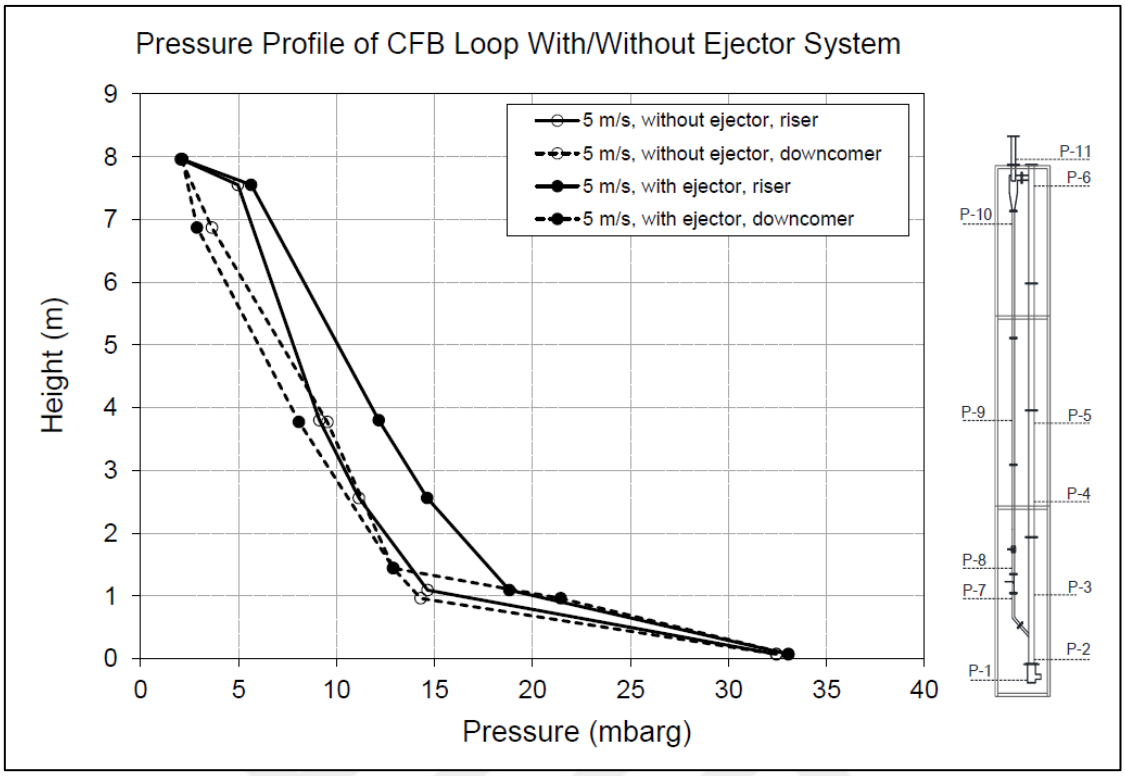

Figure 3.31. Pressure profile of CFB loop with (without) ejector system for 5 m/s

The pressure jump was observed at downcomer between P-7 and P-8 pressure ports as 8.54 mbar, which was 1.40 mbar for the experiment without ejector system. The pressure difference obtained during the experiment was less than the required pressure difference determined at previous section. The reason of this situation is explained with the solid accumulation above the ejector nozzle exit. The solid column height was approximately 300 mm which corresponded to 300 gr of solid material which means the solid material was 300 gr less in the riser with respect to experiment without ejector system. The pressure effect of 300 gr bed material on the riser pressure profile was calculated as 4.28 mbarg. Due to this reason; the required pressure difference was less than the predicted value.

The solid flux through the riser for 5 m/s condition was significantly increased with the ejector system. During the experiments without ejector system, some amount of primary air was flowing through the downcomer and the superficial gas velocity at the riser was less than the theoretically calculated values. For the experiments with ejector system, the total amount of the primary air could flow through the riser by means of the pressure

barrier formed by the ejector system. Due to the same reason, dense bed and freeboard densities decreased and increased, respectively.

For 6 m/s condition, the required pressure difference was determined as at least 19.37 mbar. In this condition, the ejector system operation was similar to the 5 m/s condition. Solid column formation was observed above the ejector nozzle exit with considerably less motive gas flowrate. The pressure profile of the CFB loop for the 6 m/s condition with and without ejector system is shown in Fig.3.32.

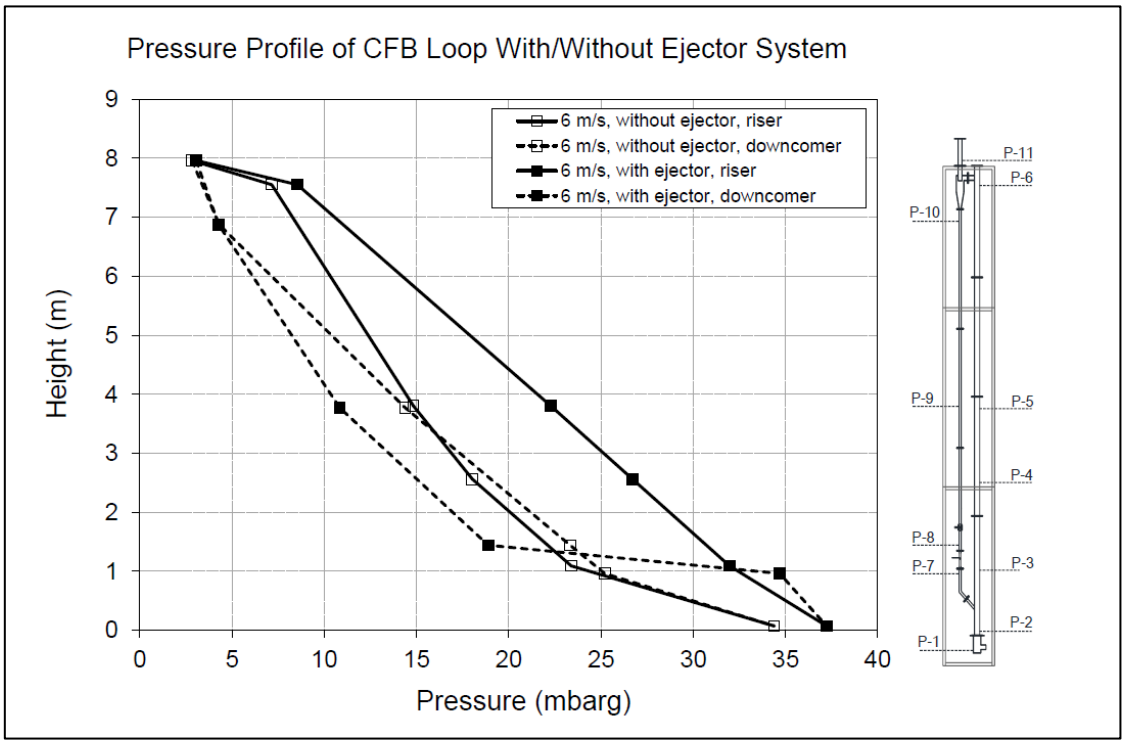

Figure 3.32. Pressure profile of CFB loop with (without) ejector system for 6 m/s

The pressure jump was observed at downcomer between P-7 and P-8 pressure ports as 15.79 mbar. The pressure difference obtained during this experiment was less than the required pressure difference determined for the without ejector case. The solid accumulation above the ejector nozzle exit explains this finding similar to the 5 m/s case. The split of primary air into two parts was prevented. Solid flux through the riser, dense bed density and freeboard density all changed considerably due to the increase of the riser air flowrate. The amount of solid particles escaping from the cyclone also decreased significantly (37 %, 59 % and 63 % for 4, 5, 6 m/s, respectively) with the ejector included system due to the absence of reverse gas flow through the downcomer.

The amount of particle escape from the cyclone also decreased with the increase of superficial velocity.

3.3.3. Solid particle flowrate at ejector vortex region

The inverse effect of the motive gas flowrate to the solid flowrate was realized at the before mentioned CFB cold model experiments. The ejector only experiments were carried out without primary air flow to the riser in order to determine the relation of motive gas and solid particles flowrates. Solid particles flowrates were measured for 10 different motive gas flowrate as shown in Fig.3.33. Initial experiments were in the absence of motive gas, the solid particle flowrate was 269.8 gr/s i.e. 465 $kg/m^2.s$ solid flux through the ejector tube. The movement of the solid particles was free fall in a vertical pipe. For the motive gas flow rates of 0.6 Nm^3/h and 1.2 Nm^3/h, the solid flowrate was slightly increased. The solid flow was promoted by the motive gas where the resistance of vortex region was not dominant. For the motive gas flowrate of 1.8 Nm^3/h, several measurements were taken and the upper and lower averages were 497 $kg/m^2.s$ and 69 $kg/m^2.s$, respectively. These different solid fluxes for the same motive gas flow rate showed that the resistance of the vortices at 1.8 Nm^3/h motive gas flowrate was unstable (Figure 3.33).

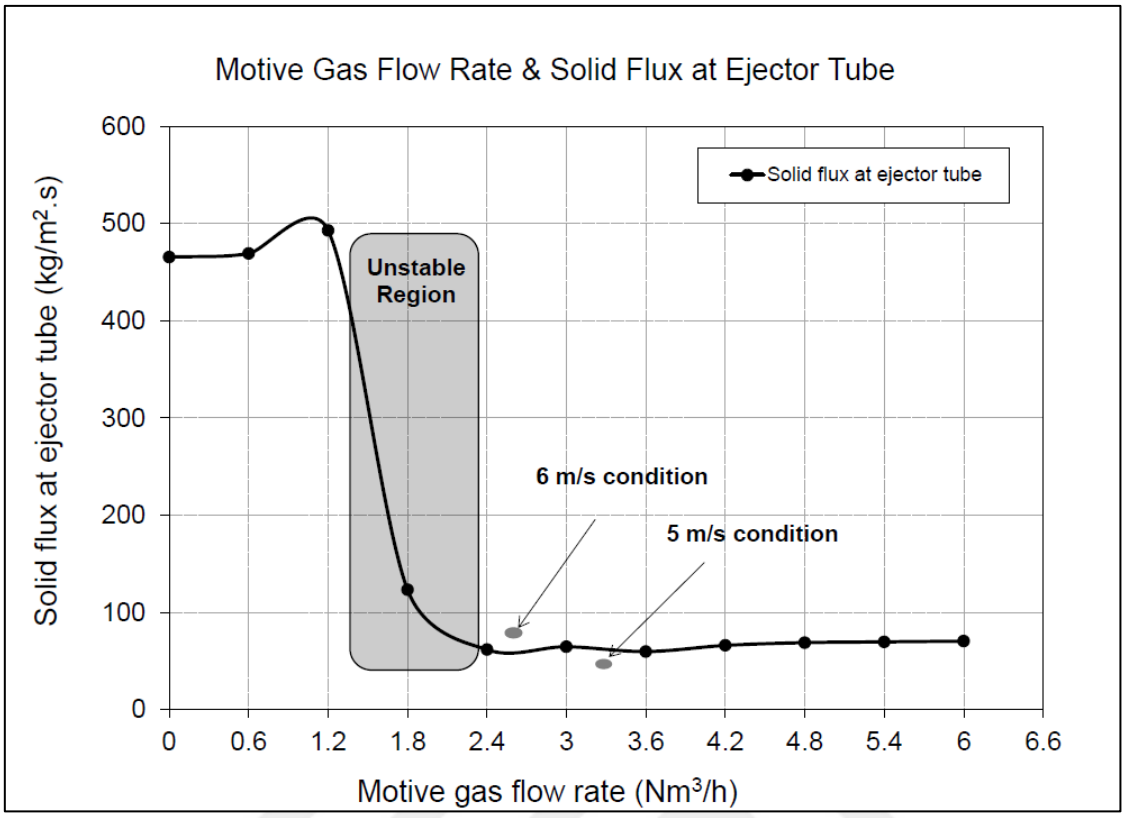

Figure 3.33. Solid particle flow rate through the ejector system

For the motive gas flowrate of 2.4 Nm^3/h to 6 Nm^3/h, solid fluxes were stable and slightly different from each other at approximately 66 $kg/m^2.s$. In other words, the solid flow rate can be assumed almost constant for the motive gas flow rates higher than the 2.4 Nm^3/h. These results show that there is a lower limit of motive gas flowrate for stable ejector operation. If motive gas flowrate is lower than this limit, solid flow become unstable and may cause loss the control of solid circulation.

3.3.4. Solid column formation conditions during cold experiment

During the experiments with the ejector system, the solid column formation was observed for 5 m/s and 6 m/s riser superficial air velocity conditions. The conditions of initial solid formation and final deformation were unknown. The ejector motive gas flowrate was held constant at a sufficient level (6 Nm^3/h) enabling solid column formation. The superficial gas velocity in the riser was increased gradually up to the point where the solid formation was observed. After observing the solid column,

superficial gas velocity was decreased gradually up to the point where solid column disappeared. The results are shown in Table 3.19.

Table 3.19. Solid Column Formation/ Disappearance Conditions during Cold Experiment

	Column Formation	**Column Disappearance**
Riser Superficial Velocity (m/s)	4.85	4.25
Bed Inventory (kg)	3.00	3.00
Motive Gas Flowrate (Nm^3/h)	6	6
Mean Particle Size (micron)	644	644
Solid Circulation Rate (kg/h)	82.6	34.5
Gs at Riser ($kg/m^2.s$)	3.31	1.38
Gs at Downcomer ($kg/m^2.s$)	25.30	10.55
Gs at Ejector Tube (kg/m2.s)	44.27	18.46

Stable solid column was first observed at 4.85 m/s superficial velocity. Solid flux through the ejector tube at this condition was 44.27 $kg/m^2.s$ which was less than the solid flux for the 5 m/s condition. At this point, the flowrate of primary air decreased gradually and solid column was observed. Solid column disappeared when the superficial gas velocity was decreased to 4.25 m/s. At this condition, solid flux through the ejector tube was 18.46 $kg/m^2.s$.

3.4. Hot Model Experimental Results

3.4.1. Operating conditions of hot experiment

Experiments were carried out with circulating fluidized bed gasifier system. Soma lignite was used as feedstock. Main operating conditions are shown at Table 3.20.

Table 3.20. Main operating conditions of hot experiments

Superficial Gas Velocity	**4 m/s**	**5 m/s**	**6 m/s**
Air Flow Rate	25 Nm^3/h	32 Nm^3/h	38 Nm^3/h
Bed material		Silica sand	
Bed material diameter		0.3 – 0.7 mm	
Initial bed inventory		3 kg	
Reactor Temperature	842 ^oC	856 ^oC	854 ^oC
Reactor Pressure		Atmospheric	
Feedstock		Soma lignite	
Fuel Feeding Rate	11.6 kg/h	13.9 kg/h	16.5 kg/h
ER	0.43	0.46	0.46
Motive Gas Flow Rate (Nm^3/h)	5.3	3.4	2.9
Dense bed Density (kg/m^3)	307	223	116
Freeboard Density (kg/m^3)	4	17	29

Total duration of each experiment was approximately 8 hours including heating of the bed material. Heating of the bed material takes 4 hour (bed material reaches 350 °C) and after reaching desired bed material temperature, coal was started to feed to the reactor. Reactor was operated 4 hours with coal feeding and related measurements were taken. Control and the monitoring of the system were done with the control system (PLC). Control screens of reactor and the fuel feeding system are shown in Fig.3.34 and Fig.3.35, respectively.

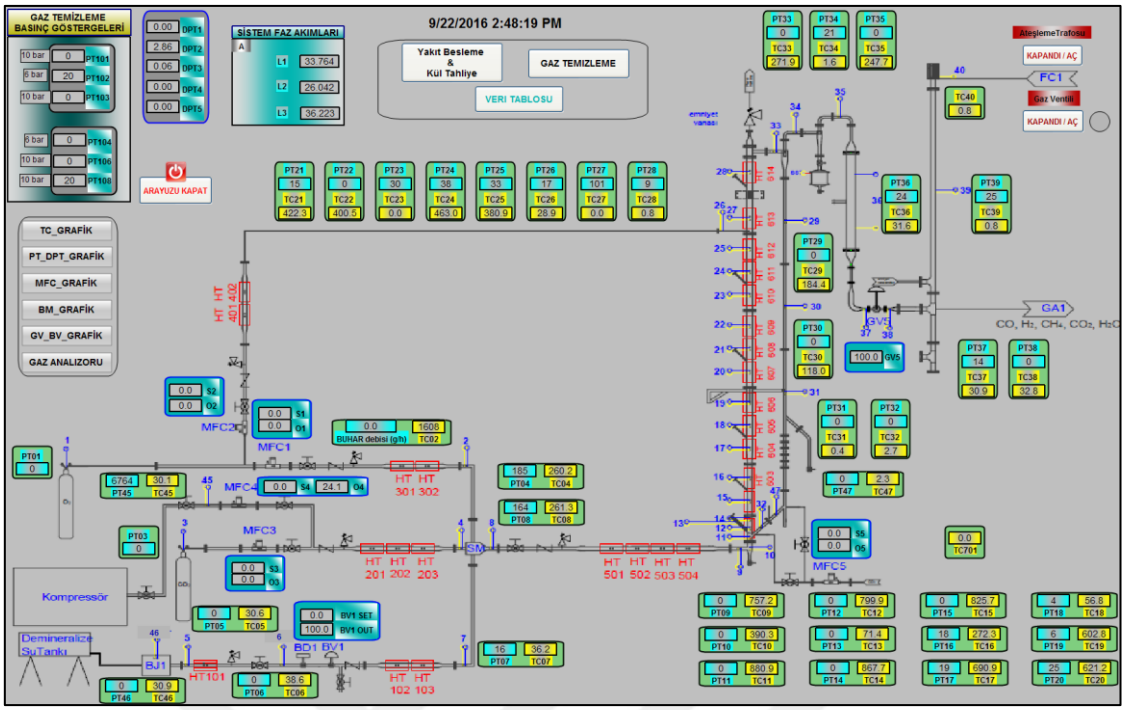

Figure 3.34. CFB gasifier reactor control screen

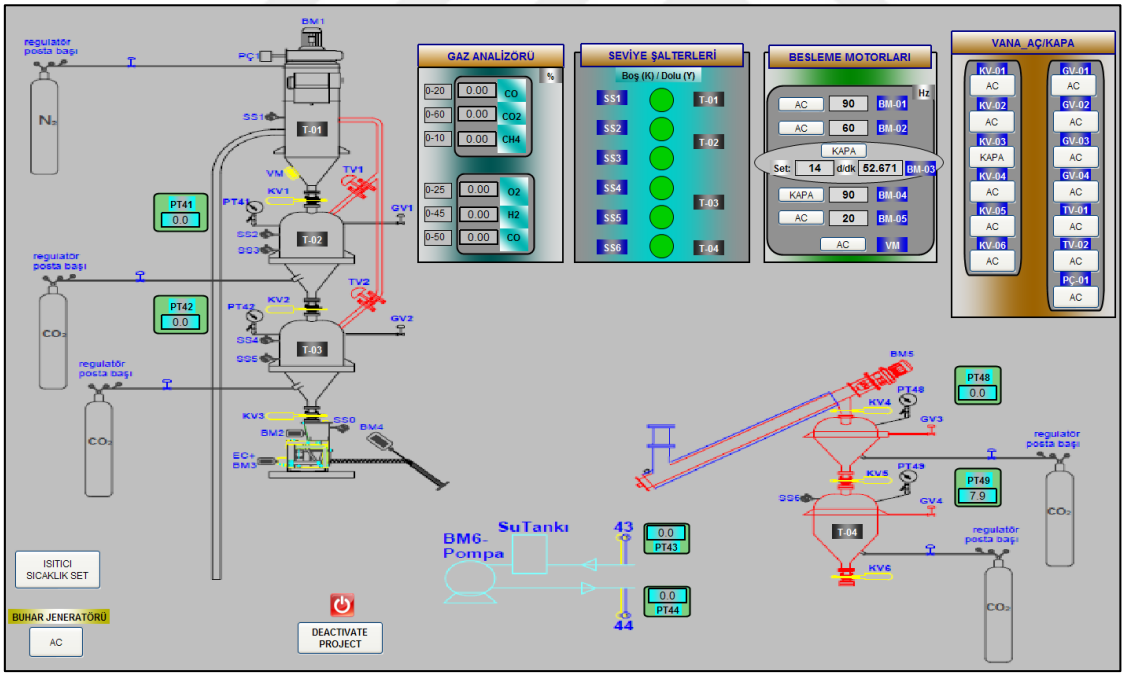

Figure 3.35. CFB gasifier Fuel feeding control screen

Air was used for gasification agent and the flowrates of air were, 25, 32 and 38 Nm^3/h for 4, 5 and 6 m/s superficial gas velocity inside the riser at approximately 850 °C reactor temperature.

Silica sand was used as bed material for gasification experiments which was the same with the bed material used at cold test facility. The size of the bed material was in between 0.3 mm at 0.7 mm. Similar to the cold tests, 3 kg of initial bed material was loaded to the reactor at the beginning of the each experiment.

Temperature of the gasifier reactor was tried to hold at desired value which was approximately 850 °C. The temperature of reactor is 842, 856 and 854 °C for 4, 5 and 6 m/s superficial gas velocity, respectively. The temperature was controlled with adjusting the coal feed rate instead of air feed rate. If the air flowrate is changed, the superficial gas velocity inside the riser is also changed which were assumed as constraint for these experiments.

Fuel feeding rate was adjusted for the control of the reactor temperature and keep the reactions at gasification region. The fuel feeding rates were 11.6, 13.9 and 16.5 kg/h for 4, 5 and 6 m/s superficial velocity conditions. In order to held reactor temperature constant at desired value (850 °C), fuel feeding rate should be also increased with the increase of superficial gas velocity i.e. air flowrate.

Another important parameter for the gasification process is the equivalence ratio (ER) which can be defined as the ratio of the air feed for gasification to the required air feed for stoichiometric combustion. Within these gasification experiments, ER values were 0.43, 0.46 and 0.46 for the 4, 5 and 6 m/s superficial gas velocity conditions.

Motive gas flowrate for ejector operation were 5.3, 3.4 and 2.9 Nm^3/h for 4, 5 and 6 m/s superficial gas velocity conditions. Similar to the cold tests with ejector application, for 4 m/s condition, there was no solid column formation and the required motive gas flowrate is higher than the other conditions. For 5 and 6 m/s conditions, there were solid column formations and some part of required pressure difference was contributed by the solid column. Because of that, required motive air flowrate were lower the 4 m/s condition.

Dense bed and freeboard densities were also calculated for the gasification experiments by using the pressure differences of dense bed region and the freeboard region. Dense bed densities were 307, 223 and 116 kg/m^3 for 4, 5 and 6 m/s superficial gas velocity conditions. Freeboard densities were 4, 17 and 29 kg/m^3 for 4, 5 and 6 m/s conditions.

Similarly to the cold experimental studies, dense bed and freeboard densities decreased and increased with the increase of superficial gas velocity, respectively.

3.4.2. Pressure profile along the CFB loop

There are 11 pressure measurement ports along the cfb loop similar to the cold test facility. Pressure profiles of cfb gasifier were taken for 3 different superficial gas velocities. In fact the results of pressure profile of hot test facility is very similar to the cold test facility.

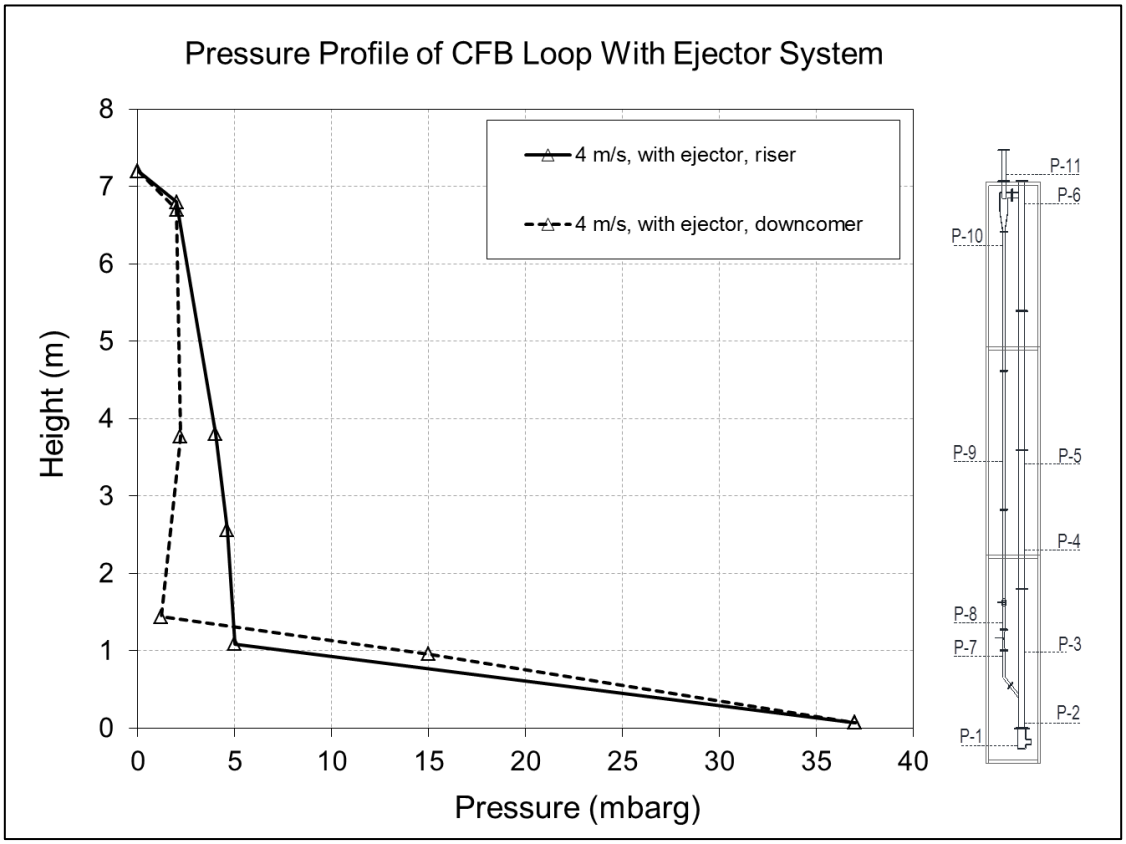

Figure 3.36. Pressure profile of CFB loop at 4 m/s superficial gas velocity

For 4 m/s condition, the system pressure profile is shown in Fig.3.36. The main bed material was located at first 1 meter of the reactor which means the regime was bubbling or turbulent fluidized bed rather than circulating fluidized bed. There was a pressure jump between pressure ports P-7 and P-8 which are exit and the inlet of the ejector, respectively. The pressure difference between the inlet and the exit of the

ejector system was approximately 13 mbar which is enough for generating the pressure barrier for reverse gas flow through the downcomer from the riser to the cyclone.

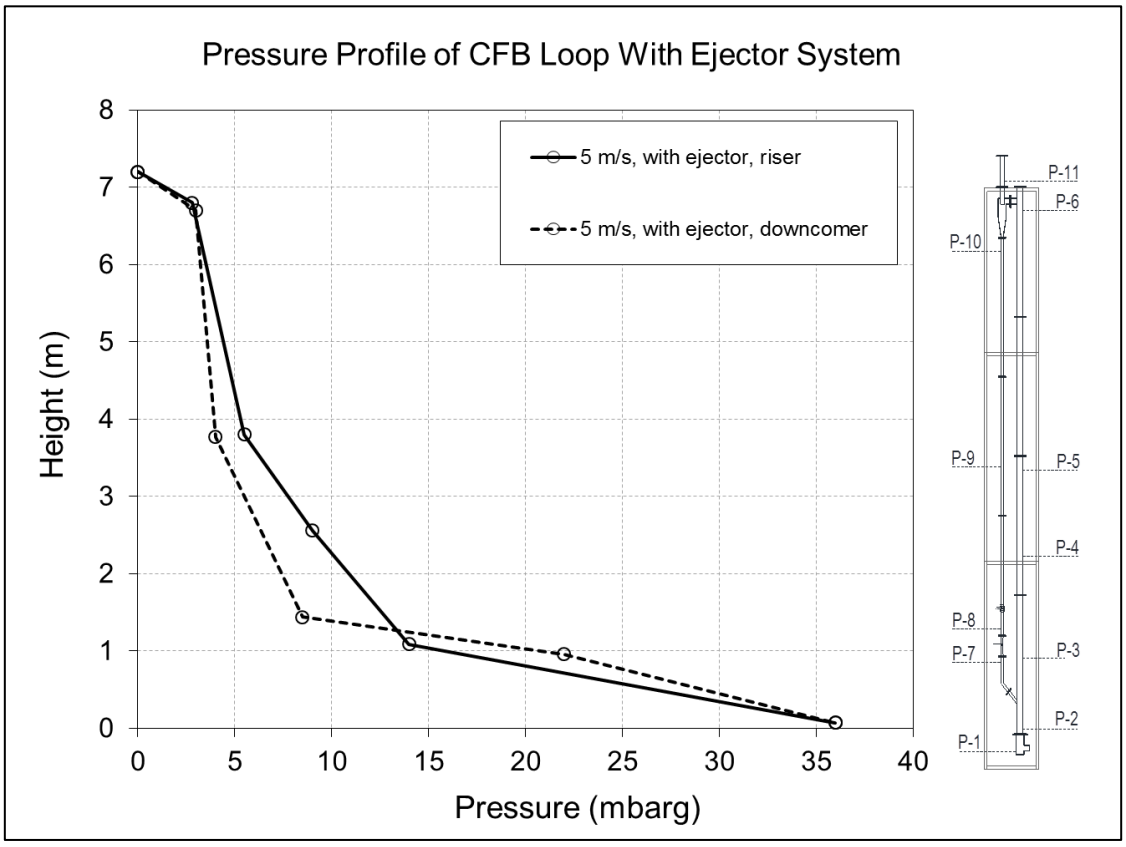

Figure 3.37. Pressure profile of CFB loop at 5 m/s superficial gas velocity

The pressure profile of CFB system for 5 m/s is shown at Fig.3.37. According to the pressure profile, it can be conclude that higher solid circulation was achieved with 5 m/s condition. Because the pressure difference of dense bed and the freeboard was lower and higher, respectively. There was also a pressure jump between pressure ports P-7 and P-8 which are exit and the inlet of the ejector, respectively. The pressure difference between the inlet and the exit of the ejector is approximately 14 mbar.

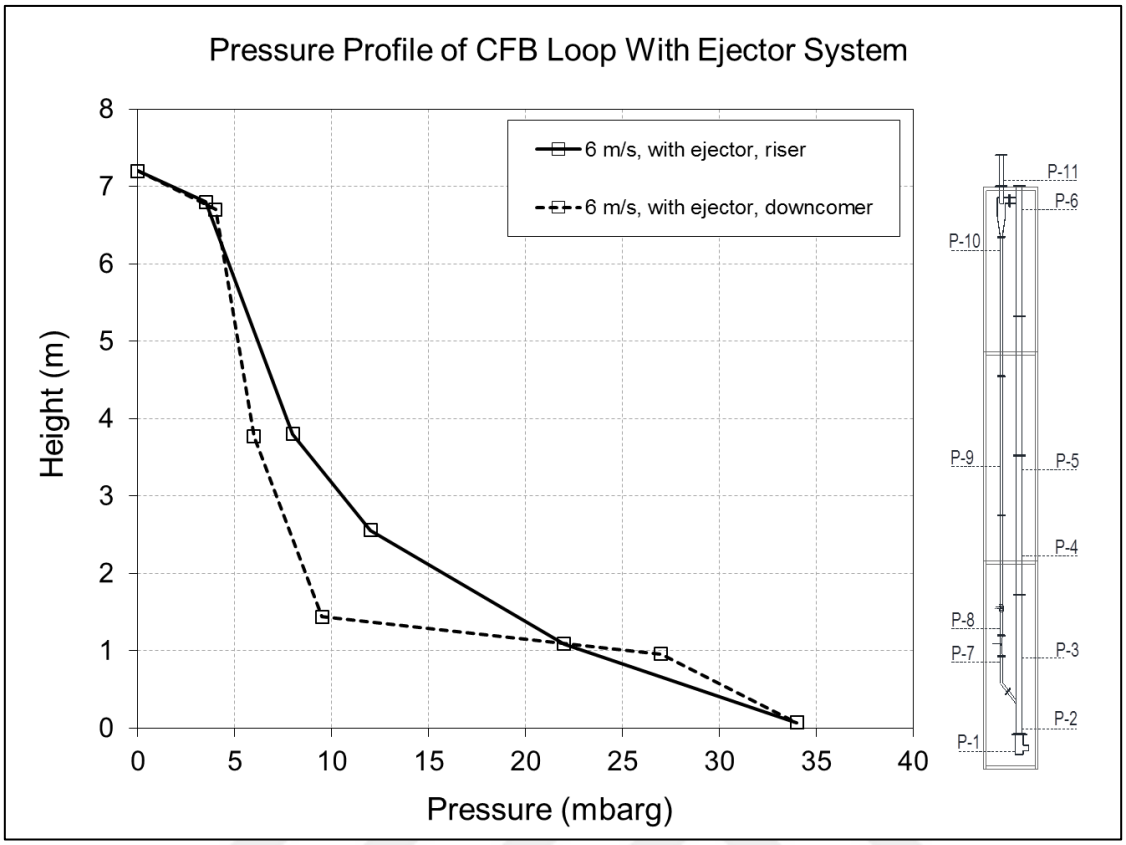

Figure 3.38. Pressure profile of CFB loop at 6 m/s superficial gas velocity

The pressure profile of CFB system for 6 m/s is shown at Fig.3.38. According to the pressure profile, it can be conclude that higher solid circulation is achieved with 6 m/s condition. Because the pressure difference of dense bed and the freeboard was lower and higher, respectively. The pressure jump due to the ejector effect is higher than the previous conditions. The pressure difference between the inlet and the exit of the ejector is approximately 17 mbar.

3.4.3. Solid circulation rate (Gs)

Cold test facility is made out of plexiglass transparent material and the visual inspection can be made in order to measure the solid circulation rates. For the case of hot gasification experiments, the system is made out of stainless steel which is not transparent. Because of that, the solid circulation could not be measured for hot system tests.

3.4.4. Gas composition

The produced gas composition of syngas during the gasification experiments were measured for each condition with gas analyzer. The composition of syngas is shown in Table 3.21 with molar basis.

Table 3.21. Gas composition of syngas at gasifier exit

	4 m/s	**5 m/s**	**6 m/s**
% CO	8.50	8.29	9.07
% H_2	9.28	9.57	10.03
% CH_4	1.82	1.92	2.09
% CO_2	12.63	14.34	14.19
% N_2	67.42	65.59	64.47

The syngas mainly consist of CO, H_2, CH_4, CO_2 and N_2 gasses. The molar compositions of the syngas for each experiment were similar to each other. There is only slight difference between gas compositions. With the increase of superficial gas velocity, N_2 content of the syngas decrease significantly and quality of the syngas decreased. In fact, this situation is related to the motive gas flowrate rather than the superficial gas velocity. For 4 m/s condition, the motive gas flowrate which was N_2, is higher than the other conditions. Similarly, for 5 m/s condition, motive gas flowrate is higher than the 6 m/s condition. Because of the higher flowrate of motive gas i.e. N_2 for lower superficial gas velocities, N_2 content of the syngas is decreasing with the increase of superficial gas velocity inside the riser.

4. CONCLUSIONS

The present work attempts to develop a first level understanding of the proper design and operational conditions of ejector type circulating fluidized bed system, by using an experimental CFB cold model and CFD analysis of ejector system. The following conclusions can be drawn from the experimental results.

Experimental work results;

- The ejector has been capable to provide the required pressure barrier for the investigated riser velocity range (4 m/s – 6 m/s).

- Depending on the solid circulation rates in CFB loop and the motive gas flowrates, there were two different operation modes of ejector type solid circulation. The main difference of these two operation modes was the solid column formation above the ejector nozzle exit.

- If the pressure barrier generated by the ejector has been broken, it has been possible to rebuild it with the continuous motive gas feed, i.e. the pressure barrier generated by the ejector has stable operation. Within this frame, a more stable solid circulation has been observed with the ejector compared to the case without the ejector.

- Solid circulation rate affected solid column formation. At low rates no solid column was formed. Above a limiting rate determined by the riser velocity, solid column formation was observed just above the ejector nozzle exit.

- During the operation of cold CFB system, solid column height was approximately constant with little fluctuations for constant motive gas flowrate and constant riser superficial velocity.

- The solid column height can be controlled with the motive gas flowrate. Increasing the motive gas flowrate decreases the solid flux through the ejector tube. Similarly, decreasing the former increases the latter.

- For the operation without solid column formation above the ejector nozzle exit, some amount of gas was recirculated by means of the vacuum effect of the ejector.

- Significantly higher pressure difference was obtained with solid column formation for the same motive gas flow rate.

- Required pressure difference between cyclone and the riser through the downcomer was increased with riser superficial gas velocity.

- Solid column formation was observed at higher superficial gas velocity, i.e. solid flux through the ejector tube than the solid column disappearance.

- For the ejector only experiments, solid flow rates were approximately constant when the motive gas flow rate was higher than a specific rate. There was also an unstable region for the motive gas flow rate where the solid flow rates were inconsistent.

- The ejector system was tested with hot gasification system and similar pressure profile was obtained with the cold test facility experiments. The pressure jump was observed at the pressure profile of the gasifier which means there was a pressure barrier generated by the ejector system.

CFD analyses results;

A CFD model was built for the gas only homogeneous case and a reference ejector system has been built to validate the CFD results. Furthermore a novel semi-empirical method was proposed as a tool for predicting the ejector performance comparable with CFD results. The following conclusions can be drawn from the CFD results.

- According to the validation results of CFD model, maximum deviations of CFD results were accurate enough for the parametric analysis of the ejector.

- Vacuum pressure i.e. pressure difference generated by the ejector is almost linearly increasing with the increase of flowrate of the motive gas.

- Vacuum pressure increases with the decrease of ejector nozzle diameter. This shows the vacuum pressure not only depends on the flowrate but also depends on the nozzle exit velocity of the motive gas.

- The static temperature of the motive air is decreasing along the nozzle due to the compressible flow effect because the Mach number is higher than the practical limit of incompressible flow (0.3) at the exit of the nozzle. After the exit of the

nozzle, temperature is again increasing due to the decrease of velocity and reaching approximately its initial value at the exit of the ejector.

-There was a limiting ejector tube length above which ejector performance does not change considerably and below which it drops steeply. This length depends on ejector nozzle exit velocity. Hence, the limiting ejector length increases with increasing flow rate.

- Vacuum pressure almost linearly increased with increase of motive gas temperature due to the increase of volumetric flow rate of motive gas.

- Vacuum pressure is decreasing nonlinearly with the increase of ejector tube diameter and the rates of changes are very sensitive to the tube diameter changes. These results show that there is strong relation with the cross-section area of the ejector tube and the vacuum pressure.

- It was realized that, there is a strong linearity relation with vacuum pressure generated by the ejector and momentum flux of motive gas with respect to ejector tube cross-section area.

- Based on the strong linearity relation between vacuum pressure and the momentum flux of motive gas, semi-empirical correlation for estimating the maximum vacuum pressure for an ejector was developed which is comparable with the CFD results.

5. FUTURE WORKS

The present work attempted to develop a first level understanding of the proper design and operational conditions of an ejector type CFB system, by using computational fluid dynamic (CFD) model, experimental CFB cold system and gasifier system. However, some studies in order to get comprehensive understanding of ejector type solid circulation for CFB systems. The studies needed for study are shown below.

- In this study, a CFD model was built for the gas only homogeneous case in order to investigate the behavior of the ejector system without any solid particle flow. CFD model analysis of ejector system with solid flow is needed. In order to understand the mechanism of the solid accumulation at ejector nozzle exit, solid flow behavior should be analyzed with CFD model. In addition to that, different motive gases may be analyzed with CFD study such as steam, CO_2 or any other gases.
- For experimental study, finer and courser particles than the particles studied in this study should be tested to analyses the behavior of ejector system with different type of particles.
- For hot experimental study, an experimental set up should be designed and manufactured that has observation window at the downcomer in order to observe solid flow and calculate the solid circulation rate through the reactor.
- The effect of ejector type circulation on agglomeration should be investigated. Due to the violent environment through the ejector nozzle exit region, there may be a potential of positive effect of ejector type solid circulation on agglomeration problem.

REFERENCES

[1] Energy Statistics Division of the International Energy Agency, (2011), Key World Energy Statistic Report.

[2] International Energy Agency, (2009), Energy Balance for World, http://www.iea.org/stats/balancetable.

[3] Republic Of Turkey Ministry Of Energy and Natural Resources, (2009), Energy Balance For Turkey.

[4] Conti, J., Holtberg, P., (2011), International Energy Outlook 2011, U.S. Energy Information Administration.

[5] Turkish Coal Enterprises, (2009), Coal Sector Report (Lignite).

[6] Balat, M., (2005), Use of biomass sources for energy in Turkey and a view to biomass potential, Biomass and Bioenergy 29, 32-41.

[7] U.S. Department Of Energy, National Energy Technology Laboratory, (2010), Gasification 2010 Worldwide Database.

[8] U.S. Energy Information Administration, (2009), International Energy Statistics.

[9] Everitt, E., (2007), Gasification and IGCC: Status and Readiness, Wyoming Coal Gasification Symposium, 2007, Wyoming.

[10] U.S. National Energy Technology Laboratory, (2010), Gasification Databases - Gasification Plant Report.

[11] Higman, C., Burgt, M., (2003), Gasification, 1st Edition, Elsevier Science, Burlington, USA.

[12] Maniatis, K., (2002), Progress in Biomass Gasification: An Overview, Europan Energy&Transport Commission.

[13] Basu, P., (2006), Combustion and Gasification in Fluidized Beds, 1st Edition, Taylor & Francis Group, London, England

[14] Kim, S.W., Kim, S.D., (2002) Effects of particle properties on solids recycle in loop-seal of a circulating fluidized bed, Powder Technology, 124, 76-84.

[15] Basu, P., Butler, J., (2009) Studies on the operation of loop-seal in circulating fluidized bed boilers, Applied Energy, 86, 1723-1731.

[16] Gül, S., Ünlü, N., Aydar, E., Karataş, H., Livatyalı, H., Nayır, T., Akgün, F., Özdoğan, Z.S., (2015) Gasification or Combustion System With Circulating Fluidized Bed, PCT/IB2015/054852

[17] Kshirsagar, S.D., Deshmukh, M.M., (2013) Combined Vapour Compression-Ejector Refrigeration System: A Review, International Journal of Engineering Research and Development, 6, 41-56.

[18] Chan, Y.J., Chen, Y.M., (2000) Enhancement of a steam-jet refrigerator using a novel application of the petal nozzle, Experimental Thermal and Fluid Science, 22, 203 – 211.

[19] E. Rusly, E., Aye, L., Charters, W.W.S., Ooi, A., (2005) CFD analysis of ejector in a combined ejector cooling system, International Journal of Refrigeration, 28, 1092–1101.

[20] Kandakure, M.T., Gaikar, V.G., Padwardhan, A.W., (2005) Hydrodynamic aspects of ejectors, Chemical Engineering Science, 60, 6391 – 6402.

[21] Bartosiewicz, Y., Aidoin, Z., Desevaux, P., Mercadier, Y., (2005) Numerical and experimental investigations on supersonic ejectors, International Journal of Heat and Fluid Flow, 26, 56–70.

[22] Bartosiewicz, Y., Aidoin, Z., Mercadier, Y., (2006) Numerical assessment of ejector operation for refrigeration applications based on CFD, Applied Thermal Engineering, 26, 604–612.

[23] Zhu, Y., Cai, W., Wen, C., Li, Y., (2009) Numerical investigation of geometry parameters for design of high performance ejectors, Applied Thermal Engineering, 29, 898–905.

[24] Pianthong, K., Seehanam, W., Behnia, M., Sriveerakul, T., Aphornratana, S., (2007) Investigation and improvement of ejector refrigeration system using computational fluid dynamics technique, Energy Conversion and Management, 48, 2556–2564.

[25] Sriveerakul, T., Aphornratana, S., Chunnanond, K., (2007) Performance prediction of steam ejector using computational fluid dynamics: Part 1. Validation of the CFD results, International Journal of Thermal Sciences, 46, 812–822.

[26] Hemidi, A., Henry, F., Leclaire, S., Seynhaeve, J.M., Bartosiewicz, Y., (2009) CFD analysis of a supersonic air ejector. Part I: Experimental validation of single-phase and two-phase operation, Applied Thermal Engineering, 29, 1523–1531.

[27] Hemidi, A., Henry, F., Leclaire, S., Seynhaeve, J.M., Bartosiewicz, Y., (2009) CFD analysis of a supersonic air ejector. Part II: Relation between global operation and local flow features, Applied Thermal Engineering, 29, 2990–2998.

[28] Varga, S., Oliveira, A.C., Diaconu, B., (2009) Influence of geometrical factors on steam ejector performance – A numerical assessment, international journal of refrigeration, 32, 1694 – 1701.

[29] Varga, S., Oliveira, A.C., Diaconu, B., (2009) Numerical assessment of steam ejector efficiencies using CFD, International journal of refrigeration, 32, 1203 – 1211.

[30] Ji, M.K., Utomo, T., Woo, J.S., Lee, Y.H., Jeong, H.M., Chung, H.S., (2010) CFD investigation on the flow structure inside thermo vapor compressor, Energy, 35, 2694–2702.

[31] Varga, S., Oliveria, A.C., Ma, X., Omer, S.A., Zhang, W., Riffat, S.B., (2011) Experimental and numerical analysis of a variable area ratio steam ejector, International journal of refrigeration, 34, 1668 – 1675.

[32] Li, C., Li, Y.Z., (2011) Investigation of entrainment behavior and characteristics of gas–liquid ejectors based on CFD simulation, Chemical Engineering Science, 66, 405–416.

[33] Ruangtrakoon, N., Thongtip, T., Aphornratana, S., Sriveerakul, T., (2013) CFD simulation on the effect of primary nozzle geometries for a steam ejector in refrigeration cycle, International Journal of Thermal Sciences, 63, 133 – 145.

[34] Varga, S., Lebre, P.M.S., Oliveria, A.C., (2013) CFD study of a variable area ratio ejector using R600a and R152a refrigerants, International journal of refrigeration, 36, 157 – 165.

[35] Ju, D., Fang, J., Zhang, T., Qiao, X., Xiao, J., Huang, Z., (2015) High-speed shadow imaging in internal flow pattern and macroscopic characteristics of a R134a flash-boiling spray discharged through a vertical twin-orifice atomizer, International Journal of Multiphase Flow, 75, 224–236.

[36] Battcock, W.V., (1972) Particulate solid fuel combustion systems, GB Patent 1291343.

[37] Donath E.E., (1975) Two stage gasification of coal, GB Patent 1393636.

[38] Yoshio, K., (1987) Fluidized bed combustion device having secondary combustion chamber, JP Patent 62190309.

[39] Per, T., Stal, A., (1988) Power plant with centrifugal separators for returning material from combustion gases to a fluidized bed, US Patent 4730563.

[40] Dumain, A., Raufast, C., (1989) Process for gas phase polymerization of olefins in a fluidized bed reactor, US Patent 4882400.

[41] Takashi, U., Akira, S., (1998) Circulating fluidized bed dryer apparatus, JP Patent 10148468.

[42] Anderson, G.L., Maryamchik, M., Wietzke, D.L., (2001) Fine solids recycle in a circulating fluidized bed, US Patent 6269778.

[43] Yoshiro, F., Susumu, N., Kazuo, O., (2003) Device for processing particles, JP Patent 2003038948.

[44] Scott, M.H., Dooley, K.A., Salmon, B.J., Lorenz, M.D., Scherrer, P.K., Lin, R., Meade, D.L., Strasser, W.S., Leonard, D.R., (2010) Process and apparatus for olefin polymerization in a fluidized bed reactor, US Patent 2010190935.

[45] Geldart, D., (1973) Types of Gas Fluidization, Powder Technology, 7, 285-292

[46] Gül, S., Ersöz, A., Baranak, M., Gul, O.F., Akgun, F., (2010) Comparative evaluation of different coal to liquid process conditions via Fischer-Tropsch synthesis, International Pittsburgh Coal Conference, 2010, Istanbul.

[47] Watanawanavet, S., (2008) CFD Optimisation Study of High-Efficiency Jet, PhD Thesis, Texas A&M University, USA

[48] Gül, S., Özdoğan, Z.S., (2016) Ejector type solid circulation system analysis for

circulating fluidized beds, International Journal of Multiphase Flow, 48, 116–128.

ÖZGEÇMİŞ

Serhat Gül 1982 yılında Osmaniye'de doğdu. Lisans ve Yüksek Lisans öğrenimini Marmara Üniversitesi Makine Mühendisliği Bölümü'nde tamamladı. Yüksek Lisans 'ta kömür ve biokütlenin dolaşımlı akışkan yatakta oksijence zenginleştirilmiş hava ortamında yakılması üzerine çalıştı. Akışkan yataklı gazlaştırma ve yakma teknolojileri üzerine birçok araştırma projesinde yer aldı. 2006 yılında çalışma hayatına başladığı TÜBİTAK Marmara Araştırma Merkezinde halen Başuzman Araştırmacı olarak çalışmaktadır.